# METEOROLOGICAL CHARACTERISTICS OF THE CANADIAN ARCTIC SHELF EXCHANGE STUDY

BY

TERESA D. FISICO

A Thesis submitted to the Faculty of Graduate Studies of

The University of Manitoba

in partial fulfillment of the requirements of the degree of

MASTER OF SCIENCE

Centre for Earth Observation Science

Department of Environment and Geography

University of Manitoba

Winnipeg, Manitoba, Canada

THE UNIVERSITY OF MANITOBA

FACULTY OF GRADUATE STUDIES

*****

COPYRIGHT PERMISSION

# METEOROLOGICAL CHARACTERISTICS OF THE CANADIAN ARTIC SHELF EXCHANGE STUDY

BY

TERESA D. FISICO

A Thesis/Practicum submitted to the Faculty of Graduate Studies of The University of Manitoba in partial fulfillment of the requirement of the degree

MASTER OF SCIENCE

# Abstract

The CASES meteorological program began October 22, 2003 and continued until June 20, 2004 (day 295 to day 172, herein "observational period " or "study period"). The program consisted of manual meteorological surface observations taken on the hour, atmospheric profiling of temperature, moisture and low-boundary layer winds, continuous cloud base height, integrated column water vapor and cloud liquid water measurements, as well as automated visibility observations. Few continuous meteorological data sets have been made during the fall-winter-spring period in the Southern Beaufort Sea sea-ice environment. Presented here is an overview of the hemispheric, synoptic and local scale meteorology observed from the CCGS *Amundsen* during the observational period. First, NCEP I reanalysis data were used to examine how the CASES year compared to the 1971-2000 30-year "normal". Second, surface 3-hourly isobaric analysis were used to track low-pressure disturbances (LPDs) affecting the CASES region during the observational period to reveal their location of origin and evolution. Third, a monthly (and overall) climatology of several meteorological variables (e.g. cloud type/amount/ceiling, adverse weather, wind, temperature) was produced. Finally, a comparison of data collected from the ship with surrounding Meteorological Service of Canada station data and an investigation into the accuracy of daily averages from NCEP I and NCEP II reanalysis data, North American Regional Reanalysis (NARR) and GEM-Regional analysis data is presented. The investigations reveal the weaknesses and strengths of popular and widely used model data with respect to actual station data with the intentions of improving atmospheric modeling in arctic regions.

# Acknowledgements

The pursuit of completing a Masters thesis is anything but a solo effort. Though only one degree will be (hopefully) awarded, all those who aided in making the completion of this document a reality are its recipients.

Firstly, I must extend my deepest gratitude to my supervisor, John Hanesiak, for his patience, understanding and guidance throughout the entire process, and for offering me the opportunity to study and experience Canada's north. I would also like to especially thank David Barber for his encouragement and support, as well as Ken Snelgrove for his collaboration and direction with MM5 and other coded endeavours.

My thanks to Edward Hudson at the Prairie and Arctic Storm Prediction Centre in Edmonton for providing the surface analysis required for the storm tracks, and to Ron Goodson of Environment Canada and Jeff Tilley at the University of North Dakota for their assistance. I also extend my acknowledgements to the Canadian Meteorological Centre for providing access to the raw output of GEM, and to the Physical Science Division of the Earth System Research Laboratory, NOAA for use of the NCAR/NCEP suite of reanalysis products.

To Wayne Chan for facilitating the 'GEM crunch', and for the much needed and appreciated boosts along the way, and to David Mosscrop, for his hardware assistance and for convincing me to 'switch'. To Tim Papakyriakou, Bob Hodgson, Jens Ehn, Ryan Galley, C.J. Mundy, Alexandre Langlois, John Iacozza, Owen Owens, and An Tat: thank you for your collaboration and assistance not only at the office, but especially in the field. I couldn't have done it alone.

I must also thank the Department of Environment and Geography, the Centre for

Earth Observation Science, and the University of Manitoba for providing the facilities and services required for completing the degree. My deepest gratitude also to the support staff, particularly Trudy Bauriess, Denise Whynot, Mary Anna, Pat Gutoski, Aggie Roberecki, and Valerie Smith, without whom I would never have found my way through the paperwork.

Mom, Dad – thank you for standing behind me the whole way. To you and the rest of my family and friends, thank you for your love, encouragement and motivation in all my undertakings.

Lastly, I would like to take this opportunity to thank Tim Hortons for dispensing their particularly effective (and addictive) brew 24-7.

# Table of Contents

# List of Tables

# List of Figures

# 1 Introduction

## 1.1 Background and Objectives

Focus on the study of the arctic environment has been increasing dramatically over recent decades. With over a century of industrial growth, the effects of introducing excessive amounts of greenhouse gases (GHGs) into the atmosphere are now becoming apparent and measurable. The Arctic Climate Impact Assessment (2004) and the Intergovernmental Panel on Climate Change Fourth Assessment Report (IPCC AR4 2007) both state that the environmentally sensitive polar regions are likely to witness the first environmental impacts as a result of continued and prolonged industrial activities and resultant byproducts. The addition of anthropogenically generated GHGs, particularly $CO_2$, into the climate system has been noted as the main cause of global average temperature rise (IPCC AR4 2007).

The polar regions are necessary heat-sinks in the global climate system. Heat and moisture are transferred to the arctic regions via the general atmospheric circulation, which, in the arctic, is influenced by shifts in semi-permanent surface pressure features. Inter-annual variability of semi-permanent surface pressure strength leads to a shift of atmospheric mass, and thus a shift in weather regime across the Northern Hemisphere. This 'see-saw' effect is called the North Atlantic Oscillation (NAO), where central pressures of the Icelandic Low and the Azores High change relative to each other. In a positive NAO state, the Icelandic Low deepens in exchange for a strengthening of the Azores High, where the opposite is true for a negative or 'low' NAO state. Figure 1.1, taken from Dickson et al. (2000) illustrates this shift in surface pressure. The NAO index, the difference between the central pressures of the Icelandic Low and the Azores High, is calculated to quantify the intensity of the mass shift. Figure 1.2 shows the winter NAO index over the last 140 years (IPCC 2001). Superimposed in this variability is what has been recently coined as the Arctic Oscillation (AO), an embedded mass shift between the polar vortex and the mid-latitudes, and its index, highly correlated with the NAO, is also provided in Figure 1.2 (IPCC 2001; Thompson and Wallace 1998). Positive NAO and AO states have been shown to drive moist warm air into the arctic region by way of cyclonic activity following a northward-deviated path (Dickson et al. 2000; McCabe et al. 2001). Since the 1960s, the NAO/AO index has been on a steady positive trend, in which time an increase in cyclonic activity and a reduction in sea ice extent have been documented (McCabe et al. 2001; Zhang et al. 2004; Barber and Hanesiak 2004; Stroeve et al. 2007). Lambert (1995) hypothesized about the relationship between $CO_2$ increase in the atmosphere and the effect on winter hemispherical cyclonic activity, and found that though storm tracks remained consistent with a $2xCO_2$ model scenario, the frequency of cyclones were reduced over all, but the frequency of intense cyclones did increase. Further and more specific investigation of cyclonic activity revealed that between 1959 and 1997, cyclonic intensity had increased at both high and mid latitudes of the Northern Hemisphere (McCabe et al. 2001). A noted 'regime shift' of increased cyclonic activity in the high latitudes and a reduction of such activity in the mid latitudes occurred around the point where the AO became strongly positive in 1989. Zhang et al. (2004) concluded similar findings, but also found that along with an increase in cyclonic activity in the last 50 years, the frequency of cyclones and intensity of cyclones originating from the mid latitudes has risen, suggesting that storm tracks were being forced northward and allowing for increased advection of heat and moisture into the Arctic. While the positive

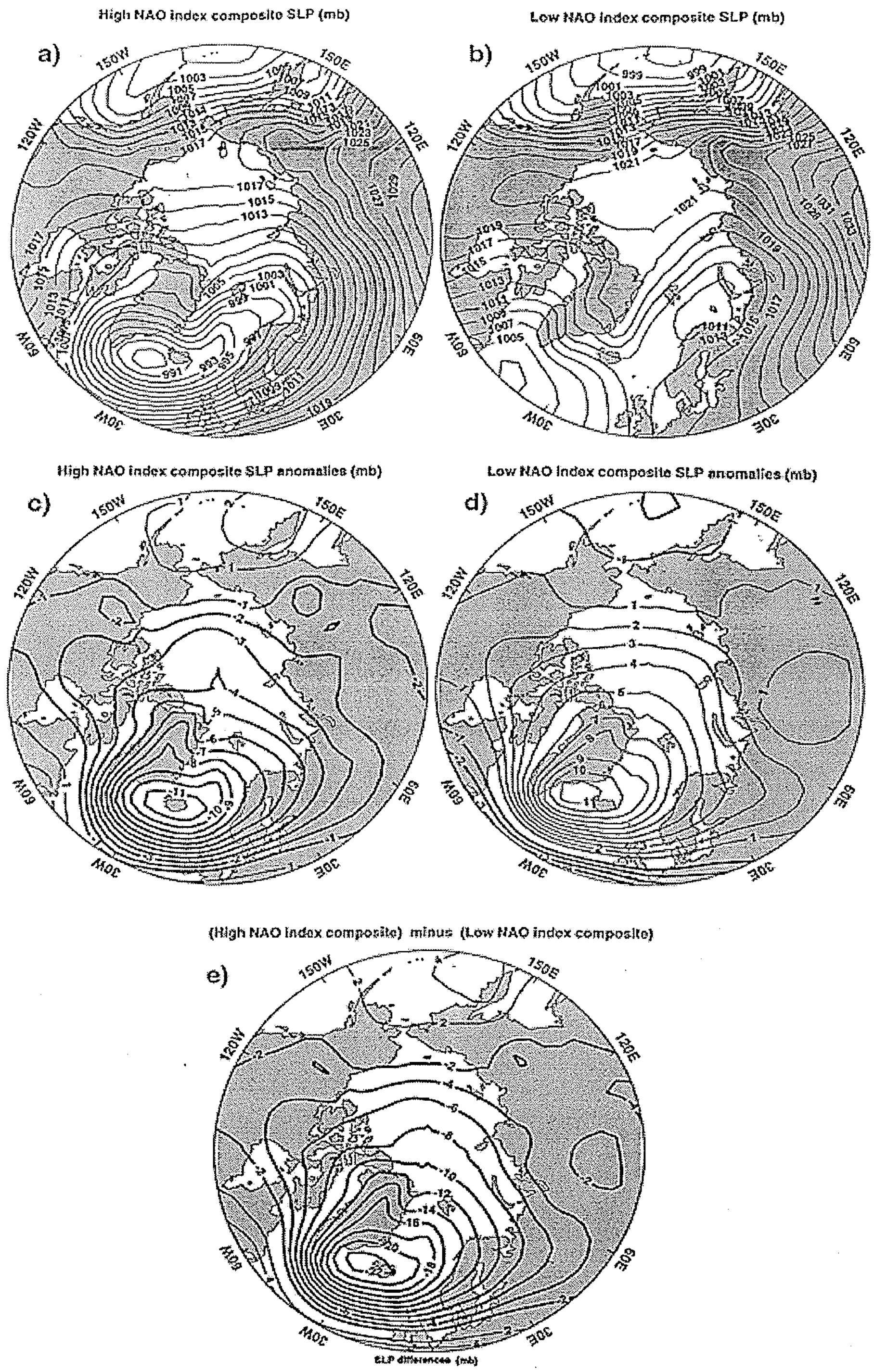


Figure 1.1: Distributions of (a), (b) winter SLP and (c), (d) SLP anomaly for composites of winter months representing high-index and low-index states of the NAO. (e) The change in SLP from the low-index composite to the high. (from Dickson et al., 2000)

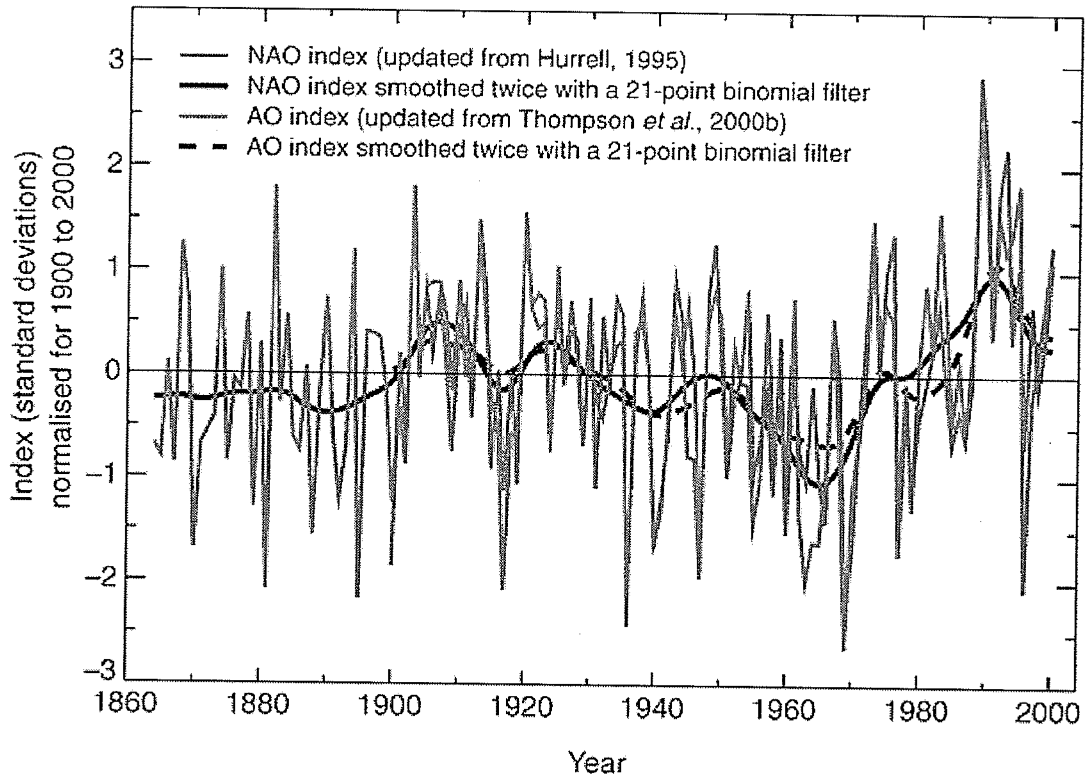


Figure 1.2: December to March North Atlantic Oscillation (NAO) indices, 1864 to 2000, and Arctic Oscillation (AO) indices, 1900 to 2000, updated from Hurrell (1995) and updated from Thompson and Wallace (2000) and Thompson et al. (2000b), respectively. The indices were normalised using the means and standard deviations from their common period, 1900 to 2000, smoothed twice using a 21-point binomial filter where indicated and then plotted according to the years of their Januarys. (taken from IPCC 2001)

shift in the AO and resulting increased cyclonic activity in the north can largely account for the recent warming measured in high latitudes, it lends a preview to what may come with further anthropogenic climate change.

Snow and sea ice are crucial to the moderation of heat and reflection of solar radiation. Unique feedbacks in the arctic climate regime are highly sensitive to fluctuations in temperature (Holland and Curry 1999). Of particular importance is the ice-ocean-atmosphere feedback mechanism, whereby surface temperature is regulated by the presence of snow and sea ice and their highly reflective properties. As warmer temperatures are introduced, the reflective properties of snow and ice are hindered due to the increased presence of liquid water. On the whole, sea ice extent decreases, as has been the case (Cosimo 2006; Barber and Hanesiak 2004; IPCC AR4 2007; ACIA 2004; Stroeve et al. 2007), allowing more heat storage in areas that are ice-free. Adding the prediction that cyclonic intensity may be on the increase suggests that surface winds and wave action may act to intensify this feedback mechanism by destroying existing ice pans. Numerous reports over the last decade have cited sea ice concentration and thickness losses in the arctic regions (Rothrock et al. 1999, Lindsay and Zhang 2005, Cosimo 2006; Barber and Hanesiak 2004; IPCC AR4 2007; ACIA 2004; Stroeve et al. 2007). Record low sea ice extent was first discovered in 2002, and levels remained nearly as low until 2005, where arctic sea ice concentration hit another record low (Lindsay and Zhang 2005). With the advent of satellite technology, sea ice coverage/extent can be more closely monitored. Up until 2006, September sea ice extent in the Arctic (at the end of the melt period) was estimated to be decreasing at a rate of -7.8%/decade for the last five decades. Reviewing this estimate with satellite inferred sea ice concentration data between 1979 to 2006 revealed a larger rate of reduction of -9.1%/decade (Stroeve et al. 2007). The mean rates of ice growth for the freeze-up period in March, though much smaller in magnitutde, are also negative (-1.8%/decade from 1956 to 2006, and -2.9%/decade when inferred with satellite data; Stroeve et al. 2007). Recently, a hypothesis was proposed that suggested model forecasts of sea ice depletion might not be as accurate as originally thought (Stroeve et al. 2007). In fact, the qualification of GHG input to the climate system simulated by global circulation models (GCMs) may be underestimating the effects of current GHG concentrations, leading to estimates of sea ice decay that are more conservative than actual rates.

It follows then that model accuracy is of great concern, especially when conclusions are being drawn regarding the future state of Earth's climate based on model simulations (Dumas et al. 2006; Zhang et al. 2004; Gregory et al. 2002; IPCC AR4 2007). The Arctic presents setbacks when attempting to maintain instrumentation and retrieve data with the hopes of providing verification for models; remote locations and the expense of transportation, harsh terrain, and extreme weather conditions are not conducive to the collection of accurate measurements and time series datasets. Previous studies have investigated the accuracy of model data against available in-situ data for various factions of the polar climate (Briegler and Bromwich 1997; Cullather et al. 2000; Wei et al. 2002; Bromwich et al. 2001; Andersen et al. 2007). With the reality of global climate change on the horizon, means and resources for *in-situ* study have become increasingly available, as policy makers and funding agencies realize the potential impacts of such a trend and the research necessary to make informed decisions. The Canadian Arctic Shelf Exchange Study was proposed as an international initiative focusing on the collection of *in-situ* data within all realms of the arctic climate system. The project was to provide insight into the role of processes and linkages between these realms, and to provide data to build and test climate models from within the Western Arctic, particularly in proximity to the Beaufort Polynya, and was successfully funded. The Canadian Arctic Shelf Exchange Study (herein CASES) took place between September 13$^{th}$, 2003 and August 31$^{st}$, 2004 (a test run of the project took place during the summer of 2002). The study was based around the use of the CCGS *Amundsen* (previously the CCGS *Sir John Franklin*), a Canadian Coast Guard icebreaker that had been retrofitted for scientific use and became the platform for most of the sampling operations. The meteorological program was carried out from October 15$^{th}$, 2003 to June

24th, 2004. The ship remained in transit for the first 30 days of the program, and then remained stationary for the next 193 days in Franklin Bay, NWT, Canada (70.05N, 126.30W; the 'over-wintering site'). While most of the meteorological instrumentation remained on the ship, a suite of meteorological instruments were also installed on the ice approximately 1.0 km ESE of the over-wintering location during this time frame. The ship reestablished transit on June 1st; 2004 and remained in transit until the end of the project. In order to address the need for meteorological support for the CASES project, to continue meteorological study in the Beaufort Sea region, and to ground-truth model data representative of the region, the data collected from the CCGS *Amundsen* and the adjacent ice camp were used in this study with the following objectives:

1. To provide a climatological context for the CASES project;
2. To provide additional knowledge into the trends of cyclonic activity in the Western Arctic;
3. To provide a meteorological summary for the CASES project;
4. To examine the differences between meteorological variables with surrounding stations;
5. To investigate the accuracy of model data within the CASES region.

## 1.2 Thesis Structure

The structure of this document will follow the order of the proposed objectives of the study. The objectives will be addressed in three separate investigations, one focusing on a summary of the meteorology and climatology of the region, the second providing data comparison between surface data from the ship, surrounding stations and models, and finally a vertical profiling study. The methods for each investigation will be included in each of the respective chapters. Firstly in Chapter 2, the site, instrumentation, and additional data used in the project will be outlined. Chapter 3 will outline the climatological and large-scale context for the CASES project, including a synoptic investigation and a local summary of the weather that occurred at the ship location, addressing objectives (1), (2), and (3). Objective (4) will be addressed in Chapter 4, while objective (5) will be covered in both Chapter 4 and Chapter 5. Chapter 4 will be the introduction to the comparisons of the ship data to other datasets. First presented is a look at how meteorological variables varied amongst adjacent permanent weather reporting stations. Secondly, an investigation of model accuracy is performed among four of the more widely used models. Chapter 4 concludes with a look at the ability of each model to represent the surface weather that occurred at the ship during the time frame of the study. In Chapter 5 the vertical structure of the atmosphere above the ship location is investigated and the accuracy of the Global Environmental Multiscale (GEM) model is tested in the vertical and presented. Chapter 6 will provide a summary of the findings and recommendations for further inquiries, and will conclude the thesis.

# 2 Site Description and Data

## 2.1 Site Description and Instrumentation

The majority of the automated measurements and manual observations were carried out from aboard the CCGS *Amundsen* (the ship). Since the meteorological program also took place during periods of ship movement, most of the instruments were placed on the upper-most level of the ship where it would be free of traffic and interference. The CCGS *Amundsen* is equipped with an AXYS Automated Voluntary Observation Ship (AVOS) system on the roof of the (bridge) wheelhouse. The AVOS system is an interactive environmental reporting system that allows for the hourly transmission of current conditions to a central land station. Temperatures (air and sea surface), pressure, relative humidity (RH), wind speed, wind direction, and current GPS location are updated every ten minutes and displayed on a computer monitor located in the wheelhouse of the ship. The AVOS system interface allows for manual observer reports to be entered into the system. The AVOS deploys a Rotronics MP 101A sensor for temperature and RH, with a resolution of 0.1°C and an accuracy of ± 0.3°C, and a 1% ± 1% accuracy for temperature and RH, respectively. Atmospheric pressure was obtained from a Vaisala PTB210 sensor with a 0.01mb resolution and an accuracy of ±0.15 mb. Wind speed and direction is collected from an RM Young 05103 anemometer, accurate to ±3° in direction and ±0.3 m/s. Manual cloud observations were taken from the ship on the hour for approximately 14 to 17 hours per day and were integrated with the AVOS prior to the hourly transmission time. On a few occasions, cloud observations were conducted from the ice in close proximity to the ship while stationary at the over-wintering site. Cloud

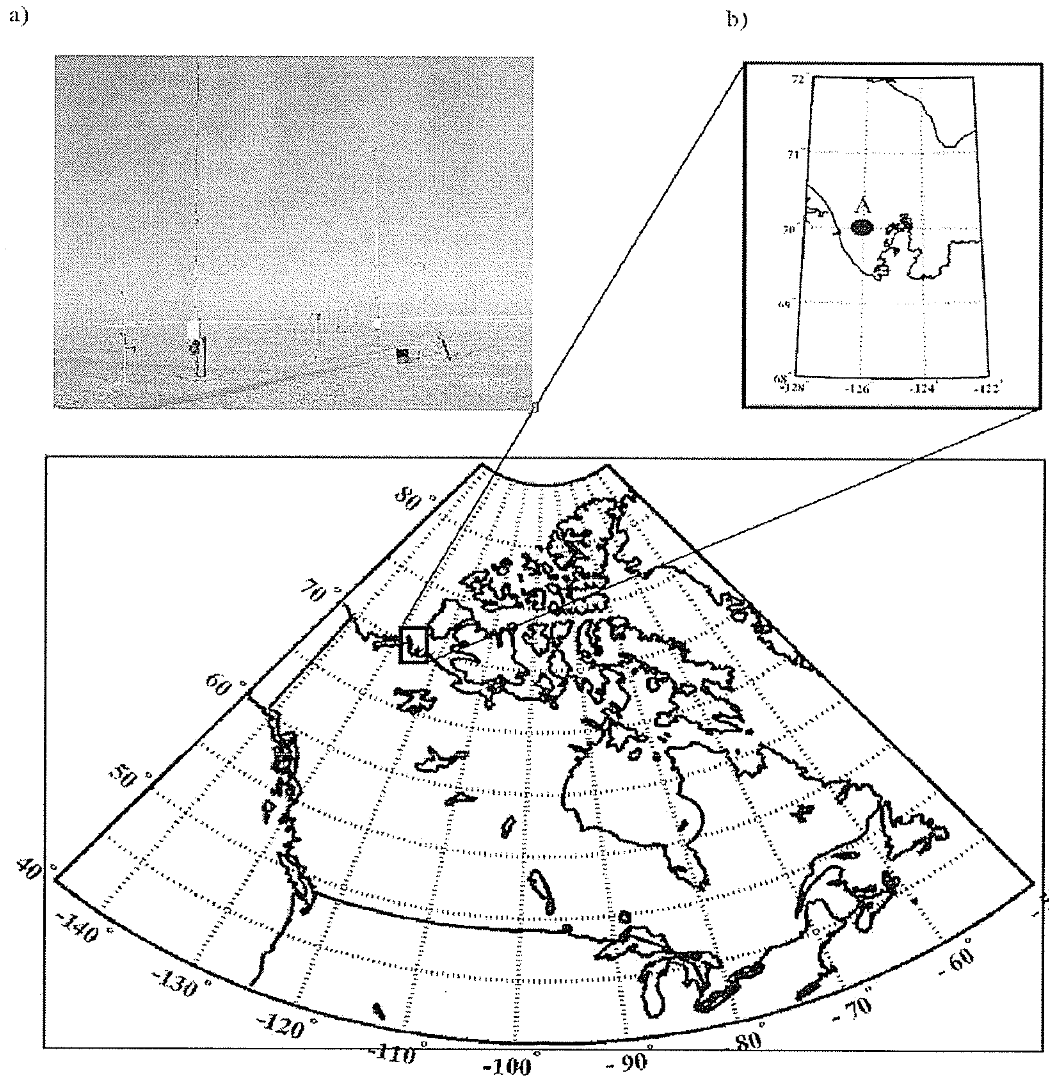


Figure 2.1: (a) Meteorological towers erected at the on-ice site 'Takauk'. (b) Over-wintering location of the CCGS *Amundsen* – 70.05N, 126.30W, Franklin Bay, North West Territories.

type and opacity were reported in octas.

Manual visibility observations were reported in conjunction with cloud observations in nautical miles and were aided by a Videograph provided by the Meteorological Service of Canada (MSC), situated adjacent to the AVOS system pointing off the port side of the ship (north, while over-wintering). Twenty-four hour manual observations were carried out on Legs 4 (day 007 to 048) and 7 (day 134 to 172) while two observers were present. Temperature, sea surface temperature (SST), pressure, relative humidity, wind speed and wind direction were archived from the AVOS. Due to the location of the AVOS and the ship's orientation while over-wintering, westerly wind conditions often caused measured wind directions and speeds to be unreliable due to turbulent flows around the frame of the ship. Multiple towers erected at an ice camp site (referred to as 'Takatuk'), located approximately one kilometre east-southeast of the ship from day 028 to day 128, provided unobstructed wind data until dismantled (see Figure 2.1). Sentry™ SVS-1 Visibility Sensors at 1.5 and 3.3 metres were also installed at Takatuk and used to collect continuous visibility measurements (accuracy ±10%). Precipitation observations were made every 6 hours UTC (00Z, 06Z, 12Z, 18Z) during an active observer shift using a Nipher snow gauge and rain gauge, which were also located on top of the ship's wheelhouse on the stern side. Integrated column water and water vapor were measured by a Radiometrics WVR-1100 microwave radiometer, situated at a position bow-ward of the *Amundsen*'s smoke stack to allow for full clearance of obstacles while scanning. Due to mechanical difficulty, data from the WVR-1100 between day 331 and 028 became unreliable. Cloud base heights were measured using a Vaisala CT25K laser ceilometer running continuously throughout the project. The CT25K was positioned on the same level as the WVR-1100 along the port railing. Its placement was well clear of the WVR-1100 scanning area and clear of any vertical obstacles. However, the exhaust from the smoke stack would occasionally drift into the field of view of the ceilometer and the WVR-1100 during periods of southerly and westerly flow, respectively.

Vaisala RS80-15G GPS wind-finding radiosondes were launched as much as once every three hours, though launches were reserved for significant weather scenarios. Significant weather scenarios included instances of severe weather, extended periods of low stratus cloud, frontal passages and clear sky cases. The radiosonde UHF and GPS antennas were placed atop a storage container on the 400 level of the ship. Radiosondes were released from the helicopter deck at the stern of the ship on the 400 level.

Data from the suite of instruments were archived regularly and are used in this study, along with additional data as described in the following section.

## 2.2 Additional Data Sources

### 2.2.1 Meteorological Service of Canada

In addition to the suite of data collected at the ship, the Meteorological Service of Canada's (MSC) Prairie and Arctic Storm Prediction Centre provided data from meteorological stations within the CASES study area from October 2003 to June 2004 inclusive for the purposes of comparison with ship data. Hourly records of cloud base height and visibility (where available), wind direction, wind speed, temperature (dry-bulb, wet-bulb and dew point), station pressure, cloud amount and opacity and present weather (where available) were provided from the following stations (where 'A' indicates an automatic station): Paulatuk A, Cape Parry A, Holman, Sachs Harbor, and Tuktoyaktuk. Daily precipitation data for each of these stations were also provided. Isobaric analyses produced at 3-hr intervals were provided by the MSC (Edmonton Office) for the CASES region in the form of image files for October 2003 to June 2004 inclusive.

### 2.2.2 National Centers for Environmental Prediction - National Center for Atmospheric Research

National Centers for Environmental Prediction – National Center for Atmospheric

Research (NCEP - NCAR) Re-analysis data (Kalnay et al. 1996, hereafter NCEP I) for the entire CASES domain were collected for the purposes of the climatological investigation and model comparison study. Based on the collection of decades of global observations at the surface and of the vertical, the NCEP I dataset is an assimilation of real data and model influence, translated into 28 vertical levels and onto two frames: a 2.5° x 2.5° grid for output on pressure surfaces, and a T62 Gaussian grid (192x94) for output of surface variables. Values of temperature, pressure, relative humidity, zonal and meridional (U and V) winds were collected on the T62 Gaussian grid, and precipitable water was taken from the former, all in the form of daily average time series data. NCEP Re-Analysis II data (NCEP II), a reworking of the original dataset with updated parameterizations and error corrections, was collected in the same fashion. NCEP II was reported to correct data in areas of the high latitudes by improving snow cover analysis and snow melt terms in the model, amongst other fixes (Kanamitsu, et al., 2002). The third and final product obtained from NCEP-NCAR was the North American Regional Reanalysis (NARR) dataset (Mesinger, et al., 2004). A subset and reworking of NCEP II and limited to the North American domain, NARR provides a higher resolution in the horizontal (35 km) and vertical (45 layers).

All products were obtained through online the NOAA-CIRES Climate Diagnostics Center, Boulder, Colorado (http://www.cdc.noaa.gov) in netCDF format.

### 2.2.3 Canadian Meteorological Centre

Global Environmental Multiscale (GEM) high-resolution 0-48 hour forecast data was provided with permission by the Canadian Meteorological Center (Rick Jones, personal communication) in GRIB Edition 1 data format and includes all of Canada and most of the United States of America in its domain. The 00z and 12z forecast runs, providing 3-hourly output for a total of 48 hours from initiation time, were downloaded and archived daily throughout the duration of the CASES year. Prior to June 16, 2004, GEM operated on a horizontal resolution of 24 km and a vertical resolution of 28 layers. On June 16, 2004, the horizontal resolution of GEM was increased from 24 km to 15 km (501 x 399). This resolution change increased the size of each forecast run substantially. Due to the nature of the automated archiving process and its dependence on network operation, the dataset is not entirely continuous.

# 3 Climatological and Meteorological Summary

## 3.1 Methods

NCEP I data were used to analyze large scale atmospheric conditions averaged over the entire primary period with meteorological field observations during CASES (September 2003 to June 2004) as well as monthly variations. This was done to reveal the climatological perspective of the CASES project (i.e. whether it was a climatologically "normal" with respect to the 1971-2000 average). A variety of atmospheric variables were investigated, including near-surface air temperature and humidity, sea level pressure, precipitable water vapor (PWV), winds, geopotential height, and 1000-500 hPa thickness. Atmospheric anomalies for each variable (over the entire period and monthly) were calculated by subtracting the overall and monthly means of September to June 1971-2000 from the overall and monthly means of September 2003 to June 2004, respectively. Positive anomalies suggest above "normal" conditions and negative anomalies below "normal" conditions.

To investigate synoptic patterns, 3-hourly isobaric surface analyses were studied and used to extract the region of origin and positions of low pressure disturbances (LPDs) as they evolved and migrated through the CASES region. LPDs were defined as any system coincident with or providing significant weather reported at the ship location. Tracks were produced manually by inspection of the analysis images covering the period of October 2003 to June 2004, inclusive. LPD tracks were classified in terms of geographic origin based on our findings with respect to the boundaries of the CASES

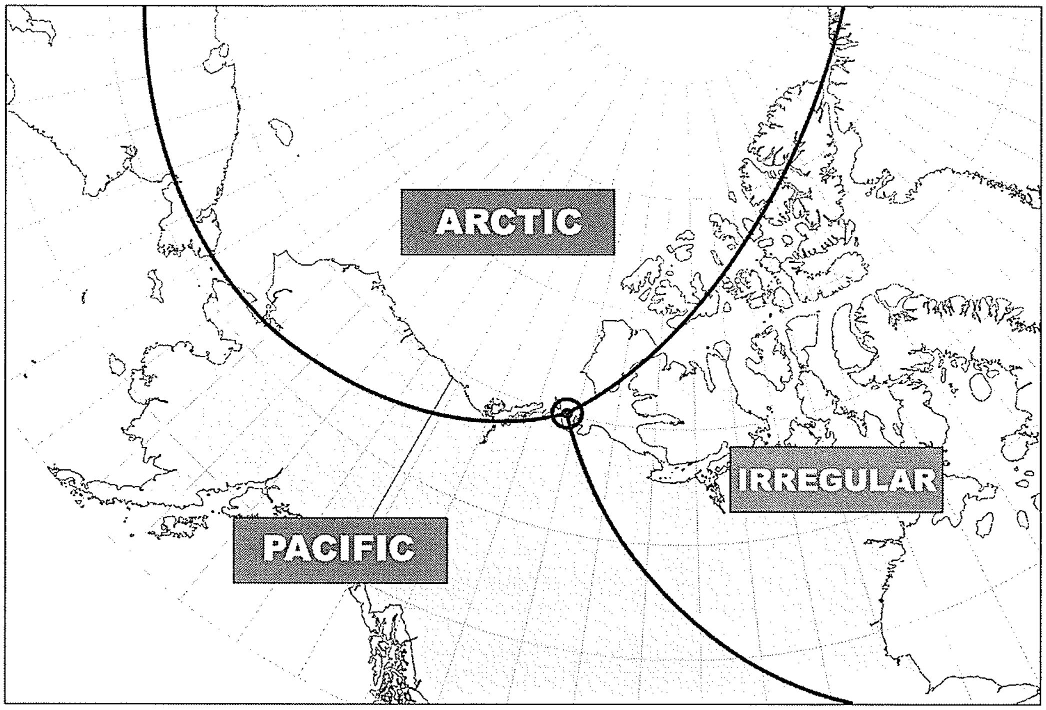


Figure 3.1: Classes of geographical origin for documented low pressure disturbances (LPDs) through the CASES domain over the duration of the project.

domain. Tracks of secondary circulations were also included. The location of cyclogenesis (and origin of disturbances lacking a closed circulation; i.e., troughs) were classified as “ARCTIC” for those which originated poleward of the ship location and “PACIFIC” for those which originated south of the Bering Strait; any LPD not corresponding to these categories were classed as “IRREGULAR”, and is illustrated in Figure 3.1. This naming convention follows those in Hudak et al. (2002). In their study, upper-air parameters regarding storm steering flow and temperature were used to class summer cyclonic origin using an automatic algorithm. An analysis in such detail was not carried out for this study. However, it can be seen in the results of our investigation that LPDs in the Western Arctic do fall under such categories based on surface analysis alone. Also, since our investigation was done using manual techniques, the use of upper-air numerical parameters to define the occurrence of LPDs was unnecessary.

Finally, data collected at the ship was analysed in daily and monthly averages to provide an overall local meteorological summary during the time frame of the project.

## 3.2 Climatological Investigation

### 3.2.1 CASES period

Results discussed here refer to the anomalies with respect to the period over September 2003 to June 2004. Overall, slightly positive air temperature anomalies (0 to +1°C) existed over the duration of the project in the CASES area with much larger positive anomalies to the west and north (+2 to +4°C) and into the entire Archipelago region (up to +7°C) (Figure 3.2). This was associated with positive sea level pressure (SLP) anomalies in the Arctic Ocean, North Pole and northern European regions (slightly positive (+1 to +2 hPa) in CASES) and negative anomalies in the eastern Arctic, North Atlantic, North Pacific and Japan regions (Figure 3.3). Near-surface relative humidity in the CASES region was near normal with only slightly positive anomalies (+3%) toward the west and east. At 500 hPa, geopotential height anomalies over CASES were +20 to +30 meters with larger positive anomalies over the Canadian Cordillera and west of CASES (over Alaska) and stretching across the Arctic Ocean, North Pole and onward to Greenland (Figure 3.4). Negative 500 hPa anomalies existed over Hudson Bay and across the north Atlantic as well as the north Pacific and Japan areas. It is not surprising that this pattern is also reflected in the 1000-500 hPa thickness field suggesting abnormally warm air over western Canada, Arctic Ocean and across to Greenland (i.e. the entire Canadian

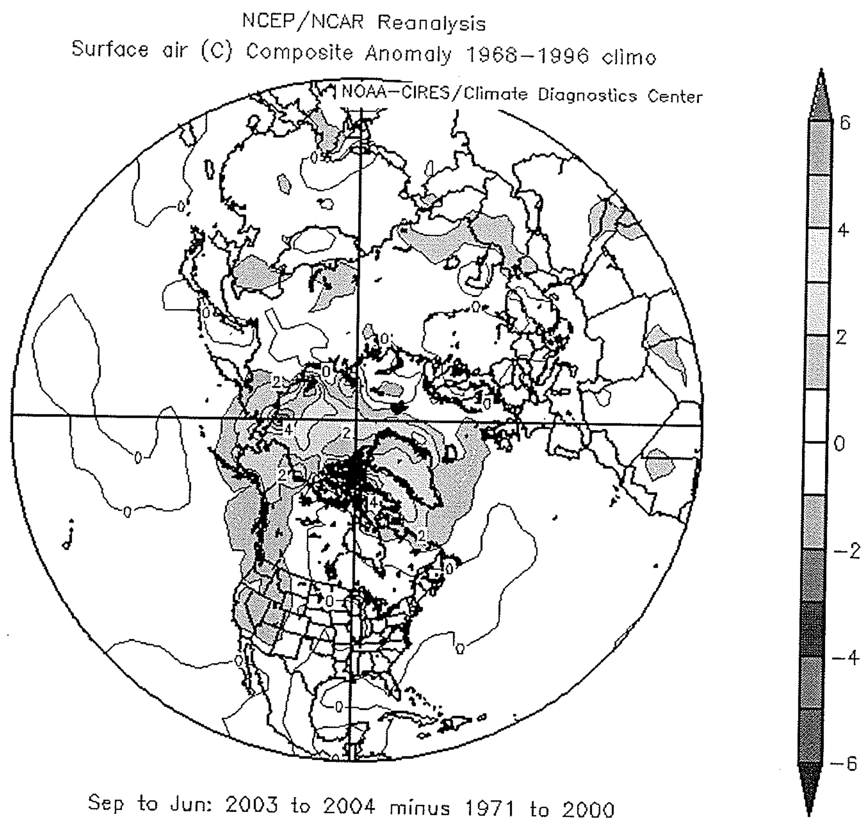


Figure 3.2: Near-surface air temperature anomalies (°C) over the CASES period (Sept. 2003 – Jun. 2004) with respect to the 1971-2000 mean.

high Arctic) (not shown). The surface and lower troposphere meridional wind anomalies were slightly negative (zero to -1 m $s^{-1}$) or greater northerly flow than average throughout the entire Arctic Ocean, CASES and western Archipelago regions but positive anomalies existed in the Gulf of Alaska, Alaska and just south of the Beaufort Sea coastline (not shown). It is also interesting to note that low-level wind vectors imply advection (warm) of large positive temperature anomalies from northern Baffin Bay/north-central Archipelago (as well as the Siberian Sea) into the western Canadian high Arctic (and CASES region) (Figure 3.5). The precipitable water vapor (PWV) anomalies are positive in the Gulf of Alaska up to the Bering Strait as well as the eastern Canadian high Arctic

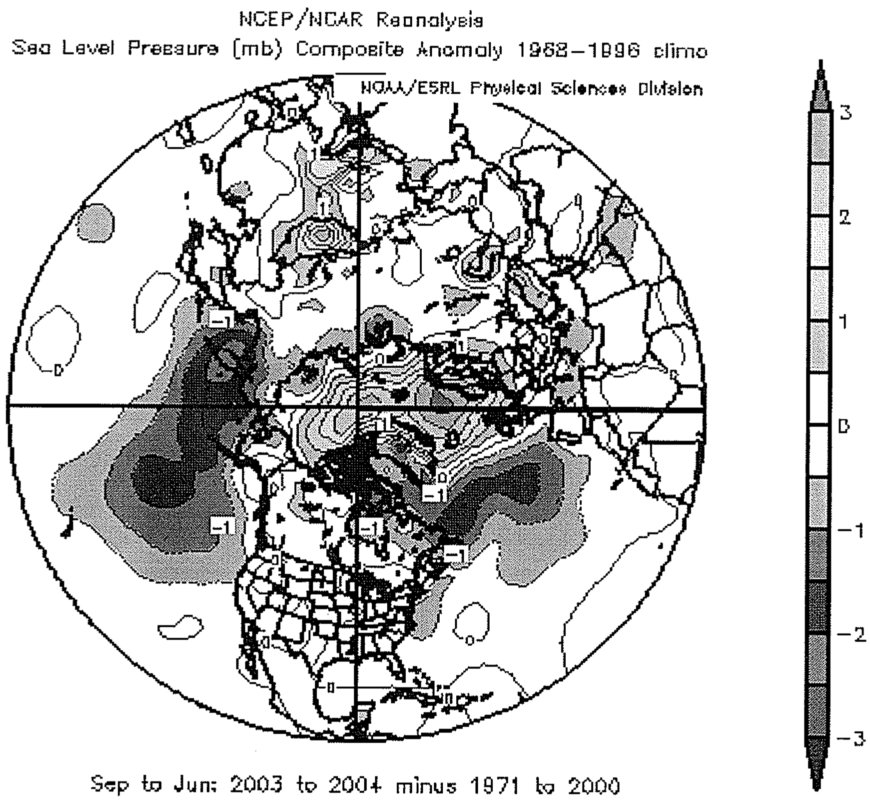


Figure 3.3: Same as Figure 1 but for sea level pressure (SLP) (hPa).

(not shown). Near normal PWV existed in the CASES and Archipelago regions (5.33 kg $m^{-2}$), which is slightly less than the average available surface-based microwave radiometer measurements retrieved from the ship (6.24 kg $m^{-2}$; further investigation of PWV measured at the ship and its comparison with the NCEP I equivalent is presented in Chapter 4).

### 3.2.2 Monthly Analysis

Given the long-term anomalies discussed above, it is useful to examine why these anomalies existed and which months/seasons were responsible for producing them. Specifically in the CASES region, the overall positive near-surface temperature anomalies in Figure 3.2 resulted from +1 to +5°C anomalies during the fall and early

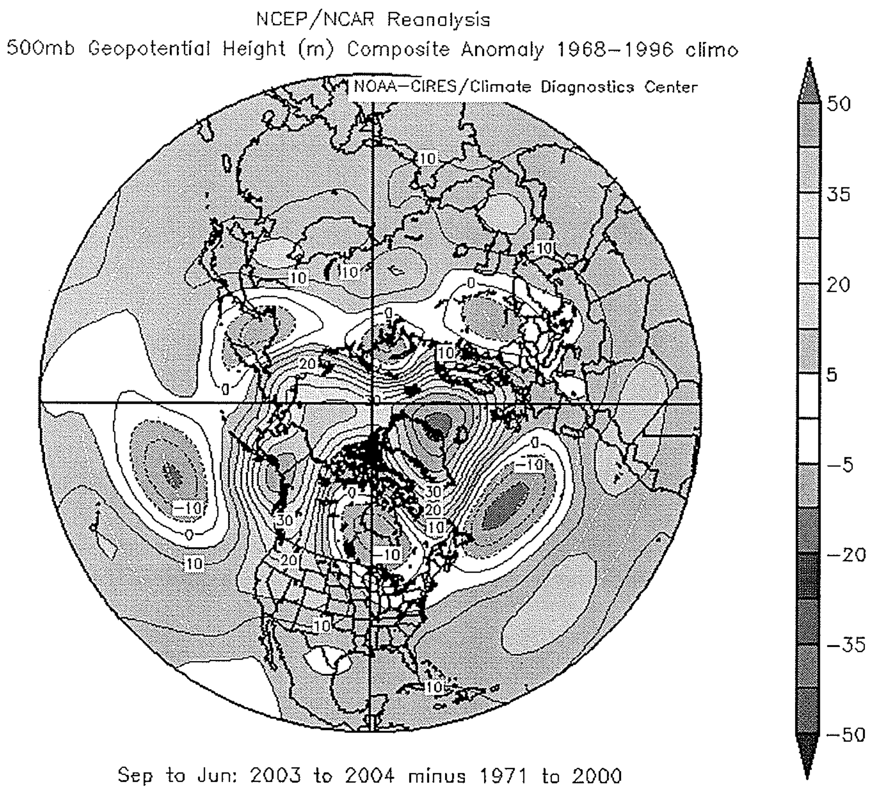


Figure 3.4: Same as Figure 1 but for 500 hPa geopotential height (m).

winter of 2003 (September to January), with October having the largest positive anomaly (Figure 3.6). In the broader picture, the entire Canadian Arctic was very warm between September to January with maximum anomalies near +11°C in October (west of the CASES region) and consistently above +6°C in the Archipelago and +4°C in the Arctic Ocean (e.g. Figure 3.7). Between February and June, air temperature anomalies were either negative (Feb, Mar, and May) or near zero (Apr and Jun) with the largest negative anomalies in Feb and Mar (-5°C). Most of the Archipelago and Alaska had consistently above normal temperatures between February and June.

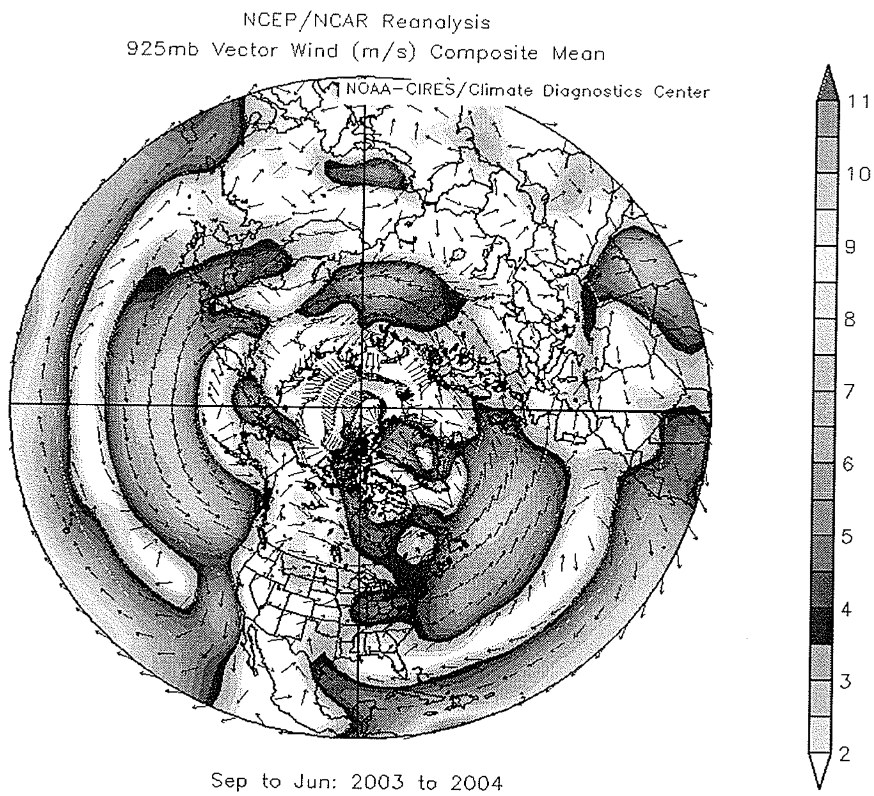


Figure 3.5: 925 hPa wind vectors averaged over the CASES period.

The warm CASES period in the fall and early winter of 2003 was partially attributed to the SLP monthly pattern with flows into the CASES region originating from the Pacific (September and November) and warm terrestrial surface to the south and southeast (October and December). This was associated with slight negative monthly SLP anomalies in the Arctic Ocean (weaker than normal Arctic high) that failed to advect cold air from the north. By late January, the Arctic Ocean high became dominant (positive monthly anomalies) producing a more significant cold northerly flow into CASES that was well-developed by February and continued into May (abnormally cold) and most of June. Lower tropospheric vector winds revealed that southerly winds should

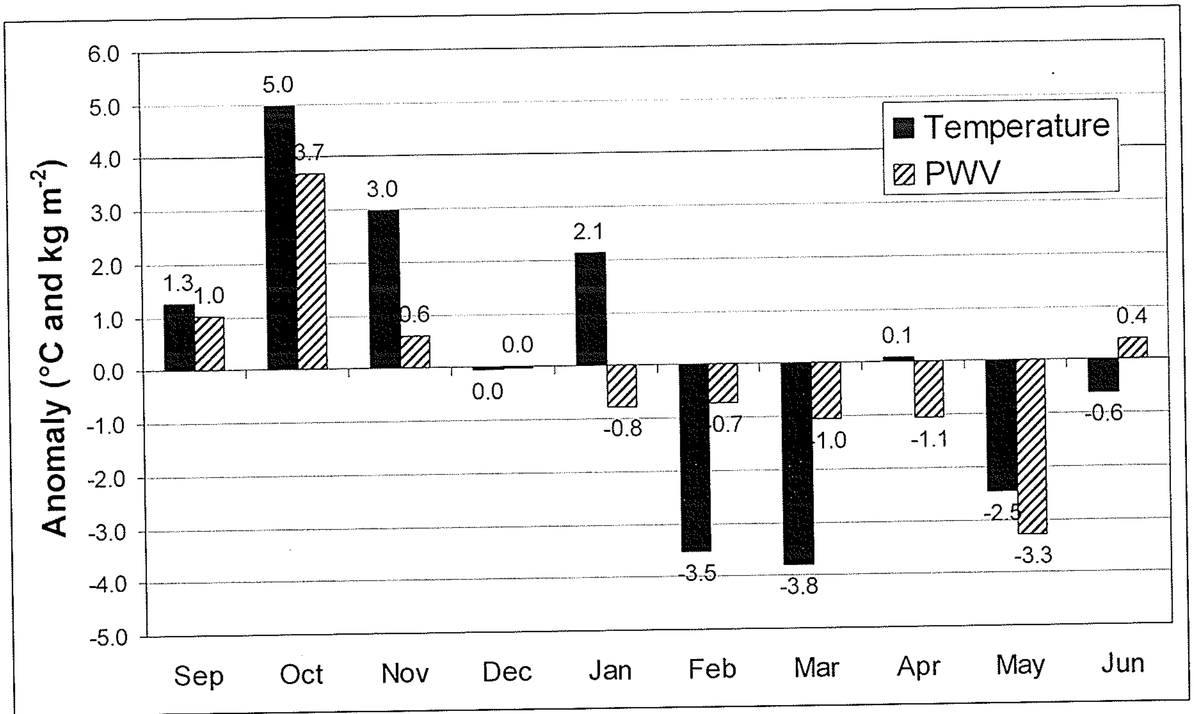


Figure 3.6: Monthly near-surface air temperature (°C) and precipitable water vapor (kg $m^{-2}$) anomalies with respect to the 1971-2000 mean directly over Franklin Bay (over wintering site of the CCGS Amundsen).

have been dominant by April into June, but did not materialize even in June (not shown). Surface wind speeds were not particularly out of the ordinary, being near normal during the fall (SON), slightly below normal (-0.5 m $s^{-1}$) in winter (DJF), above normal (+0.5 m $s^{-1}$) in March and April and below normal (-0.5 m $s^{-1}$) in May and June. This coincides with a higher frequency of blowing snow events (80% of total reported events) occurring during March of 2004.

The only notable anomalies in CASES surface humidity were negative in February (-25%), March (-20%), April (-10%) and May (-12%) associated with the strong Arctic Ocean high. Other months were either weakly positive or near normal.

At 500 hPa, the warm CASES period was associated with a zonal flow from the north

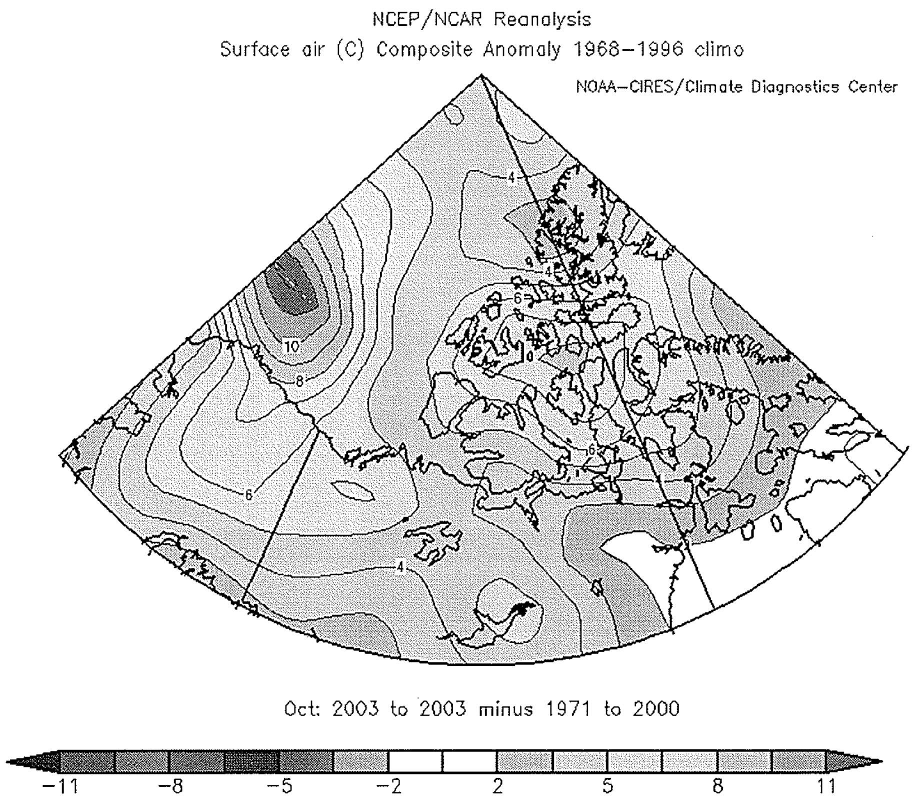


Figure 3.7: Same as Figure 3.2 but for October near-surface air temperature (°C).

Pacific (September and November) or a strong ridge over the west coast and Alaska (October and December) that fed warm Pacific air into the CASES region at mid-levels. By January, the flow began to change with colder than normal air (lower 500 hPa heights) to the west that slowly migrated toward the east from February to June. The deeper heights were centred in the east-central Archipelago that fed colder polar air into the CASES region during the late winter and spring and was supported by a building 500 hPa ridge along the west coast and Alaska between April to June.

The PWV anomalies over the CASES region went from primarily positive in fall and early winter (+0.5 to +3 kg $m^{-2}$) to negative in late winter and spring (-0.5 to

–3 kg $m^{-2}$) closely following the warm and cold periods of CASES (see Figure 3.6).

## 3.3 Synoptic Investigation

The low-pressure disturbance (LPD) tracks traced for each month can be seen in Figure 3.8 to Figure 3.16. Overall, forty-one LPDs were documented, with 56% of those originating from the ARCTIC class, 39% originating from the PACIFIC class, and 5% of the total originated from the IRREGULAR class. The most synoptically active months during the CASES year were November and March with eight and seven notable LPDs, respectively. Monthly synoptic activity was mostly dominated by northerly originating LPDs, with the exception of December, where four LPDs originated from the PACIFIC class out of its total of six for the month. Disturbances noted in the fall/early winter season generally developed and terminated west of the ship location and thus provided the Southern Beaufort Sea with warm and moist air from southern latitudes. This coincides with previous findings in our climatological investigation, where it was found, especially during the months of October and November, that temperature and moisture over the Beaufort Sea were anomalously positive compared to previous years. Conversely, in the late winter/early spring months, very little cyclonic activity was noted, indicating a strong and persistent Arctic High for much of the period, allowing the advection of frigid arctic air into the CASES region for much of this time and causing lower than normal temperatures and moisture content. In addition, cyclonic activity tended to originate north and north east of the ship location along the west coast of the Canadian Archipelago, also contributing to the influx of colder, drier air during the late winter/early spring season. This also coincides with previous findings (see Figure 3.6).

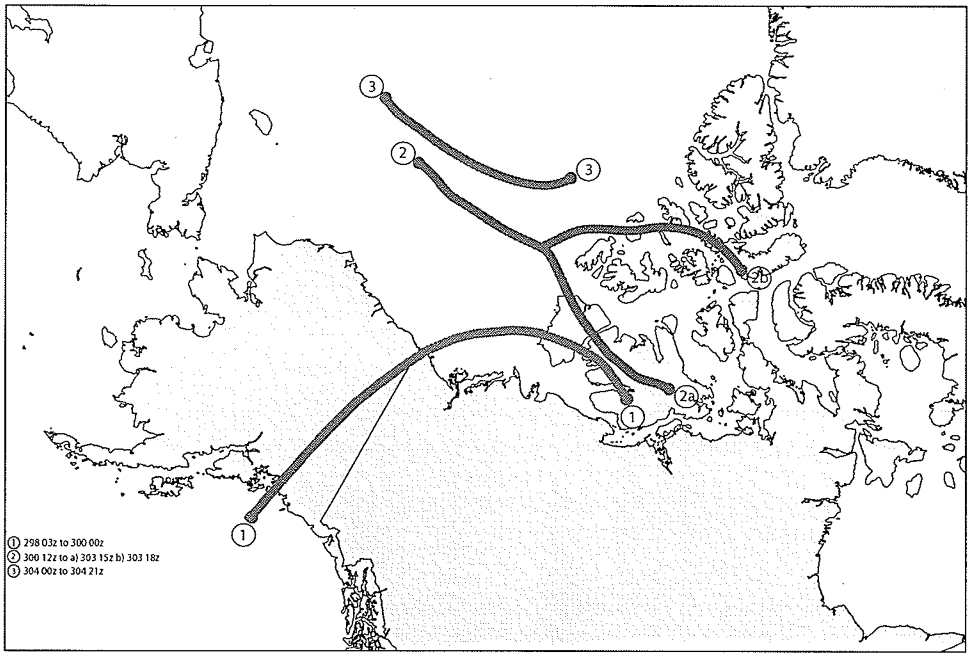


Figure 3.8: Low-pressure disturbance (LPD) tracks for October 2003. Red lines indicate LPDs of "PACIFIC" origin, blue lines of "ARCTIC" origin, and green lines of "IRREGULAR" origin. Tracks are labelled in order of their occurrence chronologically. (1) 298 03Z to 300 00Z. (2) 300 12Z to (a) 303 15Z; (b) 303 18Z. (3) 304 00Z to 304 21Z.

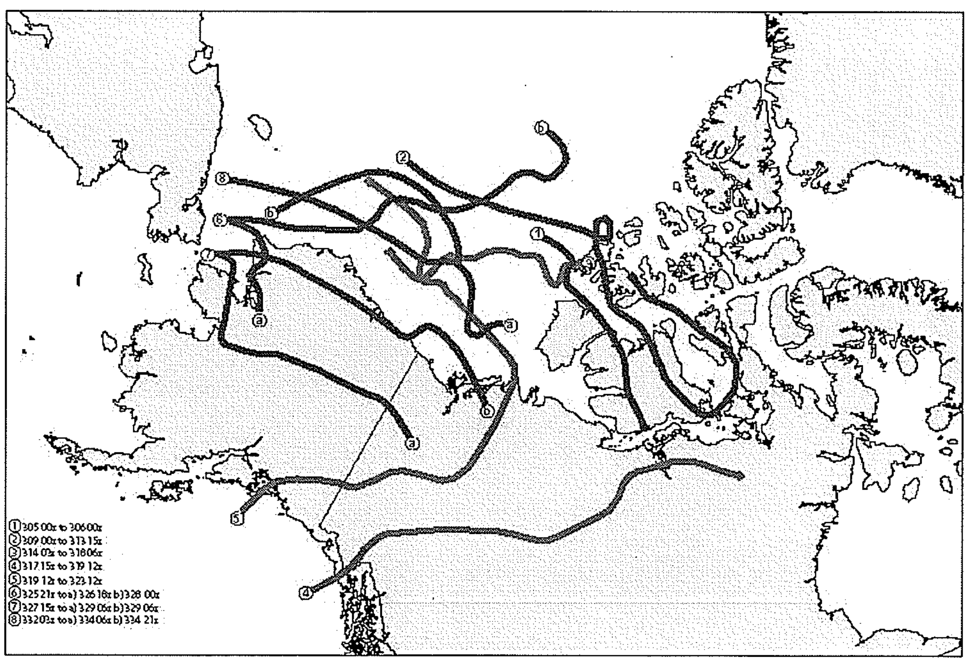


Figure 3.9: Same as Figure 3.8 for November 2003. (1) 305 00Z to 306 00Z. (2) 309 00Z to 313 15Z. (3) 314 03Z to 318 06Z. (4) 317 15Z to 319 12Z. (5) 319 12Z to 323 12Z. (6) 325 21Z to (a) 326 18Z; (b) 326 00Z. (7) 327 15Z to (a) 329 06Z; (b) 329 06Z. (8) 332 03Z to (a)334 06Z; (b) 334 21Z.

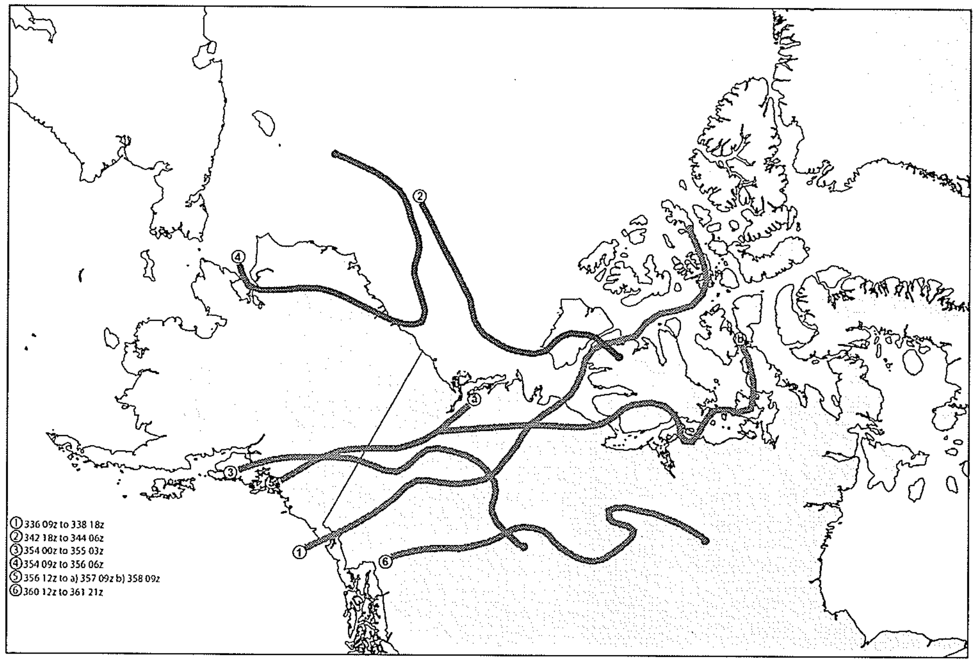


Figure 3.10: Same as Figure 3.8 for December 2003. (1) 336 09Z to 338 18Z. (2) 342 18Z to 334 06Z. (3) 354 00Z to 355 03Z. (4) 354 09Z to 356 06Z. (5) 356 12Z to (a) 357 09Z; (b) 358 09Z. (6) 360 12Z to 361 21Z.

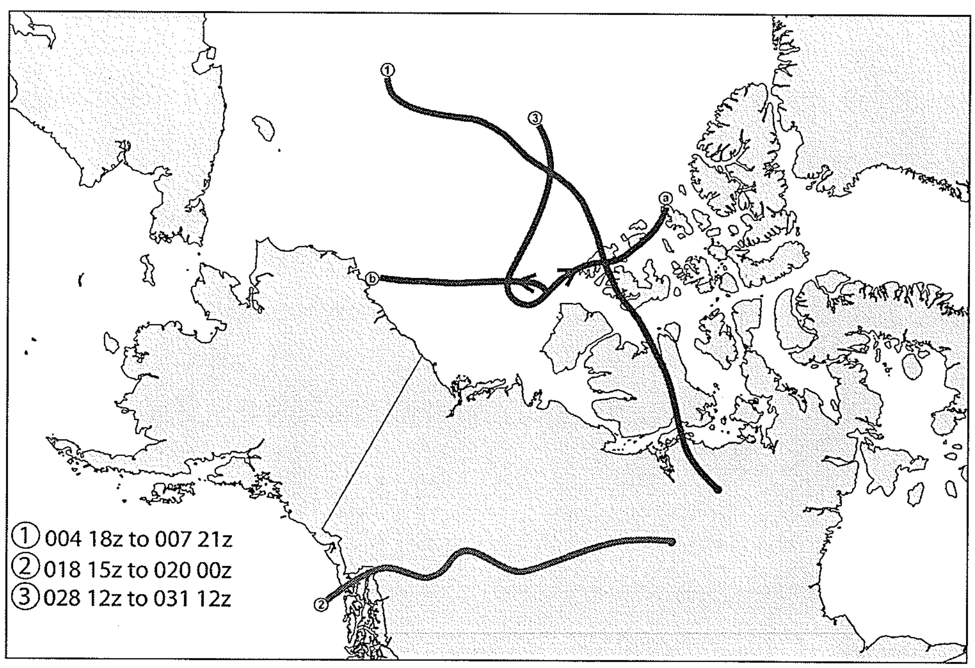


Figure 3.11: Same as Figure 3.8 for January 2004. (1) 004 18Z to 007 21Z. (2) 018 15Z to 020 00Z. (3) 028 12Z to 031 12Z.

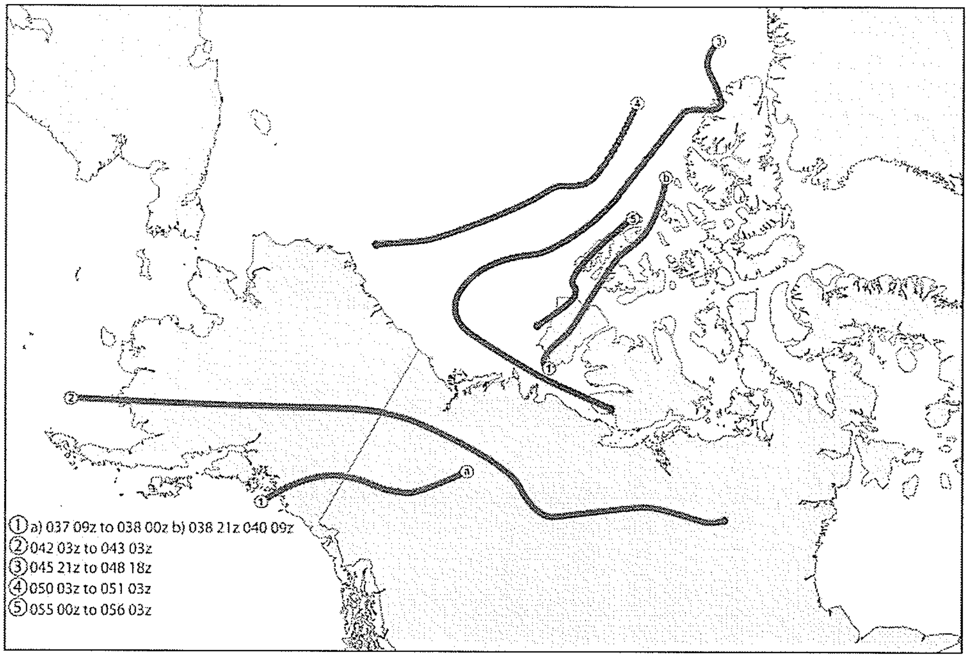


Figure 3.12: Same as Figure 3.8 for February 2004. (1) (a) 037 09Z to 038 00Z; (b) 038 21Z to 040 09Z. (2) 042 03Z to 043 03Z. (3) 045 21Z to 048 18Z. (4) 050 03Z to 051 03Z. (5) 055 00Z to 056 03Z.

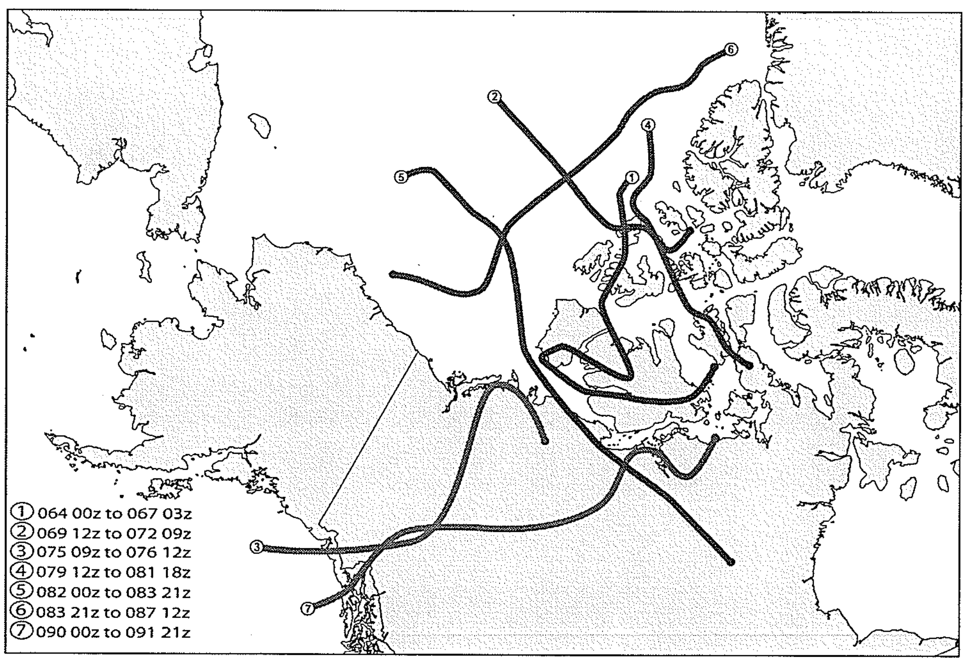


Figure 3.13: Same as Figure 3.8 for March 2004. (1) 064 00Z to 067 03Z. (2) 069 12Z to 072 09Z. (3) 075 09Z to 076 12Z. (4) 070 12Z to 081 18Z. (5) 082 00Z to 083 21Z. (6) 083 21Z to 087 12Z. (7) 090 00Z to 091 21Z.

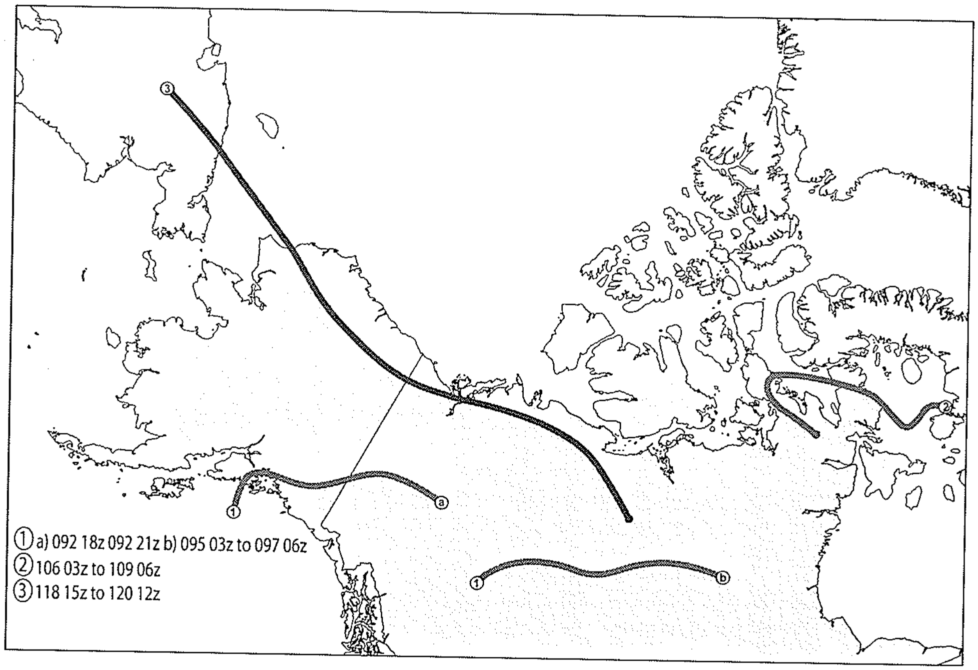


Figure 3.14: Same as Figure 3.8 for April 2004. (1) (a) 092 18z to 092 21z; (b) 095 03Z to 097 06Z. (2) 106 03Z to 109 06Z. (3) 118 15Z to 120 12Z.

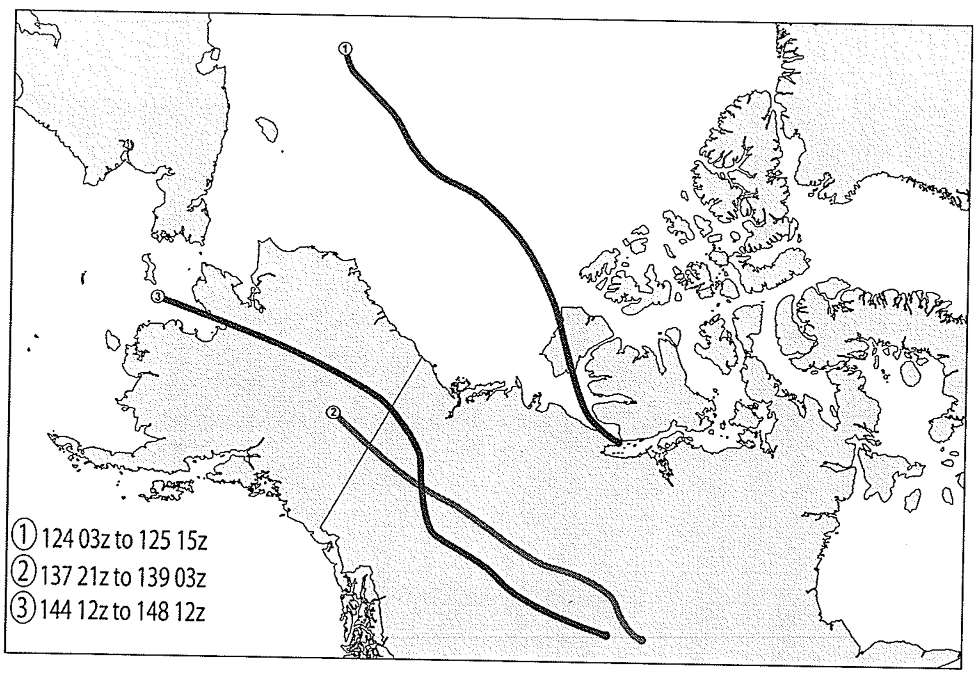


Figure 3.15: Same as Figure 3.8 for May 2004. (1) 124 03Z to 125 15Z. (2) 137 21Z to 139 03Z. (3) 144 12Z to 148 12Z.

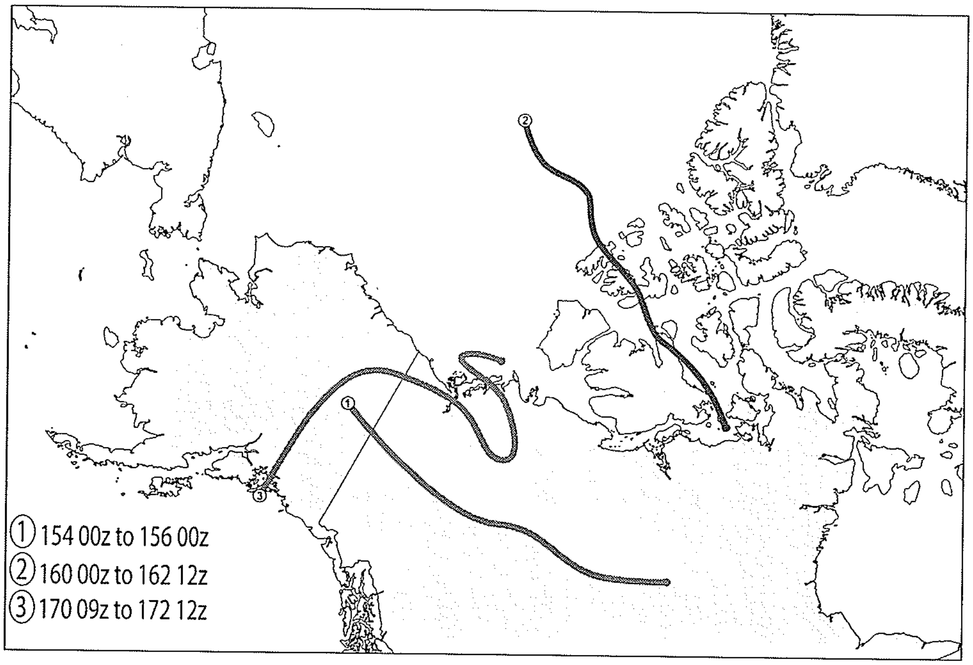


Figure 3.16: Same as Figure 3.8 for June 2004. (1) 154 00Z to 156 00Z. (2) 160 00Z to 162 12Z. (3) 170 09Z to 172 12Z.

Of all the months analysed and LPDs identified, the origin of track (3) from May 2004 was difficult to resolve. A broad area of low pressure existed over the Bering Straight where two centres, one situated to the north and one situated in the Gulf of Alaska, appeared to merge (not shown). Officially it has been classified under the "ARCTIC" category, but could also be considered as a "PACIFIC" originating disturbance.

Serreze et al. (1992) presented a synoptic overview of the Arctic Basin for 1952 to 1989 in which they demonstrate large inter-annual variability of winter cyclonic activity. They found, that though the majority of cyclonic activity in winter occurs mostly in the eastern Arctic, winter cyclonic activity was increasing overall during the period of study. Zhang et al. (2004) presented a more recent cyclone climatology for the Arctic Ocean between 1948 and 2002 using NCEP Re-analysis model data. They confirm the findings of Serreze et al. (1992) by concluding that substantial inter-annual variability in the Arctic is superimposed on a long-term positive trend of cyclonic activity. They divided their study into winter and summer categories, defining the period of October to March as their 'winter' period. They included only closed low centres in their frequency counts. To compare their climatology to what was observed during the CASES project, only closed low centres were included in calculating the total number of LPDs for the CASES region between October and March. The total number of closed lows originating locally in the Arctic Ocean and Eurasia was 19 (63.3%) while 11(36.7%) originated from the Pacific Ocean during CASES. Zhang et al (2004) displayed an average frequency of 92% when combining Eurasian and locally generated Arctic cyclones compared to 8.0% of Pacific origin from 1948 to 2002. An increase in Pacific originating cyclones implies a weaker than normal Arctic High for the CASES winter period. The large deviation from the 55-year mean suggests that significant inter-annual variability is still occurring during the winter as the previous studies suggest; though, increased frequency of disturbances of Pacific origin could be an indication of climate changes in this region. McCabe et. al. (2001) found that for the period of 1959 to 1997, the frequency of winter cyclones decreased for the mid-latitudes, which was associated with an increase in frequency of cyclonic activity in higher latitudes for the Northern Hemisphere. It is also relevant to note that the Arctic Oscillation (AO) Index, the climate indicator quantifying the large-scale pressure gradient between low and high latitudes shifted to a less negative state from 2003 to 2004 (National Oceanic and Atmospheric Administration: Climate Prediction Centre). A positive index corresponds to a lower atmospheric pressure at the surface and is generally associated with a northward displacement of mid-latitude cyclone tracks. While the AO remained negative for 2004, the slight increase could explain the higher frequency of Pacific originating storms in early 2004 and overall compared to the 55-year mean. A more detailed investigation into the relationships between the observed temperatures, sea ice concentrations and synoptic activity may serve useful in making conclusions about possible feedback mechanisms that are contributing to the weaker than normal Arctic High and the increase of cyclonic activity from Pacific origins.

## 3.4 Local Investigation

This section describes the local meteorology for the CASES project as recorded by the observers on the CCGS *Amundsen* and its suite of meteorological sensors.

Figure 3.17 illustrates the temperature record obtained during the observational period. When CASES records began (day 299 of 2003), temperatures had already fallen below the freezing mark, and dropped dramatically after the first 12 days where temperatures initially dipped below -20°C. This was in association with a significant pressure drop and tied with the passage of a low pressure disturbance of ARCTIC origin. By day 312, the centre of the low was situated over Victoria Island, north and east of the ship location, subjecting the ship to northwesterly winds. Frequent and substantial fluctuations (±10°C per 3-5 days) during the month of November relates well to the increased cyclonic activity in the region during this time period. During the start (day 005) and end of January 2004 (day 029) temperatures rose to -6.4°C and -16°C at the ship, respectively. At Cape Parry, 62 km to the northeast, temperatures were recorded as -6.6°C and -18.8°C, which came near 5°C shy of the daily maximum temperature record at Cape Parry for both days. Normal temperatures for Cape Parry are generally near -23°C to -25°C for this time of year (Environment Canada Climate Data Centre). The coldest day of the period occurred in early March of 2004 (day 067) with a temperature of -38.3°C. Cape Parry

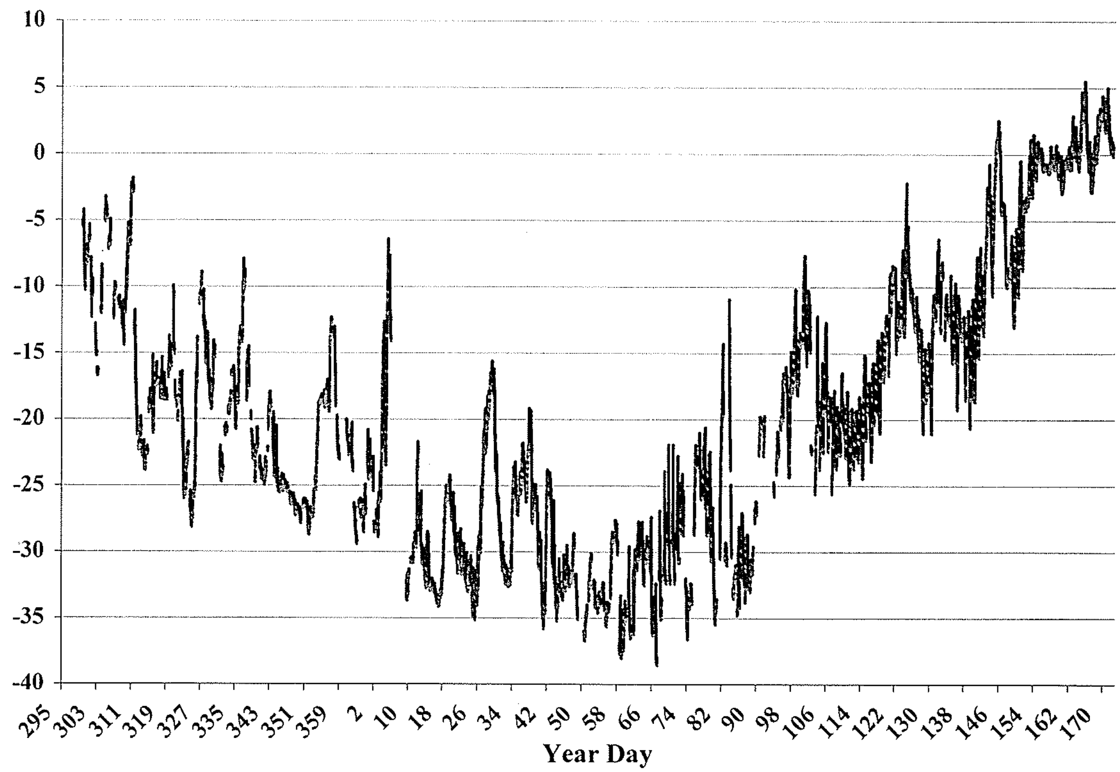


Figure 3.17: Hourly temperature record from the CCGS *Amundsen*

recorded a maximum temperature of -36.6°C on that day, over 10°C below the normal daily maximum value for Cape Parry, and near 5°C below the average daily minimum value for that day (March 7). During the remainder of the month of March temperatures varied between -20°C and -30°C, which relates to the return of frequent cyclonic activity in the CASES region. By day 090 (March 30, 2004) temperatures remained above -30°C for the rest of the season, with radical influxes of warm air peaking at day 101, 121, and 145. PACIFIC originating systems are linked to the peaks at days 101 and 145, whereas an ARCTIC originating system advancing from the north-west brought warm air advection over the ship ahead of its passage after day 121. The highest temperature of the period was recorded near the end of the study, with day 165 having a maximum temperature of 5.5°C.

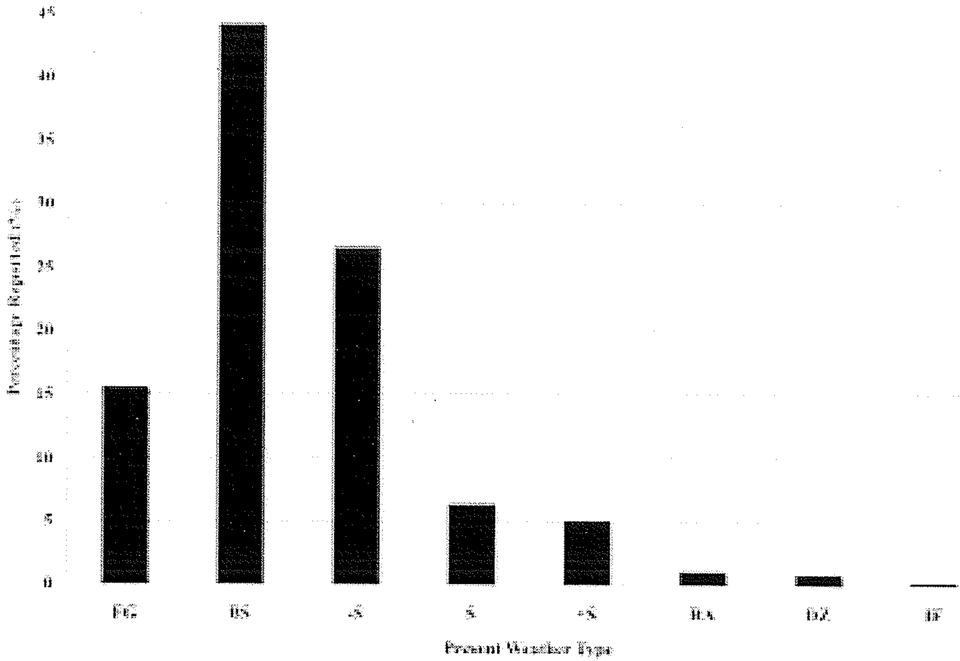


Figure 3.18: Percentage of reported weather from the CCGS *Amundsen*.

The most frequently reported weather type at the ship was blowing snow, as illustrated in Figure 3.18, followed by light snow and fog. Blowing snow events dominated from January to April by accounting for 50 to 80% of the recorded weather types. Fog was the most reported weather type during the month of May and light snow was also frequently reported during the fall and spring months. Adverse weather events occurred in all months of the study, but mainly during the months of February, March and June, as shown in Figure 3.19. 'Adverse weather' was defined as any weather event causing visibilities to drop below 5 NM. Nautical miles were used as opposed to the standard statute miles, as the videograph was calibrated in nautical miles and was used as the observer's reference; 5 NM ~ 5.75 SM, which approximately coincides with thresholds for marginal weather in industries such as aviation. Not only did blowing snow account for the majority of adverse conditions during February and March, but also for

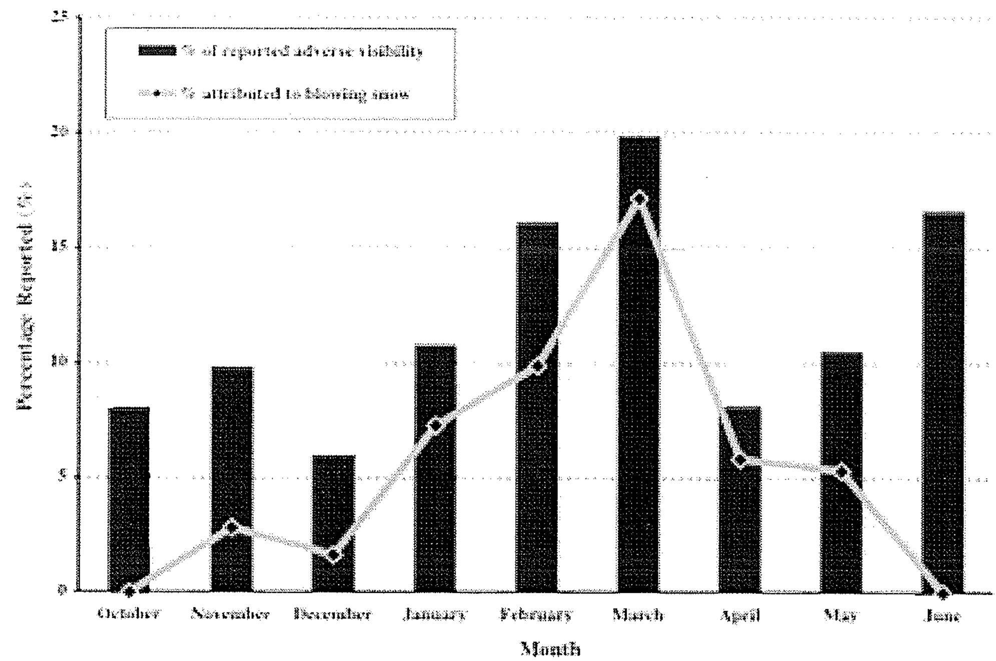


Figure 3.19: Percentage of adverse visibility versus the percentage of adverse visibility attributed to blowing snow events. Adverse visibility is defined as a visibility less than or equal to 5 NM.

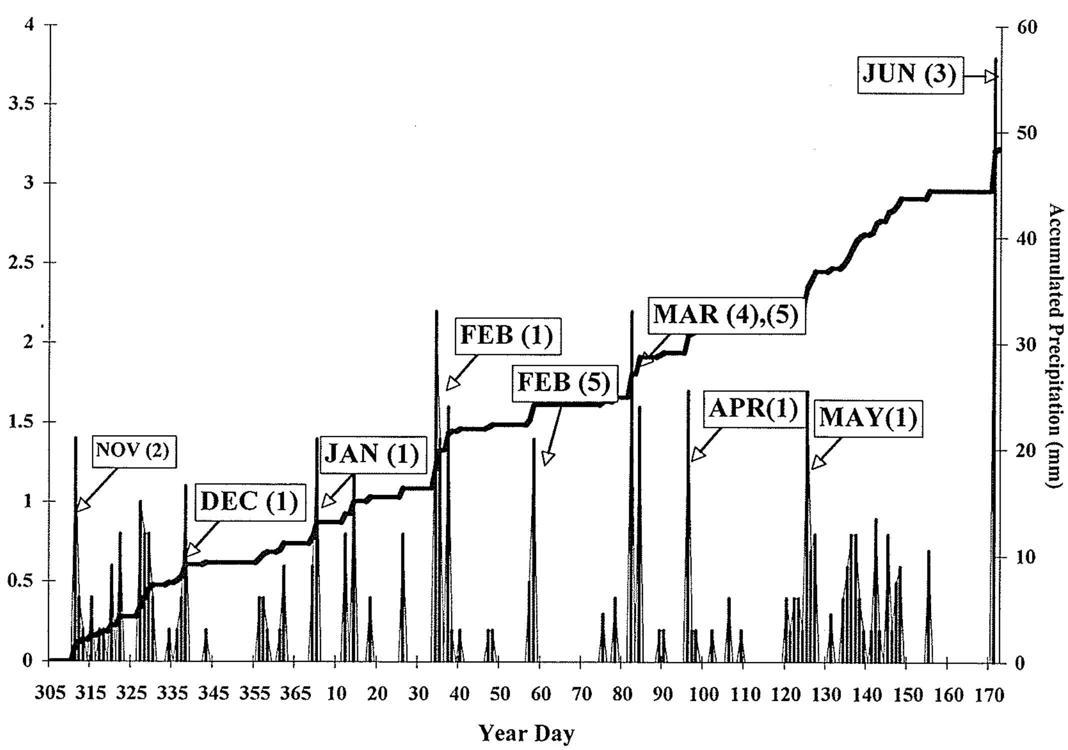


Figure 3.20: Daily reported and accumulated precipitation recorded aboard the CCGS *Amundsen*. LPDs responsible for particular events are included, where (#) corresponds to the monthly LPD label, as outlined in Section 3.3.

January through to May. Dense fog was the main cause of poor visibility for June, when the ship broke out of its ice location and began to sail into open water. The combination of newly available moisture from open water leads and still relatively cool air gave way to frequent periods of mist and dense fog.

Precipitation data (raw) recorded during the observational period is outlined in Figure 3.20. Significant precipitation events have been correlated to specific LPDs as outlined in Section 3.3. The total accumulated precipitation amounted to 48.4 mm, which if compared to the seasonal average precipitation to surrounding stations, appears to be below average for the region for the months of September to June (Cape Parry on average receives 87.7 mm of precipitation (liquid and solid) in this time frame. A Nipher snow gauge was used in collected snow accumulation and a rain gauge for liquid precipitation, from atop the ship with the rest of the instrumentation. Turbulent effects may have played a role in reducing the catch, as well as the inherent catch errors that the Nipher snow gauge exhibits (Sugiura et. al., 2003).

The area of study is also prone to extended periods of low-level stratus (Crane and Barry, 1984), which remained true during the observation period, with stratus clouds being the most reported cloud type throughout the study (Figure 3.21). After stratus, cirrostratus and altostratus follow in reported frequency. Breaking the cloud observations into the standard sky conditions (sky clear (0 octas), few (1-2 octas), scattered (2-3 octas), broken (5-7 octas) and overcast (8 octas)), overcast conditions was the most reported sky type, being reported nearly 30% of the time overall. Few clouds followed, being reported 22% of the time. A monthly look at sky conditions (Figure 3.23) reveals that October was overcast almost 80% of the time, but this peak is amplified due to few

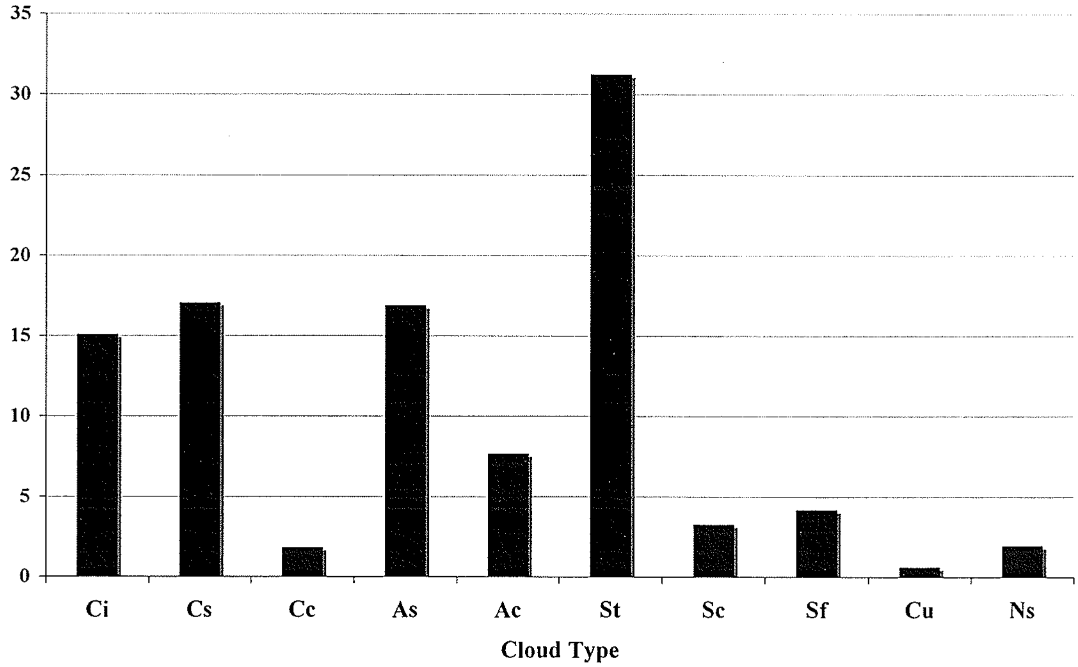


Figure 3.21: Percentage of reported cloud type by number of total hours reported from the CCGS *Amundsen*.

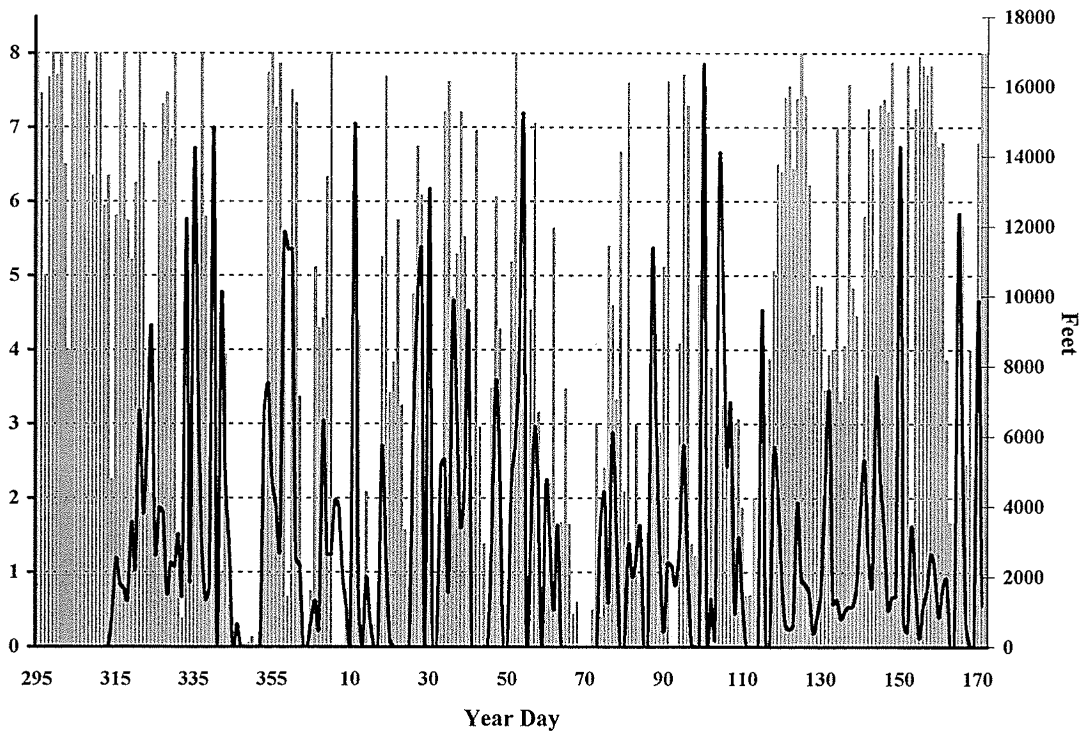


Figure 3.22: Cloud amount (grey bars) versus cloud base height (black solid line) as recorded from the CCGS *Amundsen*.

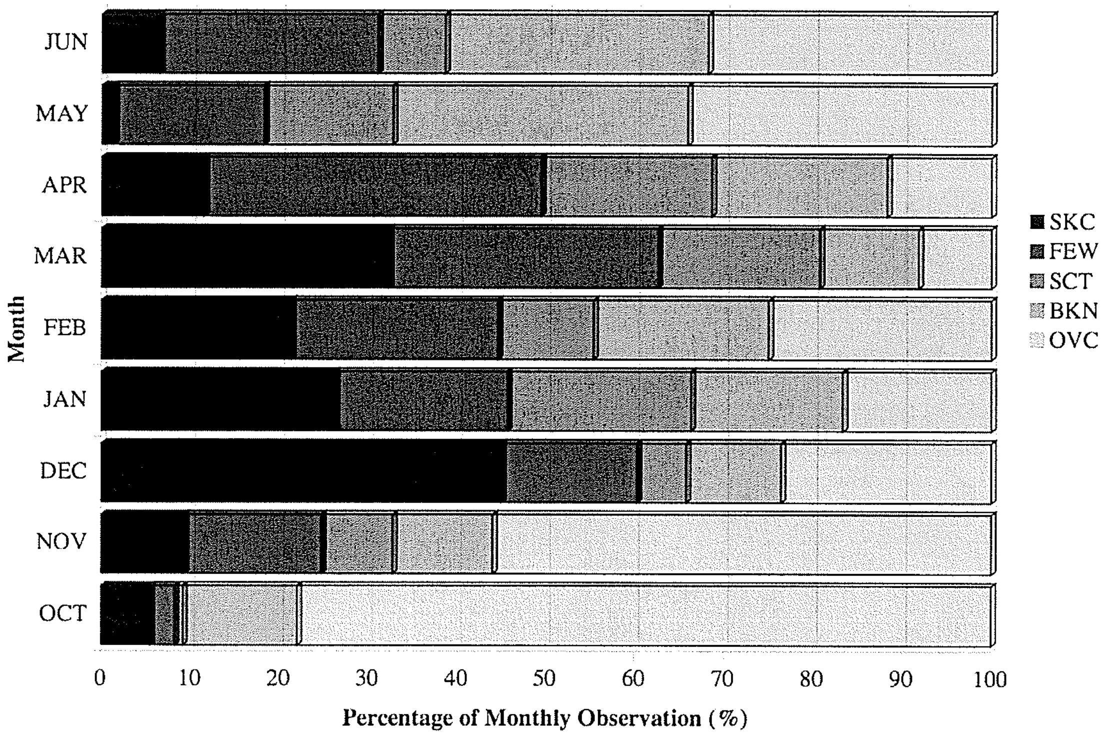


Figure 3.23: Monthly percentage of reported sky condition based on reported cloud amounts as recorded from the CCGS *Amundsen*. Categories are SKC (Clear Sky, 0 octas), FEW (Few clouds, 1-2 octas), SCT (Scattered clouds, 3-4 octas), BKN (broken ceiling, 5-7 octas), and OVC (Overcast, or full ceiling, 8 octas).

records for the month of October (measurements began October $22^{nd}$) compared to all other months. Overall, November, the most synoptically active month, was the cloudiest, being overcast 55% of the time. The second most synoptically active month, March, appears to have had extended periods of sky coverage 0 to 2 octas. A general pattern existed where less cloudy skies are present through the winter months, where as the summer-winter and winter-spring transitions contain the cloudiest days of the period.

Winds at the ship location predominantly blew from either easterly or westerly directions throughout the course of the study (See Figure 3.24). A monthly breakdown of wind direction frequency (Figure 3.25) reveals that winds were predominantly easterly in the fall/early winter months, becoming increasingly westerly through the winter. The frequency of easterly wind directions again increases with the return of spring (April to June). Upon further inspection of the distribution of wind direction, a minimum from the west-southwesterly direction (240° to 260°) is apparent, which is mostly likely attributed to the orientation of the ship and the location of the anemometer (the lack of proper exposure to the direct wind flow). A wind blowing from the southwest would most likely create a turbulent flow around the wheelhouse of the ship, significantly reducing wind magnitude at the anemometer.

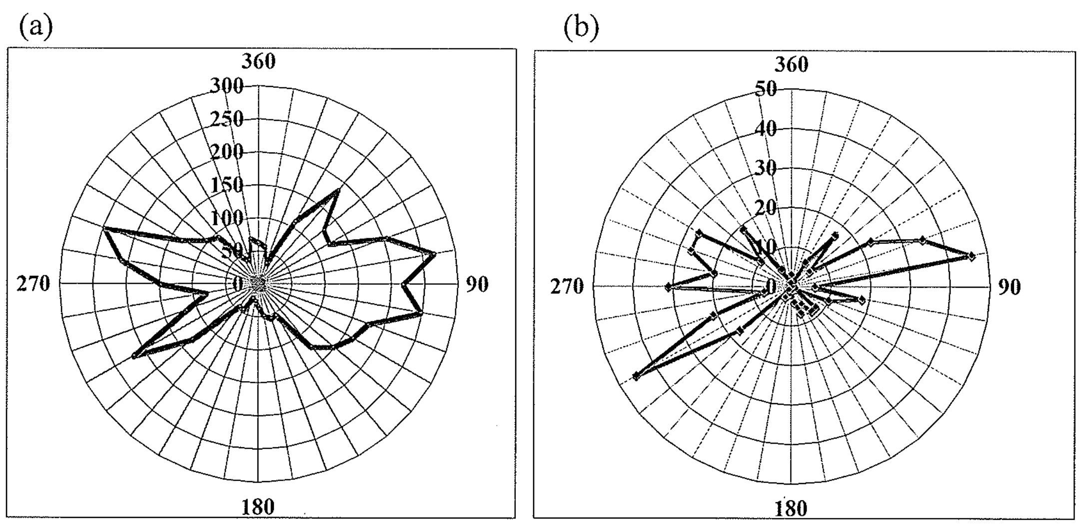


Figure 3.24: Directional frequency of winds reported at the CCGS *Amundsen* for (a) all speeds, and (b) speeds over 20 kts (10 m $s^{-1}$). Each concentric circle represents an additional (a) 50 and (b) 10 occurrences of reported wind direction, and each radial indicates the direction the winds were recorded to be coming from.

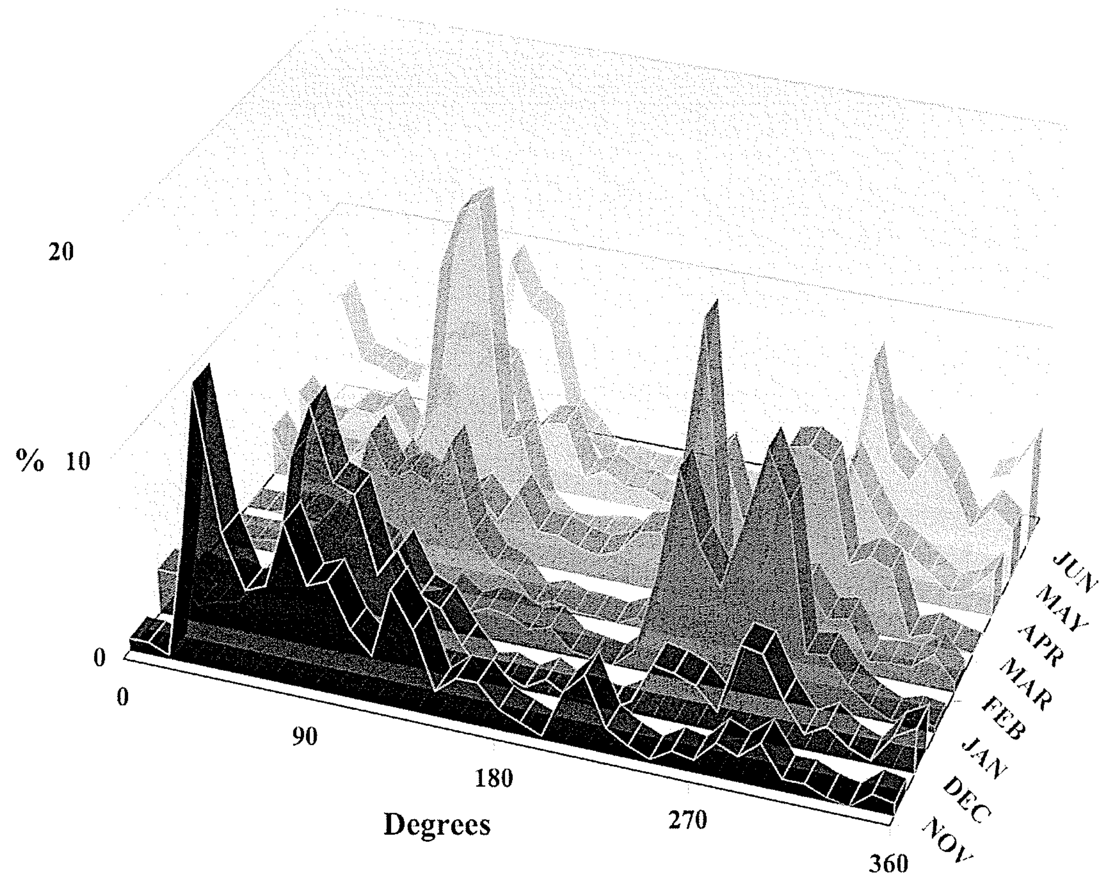


Figure 3.25: Monthly directional frequency of winds reported at the CCGS *Amundsen* for all speeds. The x-axis represents the direction (in degrees) from which winds were reported to be from, and the z-axis represents the percentage of the total number of wind measurements for the particular month, indicated on the y-axis.

# 4 Data Comparison

Many studies that focus on uncovering long-term atmospheric trends use available modelled data, especially for studies in the Arctic where in-situ data is sparse and often unreliable (Zhang et al. 2004; Barber and Hanesiak 2004; Hudak and Young 2002; Serreze et al. 1993). The NCEP-NCAR suite of reanalysis products is often commonly used to represent in-situ data in areas of sparse station coverage such as on ice areas. Given the nature of the terrain in Arctic regions and ice field topography, meteorological data at low resolutions reduce the accuracy of characterizing the local scale meteorological fields such as temperature, wind speed, wind direction and moisture. These influences also come into play when using surrounding land-based station data in place of on-ice data when there is none available. Presented first is a comparison of data collected at the ship with data collected at Cape Perry and Paulatuk, the closest MSC stations geographically. Secondly, the accuracy of common NCEP-NCAR products is investigated in reference to the data collected at the ship and the aforementioned MSC stations.

## 4.1 Methods

Daily average time series data were calculated from the data collected from the CCGS *Amundsen*. Data collected from MSC station Cape Parry and Paulatuk were also reduced to daily averages. Pressure, temperature, relative humidity (only available at Paulauk and the ship), visibility, and zonal and meridional winds were available for comparison. The daily average bias was calculated by subtracting the ship data set from the station data set for each day, as outlined below:

$$BIAS_{DAILY} = X_{STN} - X_{SHIP} \quad \textbf{(4.1);}$$

$$BIAS_{MONTHLY} = \frac{1}{n}\sum_{i=1}^{n}(BIAS_{DAILY})_i \quad \textbf{(4.2);}$$

where $X_{StTN}$ and $X_{SHIP}$ are the daily averages of the station (Cape Parry or Paulatuk) data and ship data, respectively. A monthly average bias was created by averaging the daily biases over the course of each month, as in equation (4.2), during the observational period to reveal a seasonal summary of the differences of meteorological fields between the stations, where $n$ is the number of days per month with available data. The results of this study are outlined in Section 4.2.

Data from NCEP I, NCEP II, NARR and GEM were extracted at grid points surrounding each of the stations lat/long positions with respect to each of the model grids. Table 4.1, 4.2 and 4.3 outline the grid points for each model and the respective distances to the corresponding ground station. In the case of GEM, zonal and meridional wind components are provided as grid referenced as opposed to true. A rotation scheme for the wind data was necessary before a comparison could be fairly done between the modelled GEM winds and the winds reported at the stations. The zonal ($U$) and meridional ($V$) wind components were rotated by:

$$U_{TRUE} = U_{GRID}\cos\theta + V_{GRID}\sin\theta \quad \textbf{(4.3);}$$

$$V_{TRUE} = V_{GRID}\cos\theta - U_{GRID}\sin\theta \quad \textbf{(4.4);}$$

where

ship's longitude ($15.3^0$).

The PWV parameter was not a set field in the GEM output; PWV for GEM was calculated by integrating specific humidity ($\boldsymbol{Q}$) over the entire column:

$$PWV = \frac{1}{g}\sum_{k=1}^{28} Q_k \Delta p \quad \textbf{(4.5);}$$

where $\boldsymbol{Q_k}$ is the modeled specific humidity at the $\boldsymbol{k_{th}}$ level,      is the change in pressure between levels, and $\boldsymbol{g}$ is the acceleration due to gravity.

In order to create datasets that were representative of the same latitude and longitude of each of the three stations, an inverse distance weighting (IDW) interpolation technique was carried out as follows:

$$Z_{est} = \frac{\sum_{i=1}^{n} \frac{Z_i}{h_i^2}}{\sum_{i=1}^{n} \frac{1}{h_i^2}} \quad \textbf{(4.6);}$$

where $\boldsymbol{Z_{est}}$ is the estimated value for the required location, $\boldsymbol{Z_i}$ is the modelled value at grid point $\boldsymbol{i}$, and $\boldsymbol{h_i}$ is the distance between the grid point location and the point of interest (the location of the ship, Cape Parry, or Paulatuk). The closest four surrounding grid points from each model were used in the interpolation ($\boldsymbol{n}$=4). Deviations were calculated by subtracting the station's daily averaged value from the modeled value, and monthly average biases were calculated as per equation (4.1) and (4.2). Daily averages for GEM were calculated solely on the 00z and 12z output time steps. Daily averages of NCEP I, NCEP II and NARR were available pre-calculated based on a 4-hourly (00z, 06z, 12z, and 18z) and 8-hourly (every three hours UTC, NARR only) availability. In order to retain consistency, daily averages of station data were calculated based on the methods described per each model for the comparison study (i.e., for NARR comparison, station data was averaged following the same 8-hourly averaging convention, etc).

Table 4.1: Grid point references and distances used in the interpolation process to create corresponding datasets for Cape Parry, Paulatuk and the CCGS *Amundsen* from NCEP I and NCEP II model data. (a) Grid references from the T62 Gaussian grid; (b) Grid references from the 2.5°x 2.5° grid.

(a)

| **NCEP I and NCEP II** **Gaussian Grid: T62** Station | Grid Point | Lat | Long | Distance from Station (m) |
|---|---|---|---|---|
| **SHIP** | STN | 70.05 | -126.3 | 0 |
| NCEP | (10,125) | 69.521697 | -125.625 | 64432.586 |
| NCEP | (10,124) | 69.521697 | -127.5 | 74941.788 |
| NCEP | (9,125) | 71.5871489 | -125.625 | 173278.662 |
| NCEP | (9,124) | 71.5871489 | -127.5 | 177054.059 |
| **CAPE PARRY** | STN | 70.16667 | -124.716667 | 0 |
| NCEP | (10,126) | 69.521697 | -123.75 | 80994.371 |
| NCEP | (10,125) | 69.521697 | -125.625 | 79989.07 |
| NCEP | (9,126) | 71.5871489 | -123.75 | 162378.013 |
| NCEP | (9,125) | 71.5871489 | -125.625 | 161927.401 |
| **PAULATUK** | STN | 69.35 | -124.06667 | 0 |
| NCEP | (11,126) | 67.81940426 | -123.75 | 171214.831 |
| NCEP | (11,125) | 67.81940426 | -125.625 | 182148.88 |
| NCEP | (10,126) | 69.521697 | -123.75 | 22827.291 |
| NCEP | (10,125) | 69.521697 | -125.625 | 64041.973 |

(b)

| **NCEP I and NCEP II** **2.5° x 2.5°** Station | Grid Point | Lat | Long | Distance from Station (m) |
|---|---|---|---|---|
| **SHIP** | STN | 70.05 | -126.3 | 0 |
| NCEP | (7,93) | 72.5 | -127.50 | 276714.433 |
| NCEP | (7,94) | 72.5 | -125.00 | 277291.777 |
| NCEP | (8,93) | 70 | -127.50 | 46106.852 |
| NCEP | (8,94) | 70 | -125.00 | 49894.847 |
| | | | | |
| **CAPE PARRY** | STN | 70.16667 | -124.716667 | 0 |
| NCEP | (7,94) | 72.5 | -125.00 | 260545.415 |
| NCEP | (7,95) | 72.5 | -122.5 | 272089.337 |
| NCEP | (8,94) | 70 | -125.00 | 21490.876 |
| NCEP | (8,95) | 70 | -122.5 | 86329.567 |
| | | | | |
| **PAULATUK** | STN | 69.35 | -124.06667 | 0 |
| NCEP | (8,94) | 70 | -125.00 | 81042.063 |
| NCEP | (8,95) | 70 | -122.5 | 94595.486 |
| NCEP | (9,94) | 67.5 | -125.00 | 209872.607 |
| NCEP | (9,95) | 67.5 | -122.5 | 216125.347 |

Table 4.2: Grid point references and distances used in the interpolation process create corresponding datasets for Cape Parry, Paulatuk and the CCGS *Amundsen* from NARR model data.

| NARR Grid (349x277)<br><br>Station | Grid Point | Lat | Long | Distance from Station (m) |
|---|---|---|---|---|
| **SHIP** | STN | 70.05 | -126.3 | 0 |
| NARR | (150, 217) | 70.1352 | -126.7269 | 18808.041 |
| NARR | (151, 217) | 70.2043 | -125.9568 | 21586.989 |
| NARR | (150, 216) | 69.8738 | -126.5216 | 21407.272 |
| NARR | (151, 216) | 69.9424 | -125.7588 | 23903.012 |
| | | | | |
| **CAPE PARRY** | STN | 70.16667 | -124.716667 | 0 |
| NARR | (152, 217) | 70.2707 | -125.1826 | 21087.227 |
| NARR | (153, 217) | 70.3343 | -124.4044 | 22103.377 |
| NARR | (152, 216) | 70.0082 | -124.9921 | 20548.634 |
| NARR | (153, 216) | 70.0713 | -124.2214 | 21605.763 |
| | | | | |
| **PAULATUK** | STN | 69.35 | -124.06667 | 0 |
| NARR | (152, 214) | 69.481 | -124.6225 | 26260.325 |
| NARR | (153, 214) | 69.5432 | -123.8666 | 22934.762 |
| NARR | (152, 213) | 69.2163 | -124.4433 | 21064.504 |
| NARR | (153, 213) | 69.278 | -123.6945 | 16731.651 |

Table 4.3: Grid point references and distances used in the interpolation process create corresponding datasets for Cape Parry, Paulatuk and the CCGS *Amundsen* from GEM model data. (a) Prior to the June 16, 2004 resolution change (24 km). (b) Post June 16, 2004 resolution change (15 km).

(a)

| **GEM Grid** <br> **24 km** | Grid Point | Lat | Long | Distance From Station (m) |
|---|---|---|---|---|
| **SHIP** | STN | 70.05 | -126.3 | 0 |
| | (86,165) | 70.057 | -126.313 | 922.4 |
| | (85,165) | 69.996 | -126.945 | 25255.5 |
| | (85,164) | 69.78 | -126.767 | 34951.6 |
| | (86,164) | 69.84 | -126.741 | 24151.7 |
| **CAPE PARRY** | STN | 70.16667 | -124.716667 | 0 |
| | (88,165) | 70.17 | -125.036 | 12062.2 |
| | (89,165) | 70.223 | -124.392 | 13701.6 |
| | (88,164) | 69.952 | -124.878 | 24787.5 |
| | (89,164) | 70.005 | -124.241 | 25564.5 |
| **PAULTUK** | STN | 69.35 | -124.06667 | 0 |
| | (88,161) | 69.299 | -124.422 | 17505.7 |
| | (89,161) | 69.35 | -123.804 | 7220.7 |
| | (88,160) | 69.081 | -124.276 | 31858.1 |
| | (89,160) | 69.132 | -123.665 | 27645.8 |

(b)

| GEM Grid 15 km | Grid Point | Lat | Long | Distance From Station (m) |
|---|---|---|---|---|
| SHIP | STN | 70.05 | -126.3 | 0 |
| | (138,265) | 70.1032 | -126.4359 | 7851.5 |
| | (138,264) | 69.968 | -126.3269 | 9185.2 |
| | (139,264) | 70.0046 | -125.9314 | 14898.5 |
| | (139,265) | 70.1401 | -126.0378 | 14118.8 |
| CAPE PARRY | STN | 70.16667 | -124.716667 | 0 |
| | (143,265) | 70.2781 | -124.431 | 16328.2 |
| | (142,265) | 70.245 | -124.8359 | 6606.2 |
| | (143,264) | 70.1416 | -124.3351 | 14710.8 |
| | (142,264) | 70.1088 | -124.7363 | 9683.6 |
| PAULATUK | STN | 69.35 | -124.06667 | 0 |
| | (142,258) | 69.2913 | -124.1726 | 9400.9 |
| | (143,258) | 69.3227 | -123.7867 | 8937.6 |
| | (142,259) | 69.4275 | -124.2633 | 13429.1 |
| | (143,259) | 69.4591 | -123.875 | 16326.6 |

## 4.2 Station Comparison

### 4.2.1 Cape Parry vs. CCGS Amundsen

Cape Parry, the closest permanent observation station to the ship's overwintering location, is situated approximately 62 km to the east-northeast atop a rocky escarpment 86.6 m above the Arctic Ocean. The monthly anomalies are illustrated in Figure 4.1. The station pressure recorded at Cape Parry was consistently 1.0 mb to 1.3 mb below the ship's recorded monthly average pressure, which can be attributed to the difference in elevation (the hypsometric equation using an approximate yearly average temperature for Cape Parry at -17.73 °C, and using the standard surface pressure of 101.325 mb as the base reference yields a layer height of about 74 m for 1.0 mb and 94 m for 1.3 mb change). Making note of the lack of fluctuation in the deviations of monthly pressure

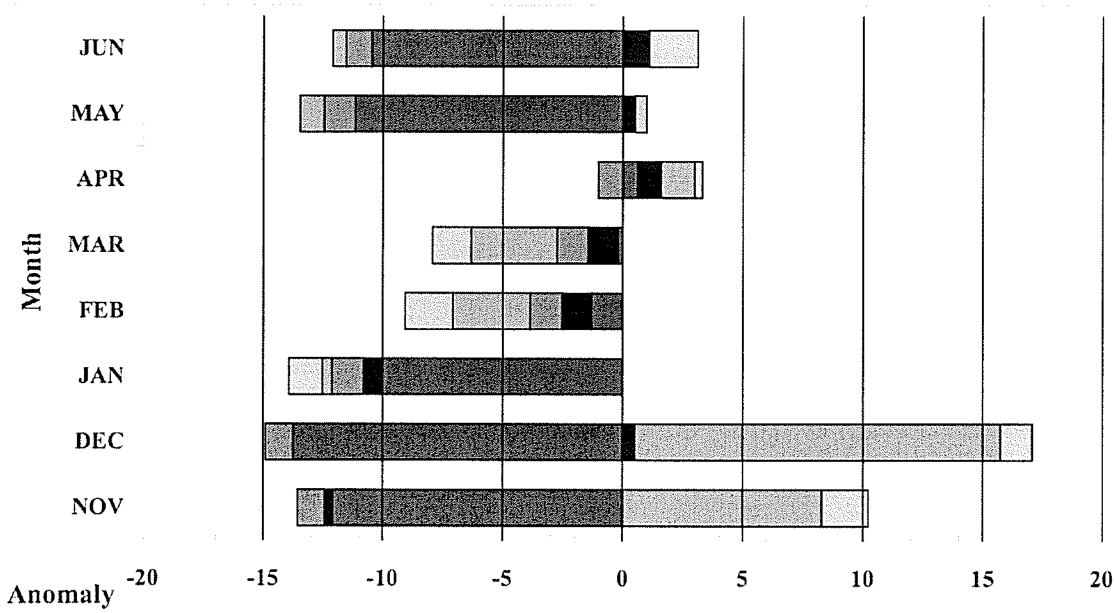


| | NOV | DEC | JAN | FEB | MAR | APR | MAY | JUN |
|---|---|---|---|---|---|---|---|---|
| V (m/s) | 1.92871333 | 1.325115 | -1.3974393 | -1.9830276 | -1.5929452 | 0.31931667 | 0.47505484 | 2.027125 |
| U (m/s) | 8.29791 | 15.2295217 | -0.3982036 | -3.2188724 | -3.5935581 | 1.40221667 | -1.0066032 | -0.5655055 |
| P (mb) | -1.1359333 | -1.1622167 | -1.3296071 | -1.3266897 | -1.2808065 | -1.0237857 | -1.3109677 | -1.08665 |
| TEMP (°C) | -0.3416667 | 0.52 | -0.7992857 | -1.2175862 | -1.2574194 | 0.97571429 | 0.5183871 | 1.0965 |
| VIS (SM) | -12.079611 | -13.738164 | -9.9930246 | -1.3127931 | -0.1924839 | 0.62426667 | -11.147783 | -10.462186 |

Figure 4.1: Anomalies of Temperature, station pressure, visibility, zonal wind and meridional winds between Cape Parry and the CCGS *Amundsen* from November 2003 to June 2004.

between the two stations, the pressure recorded at the ship is mirrored well in Cape Parry's record and could be corrected and used as an estimate of on-ice data within this range. Deviations in monthly-averaged temperature fluctuated more often from month to month but remained within ±1.5 °C with the largest deviation occurring during the months of February (-1.22 °C) and March (-1.26 °C). November, and January to March were warmer months (negative deviations) at the ship compared to Cape Parry's average monthly temperatures, whereas December was a colder month at the ship, as well as the remaining spring months.

A comparison of monthly average zonal winds at both stations has proven to be highly variable, especially in the late fall and early winter months of October, November and December. The few ship observations available for the month of October are not indicative of a full monthly average, but do indicate that for the later part of the month the zonal wind was much stronger at Cape Parry than at the ship location. This is continued through November and December with zonal winds at Cape Parry greater than at the ship by 7.0 m $s^{-1}$ and 11.8 m $s^{-1}$, respectively. In January and for the rest of the study period, zonal wind flow was in much better agreement. Monthly average zonal winds for the ship were greater than those recorded at Cape Parry through the months of January (-2.0 m $s^{-1}$), February (-2.1 m $s^{-1}$) and March (-4.0 m $s^{-1}$). From April to June, Cape Parry average zonal winds were dominant, but remained in good agreement. Though the monthly average deviation for April was greatest in this period (+3.6 m $s^{-1}$), anomalies decreased through May (+1.4 m $s^{-1}$) and June (+0.9 m $s^{-1}$). Monthly average meridional wind anomalies, however, remained in fairly good agreement throughout the study period, ranging from about ± 3.0 m $s^{-1}$. The meridional wind component during the winter at Cape Parry was predominantly greater than recorded at the ship, with January, February and March yielding negative anomalies; however, the overall alternation from positive anomalies to negative anomalies does tend to follow the transitions of the seasons, where positive anomalies dominated the later part of the fall and spring and negative anomalies in the winter. Maximum deviations came in December with +1.9 m $s^{-1}$, March with -2.0 m $s^{-1}$, and June with +2.6 m $s^{-1}$.

Reported visibilities at the ship were carried out manually with the aid of a videograph mounted on the ship. Between the end of January (day 28) and the end of April (day 122), visibility sensors were installed at the ice camp Takatuk (discussed above) and visibility was observed at both 1.5 m and 3.0 m. Over the study period, manual observations are consistently overestimated according to the visibilities recorded at Takatuk, and observations recorded from the visibility sensors were markedly closer in comparison to the observations taken at Cape Parry, compared to those taken by observers. Human error involved in manual observations, the calibration of the videograph and the location where the manual observations were made (atop the wheelhouse, which would introduce a bias towards higher visibilities) are possible explanations for these large differences. However, systematic biases are introduced when maximum reported visibility (which can vary amongst the design of an automatic station) is not taken into account. Manual observations used an upper limit of 20 SM as the maximum reported visibility, where as the sensors placed at Takatuk and the sensor at Cape Parry have much lower maximums (9.99 SM, and 9.32 SM ± 10%, respectively). Focusing only on visibilities taken at Takatuk, the monthly average observations at Takatuk came within ±1.5 SM from the observations at Cape Parry between February and April. The biggest deviation came during the month of February where the monthly average at Takatuk was 1.3 SM greater. Monthly average visibility during March was also slightly greater by 0.19 SM. By limiting the maximum visibility observation at the ship to the maximum reported visibility at Cape Parry for the whole period, ship reported visibilities are much more closely related with an improved range of -5.2 SM to +0.23 SM (previous range: -15 SM to -0.25 SM). While the comparison for months of February to April remain the largely the same, ship visibilities continue to be larger than reported at Cape Parry on the whole. The comparison improves throughout the winter months from -4.0 SM to +0.23 SM, and varied greatest during the fall and spring months.

### 4.2.2 Paulatuk vs CCGS Amundsen

The MSC station at Paulatuk is located approximately 117 km SE of the CCGS

*Amundsen*'s over-wintering location at an elevation of 5.50 m above sea level. As a result, pressure measurements taken at the ship closely resemble the measurements recorded at Paulatuk, ranging from -0.17 mb to 0.01 mb (varing within the margin of error for the pressure sensor at the ship (± 0.15 mb)), with the largest deviations in the months of December to March (Figure 4.2), where ship values were greater than values reported at Paulatuk. This trend was consistent through the study period, with the exception of the months of October, November, and April, where pressure recorded at Paulatuk was slightly higher than ship pressure by a small margin. Temperature anomalies varied by -1.7 °C to 3.7 °C, with ship temperatures being warmer on average during the months of November to January. The regime shifted by 2.6 °C from January to February (February being the coldest month at the ship), and from February to June, monthly averaged temperatures measured at the ship became increasingly cooler than reported at Paulatuk, with the highest positive deviation in June (+3.7 °C). Unlike Cape Parry, relative humidity was available at the Paulatuk station site and included here. Monthly average relative humidity for both the ship and Paulatuk are in good agreement in the late fall and winter months. On average, higher humidity was reported at the CCGS *Amudsen* in November and December, and the opposite is true for the months of January to March, with all deviations remaining within ± 3%. Much larger deviations occur during the spring months, where relative humidity at the ship for the months of April, May and June was higher by 6% to 12% on average, which corresponds to the ship being exposed to and returning to open waters.

Based on available wind data from between 1988 and 2003 (Environment Canada, personal communication), Paulatuk appears to have two modes for summer and winter. Between the months of October and February, winds are predominantly and increasingly

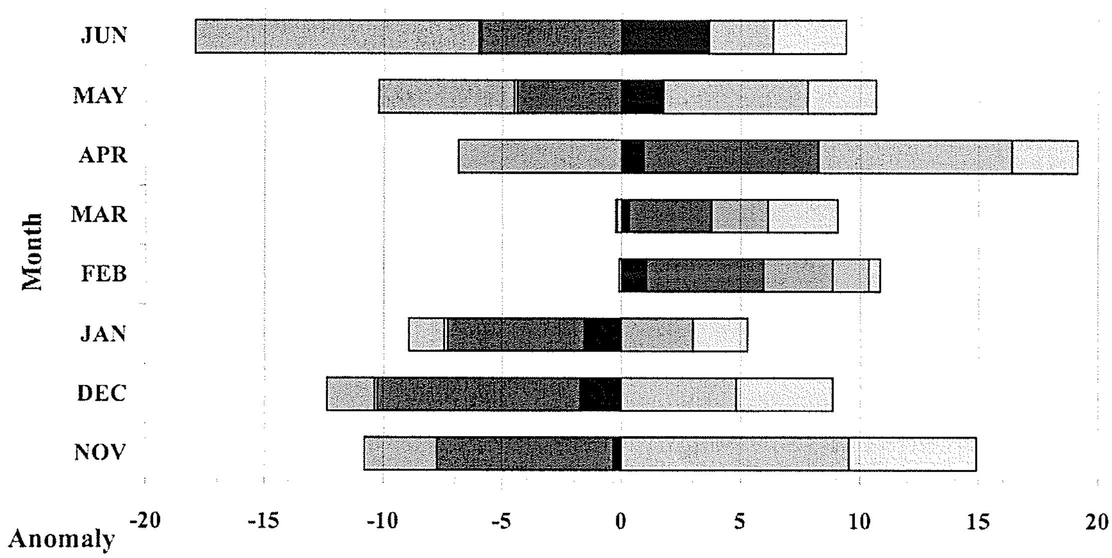


| | NOV | DEC | JAN | FEB | MAR | APR | MAY | JUN |
|---|---|---|---|---|---|---|---|---|
| V (m/s) | 5.35038 | 4.0433556 | 2.2717222 | 0.4780037 | 2.93978 | 2.7532429 | 2.886671 | 3.0699 |
| U (m/s) | 9.5465933 | 4.8292667 | -1.4962815 | 1.5170222 | -0.0663733 | 8.1224179 | 6.0450935 | 2.6658795 |
| RH (%) | -3.0626667 | -1.9983871 | 3.0212 | 2.8958621 | 2.375 | -6.8507143 | -5.6935484 | -11.940714 |
| P (mb) | 0.0077333 | -0.1210645 | -0.1188929 | -0.0956552 | -0.1658667 | 0.0222857 | -0.1058065 | -0.09065 |
| VIS (SM) | -7.4262777 | -8.5399554 | -5.7751675 | 4.921 | 3.4336667 | 7.2982667 | -4.4122991 | -5.9111856 |
| TEMP(°C) | -0.3053333 | -1.7041935 | -1.5403571 | 1.0451724 | 0.3336667 | 0.9453571 | 1.7480645 | 3.6725 |

Figure 4.2: Anomalies of temperature, station pressure, visibility, relative humidity, zonal wind and meridional winds between Paulatuk and the CCGS *Amundsen* from November 2003 to June 2004.

southwesterly (wind magnitude increases). A transition occurs to a northwesterly-northeasterly mode during the months of March to July. After separating the reported wind vectors into their components, zonal winds at Paulatuk were stronger during the late fall/early winter months as well as the spring months compared to winds reported at the ship. Maximum deviations between the two stations are positive deviations (more westerly at Paulatuk than at the ship) during the months of November and April at +7.7 m $s^{-1}$ and + 7.1 m $s^{-1}$, respectively, months in which the ship reported winds predominately out of the east (see Figure 3.25). Zonal winds relate well during the winter months, varying between ±2 m $s^{-1}$, with the smallest anomaly in February (0.4 m $s^{-1}$). Overall, during the fall and spring, the monthly averaged magnitude of westerly winds at Paulatuk was greater than that of the ship. In the case of meridional winds, anomalies remained consistently positive throughout the entire period with the exception of February, which yielded a negative anomaly of -0.8 m $s^{-1}$. The largest southerly wind anomalies came in November (+3.4 m $s^{-1}$), and June (+3.2 m $s^{-1}$). For the rest of the period, southerly wind anomalies remained within +3 m $s^{-1}$.

The automated visibility sensor for Paulatuk reports maximum visibilities of 14.98 SM. As in the case for Cape Parry, and even with a higher maximum value compared to Cape Parry, visibilities reported at the ship are much larger than those reported at Paulatuk by between 5.3 and 8.5 SM from November to June. Replacing the monthly averaged manual visibility observations from the ship with the automated measurements taken at Takatuk at 1.5 m, Paulatuk visibilities appear to be much greater by 3.4 to 7.3 SM between February and April. The maximum observation for the visibility sensors is 9.32 SM. The automatic difference between to the two maximums introduces a systematic error through the time series. As before, reducing the maximum reported visibility at the ship to match that of Paulatuk, monthly averaged visibility remains large on the whole outside of the availability of automated data from Takatuk. Although still larger, ship visibility measurements are in much better agreement, with the best comparisons being made during the months of December (-1.9 SM), May (-0.04 SM), and June (-1.85 SM), and the maximum deviation coming in November (-3.25 SM).

## 4.3 Model Comparison:

Table 4.1 lists the root mean square errors (RMSE) for each station/model comparison and for each meteorological field as a representation of relative accuracy between each model and each station over the observational period of CASES. Overall, relative humidity (when available) was represented poorly amongst the remaining variables, while pressure was relatively well-resolved in comparison. Plots of station data versus model daily average data (Figures 4.3 to 4.10; Figures 4.12 to 4.18), assuming that the perfect model representation would yield a 1:1 relationship, illustrate the overall deviation of the model throughout the period against a superimposed y=x line, and by separating the biases into seasonal categories: fall (OND), winter (JFM) and spring (AMJ).

Table 4.4: RMSE values for model comparisons with meteorological data collected at Cape Parry, Paulatuk and CCGS *Amundsen* from October 2003 to June 2004.

| | Field | GEM | NCEP I | NCEP II | NARR |
|---|---|---|---|---|---|
| *CCGS Amudsen* | Temperature (T) | 1.78 | 4.20 | 3.96 | 4.76 |
| | Pressure (MSLP) | 1.96 | 2.12 | 2.26 | 3.04 |
| | Relative Humidity (RH) | 4.98 | 14.73 | - | 8.10 |
| | Zonal Winds (U) | 6.73 | 7.65 | 6.96 | 9.23 |
| | Meridional Winds (V) | 4.85 | 4.02 | 3.80 | 4.15 |
| | Precipitable Water (PWTR) | 1.69 | 3.09 | 2.93 | 2.86 |
| *Cape Parry* | Temperature (T) | 2.04 | 4.28 | 3.10 | 5.27 |
| | Pressure (MSLP) | 0.38 | 0.98 | 1.10 | 5.65 |
| | Zonal Winds (U) | 3.05 | 4.18 | 3.46 | 5.54 |
| | Meridional Winds (V) | 1.59 | 1.40 | 1.96 | 1.96 |
| *Paulatuk* | Temperature (T) | 2.05 | 4.37 | 3.16 | 4.54 |
| | Pressure (MSLP) | 0.55 | 1.48 | 1.49 | 0.93 |
| | Relative Humidity (RH) | 10.64 | 21.08 | - | 10.15 |
| | Zonal Winds (U) | 2.29 | 3.57 | 4.22 | 2.43 |
| | Meridional Winds (V) | 2.21 | 2.79 | 2.85 | 2.18 |

### 4.3.1 Temperature Representation

For all stations, GEM provided the best fit for temperature, with correlation coefficients ($r$) greater than 0.98 for each station, and the greatest linear relationship demonstrated with Paulatuk. Seasonally, GEM also provided the most consistent fit, where in the case of NCEP I, NCEP II and NARR, there appear to be distinct seasonal discrepancies. Temperatures during the winter months at Cape Parry were mainly underestimated by NCEP I with an average bias of -1.30 K, where the opposite is true for NARR (+4.01K), where maximum deviations exist below temperatures of 240K with magnitudes as much as +15K. Similarly, NARR overestimated winter temperatures for the ship and Paulatuk as well (+2.70K and +2.55K), but to a lesser extent. Similarly, winter temperatures at Paulatuk are overestimated by NCEP II on the whole. Fall estimates are underestimated by NCEP I and NARR for all stations. NARR exhibited the lowest linearity and highest variability throughout the study period for all stations, with $r$ ranging around 0.92 and with RMSE of 4.76, 5.27, and 4.54 for the ship, Cape Parry and Paulatuk, respectively.

(a)

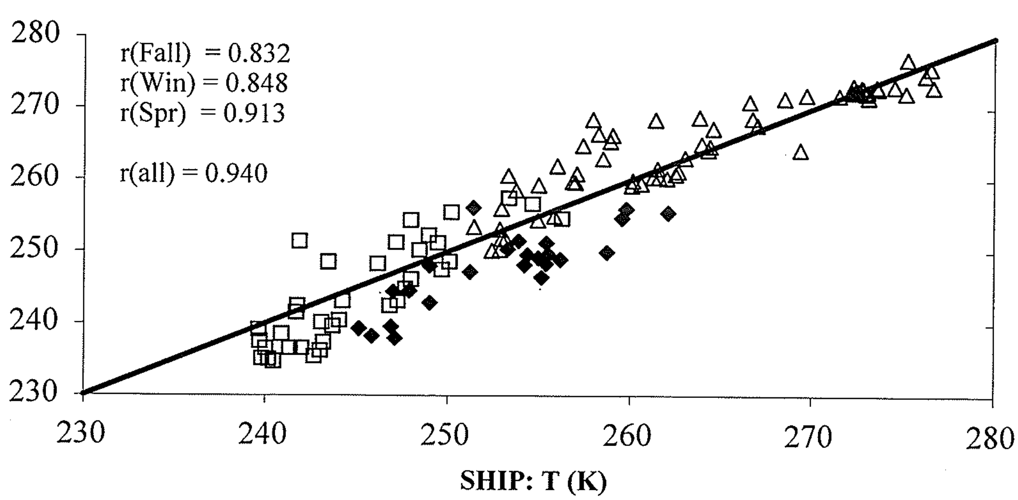

(b)

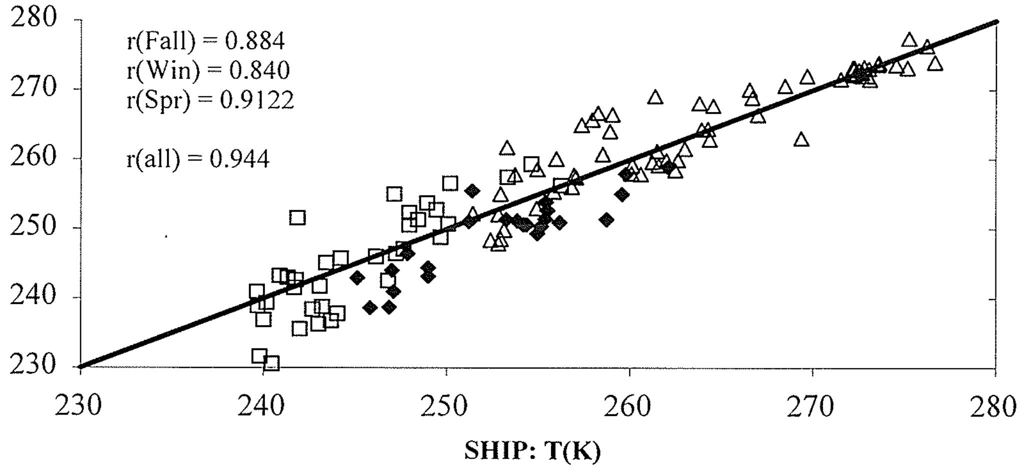


(c)

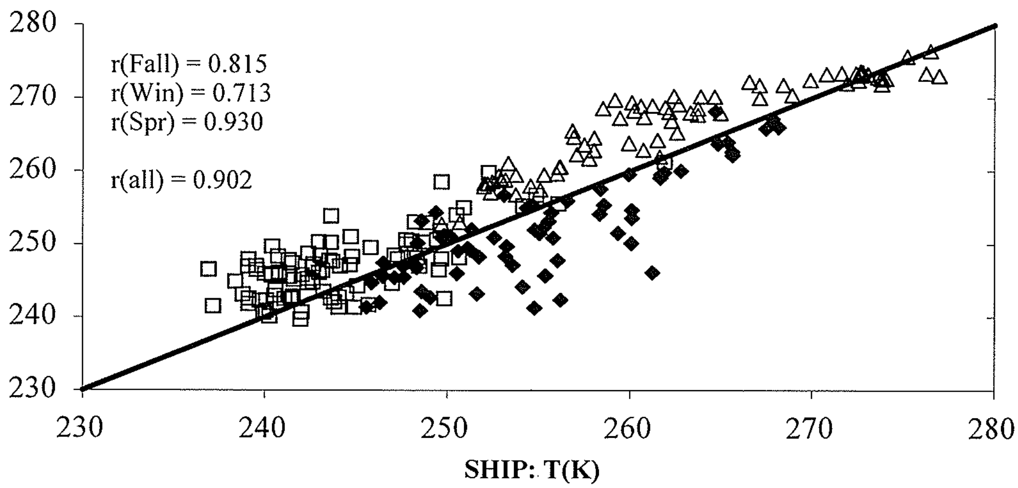


(d)

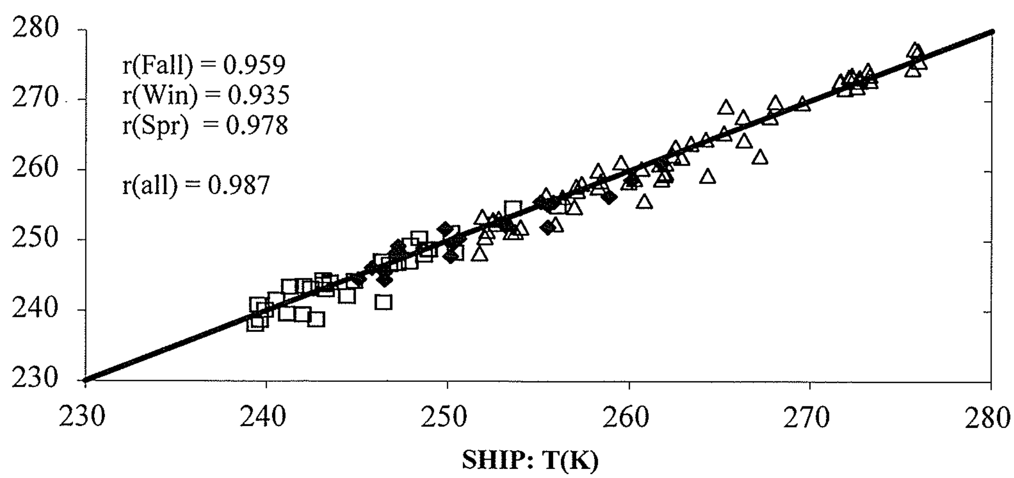


Figure 4.3: Temperature comparisons between the CCGS *Amundsen* and (a) NCEP I, (b) NCEP II, (c) NARR, and (d) GEM. Solid diamonds represent Fall (OND) data, open squares the Winter (JFM), and open triangles the Spring (AMJ).

(a)

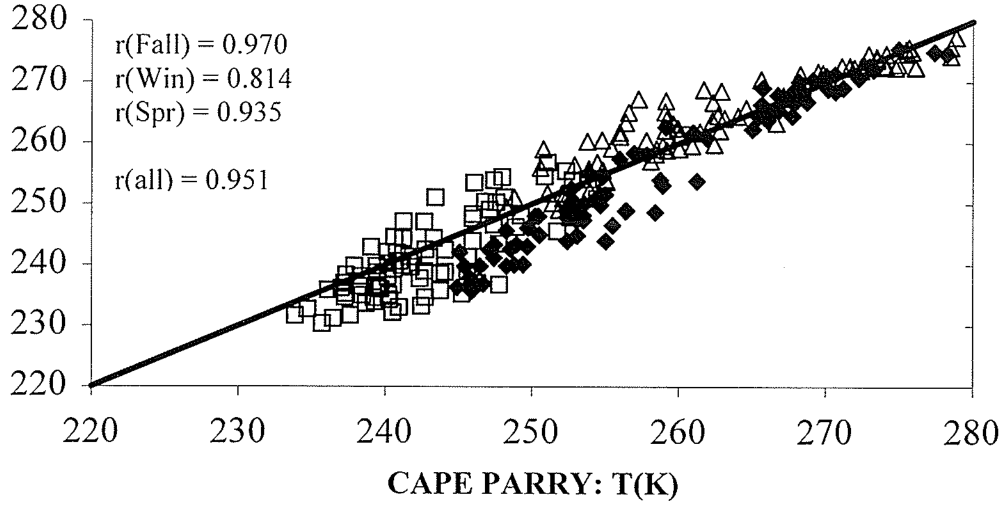
r(Fall) = 0.970
r(Win) = 0.814
r(Spr) = 0.935
r(all) = 0.951
280
270
260
250
240
230
220
220
230
240
250
260
270
280
CAPE PARRY: T(K)

(b)

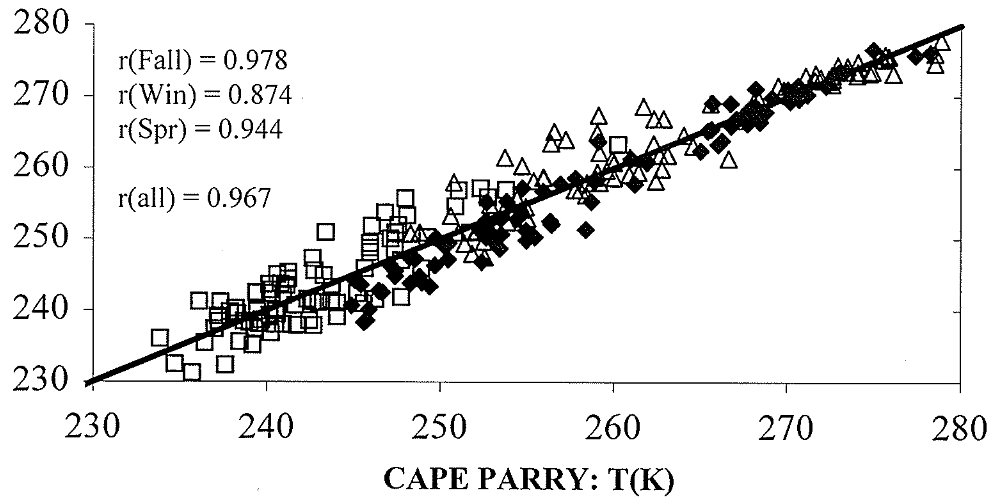
r(Fall) = 0.978
r(Win) = 0.874
r(Spr) = 0.944
r(all) = 0.967
280
270
260
250
240
230
230
240
250
260
270
280
CAPE PARRY: T(K)

(c)

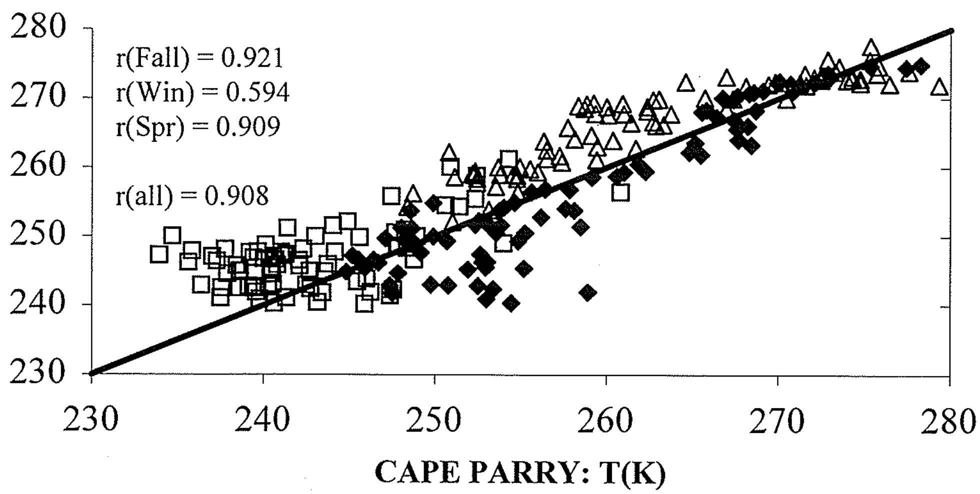
r(Fall) = 0.921
r(Win) = 0.594
r(Spr) = 0.909
r(all) = 0.908
280
270
260
250
240
230
230
240
250
260
270
280
CAPE PARRY: T(K)

(d)

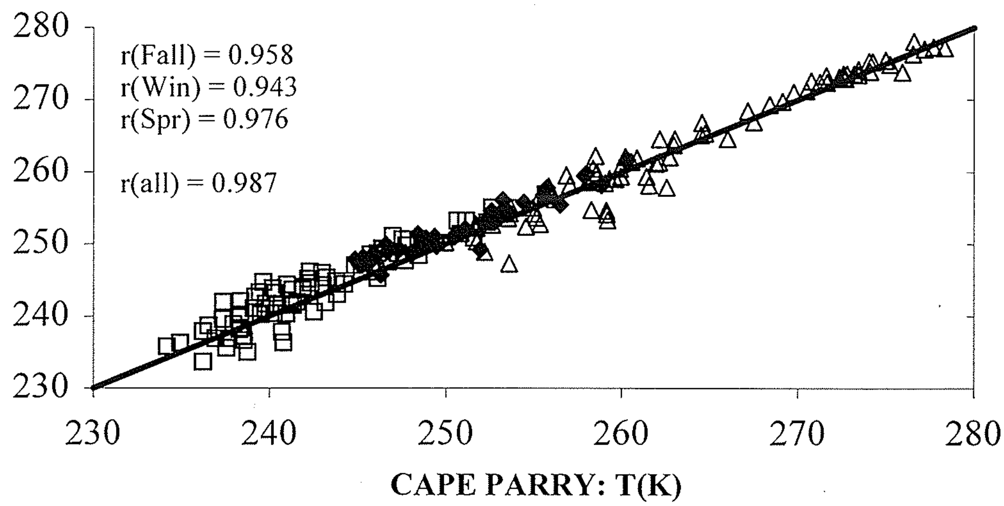


Figure 4.4: Same as Figure 4.3 for data from Cape Parry.

(a)

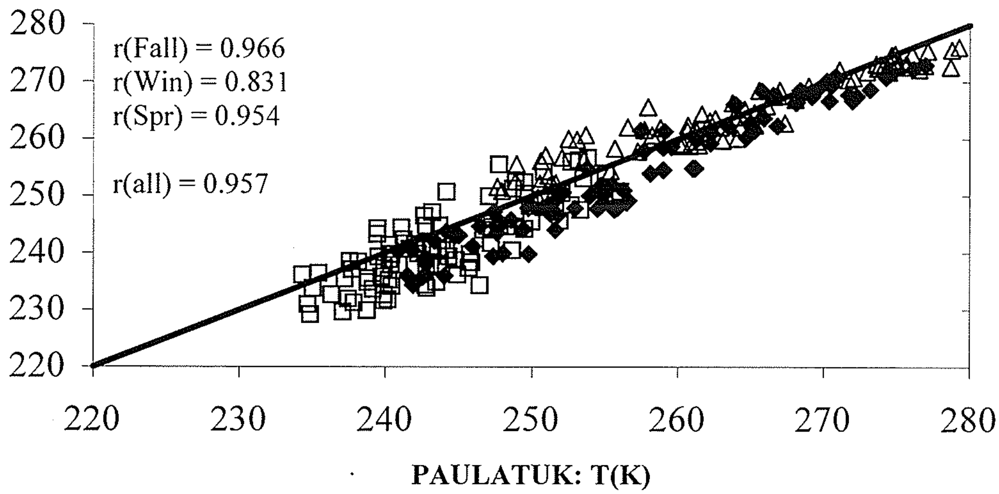
r(Fall) = 0.966
r(Win) = 0.831
r(Spr) = 0.954
r(all) = 0.957
280
270
260
250
240
230
220
220
230
240
250
260
270
280
PAULATUK: T(K)

(b)

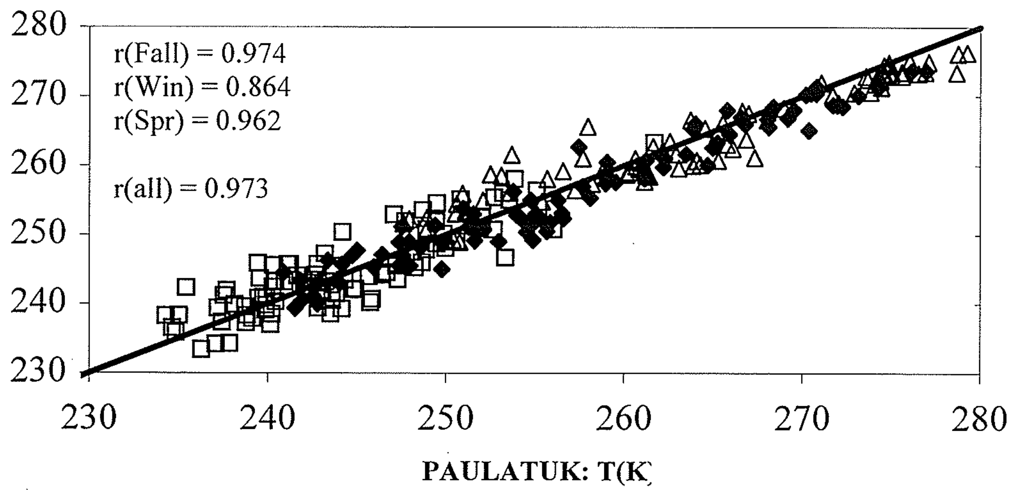
r(Fall) = 0.974
r(Win) = 0.864
r(Spr) = 0.962
r(all) = 0.973
280
270
260
250
240
230
230
240
250
260
270
280
PAULATUK: T(K)

(c)

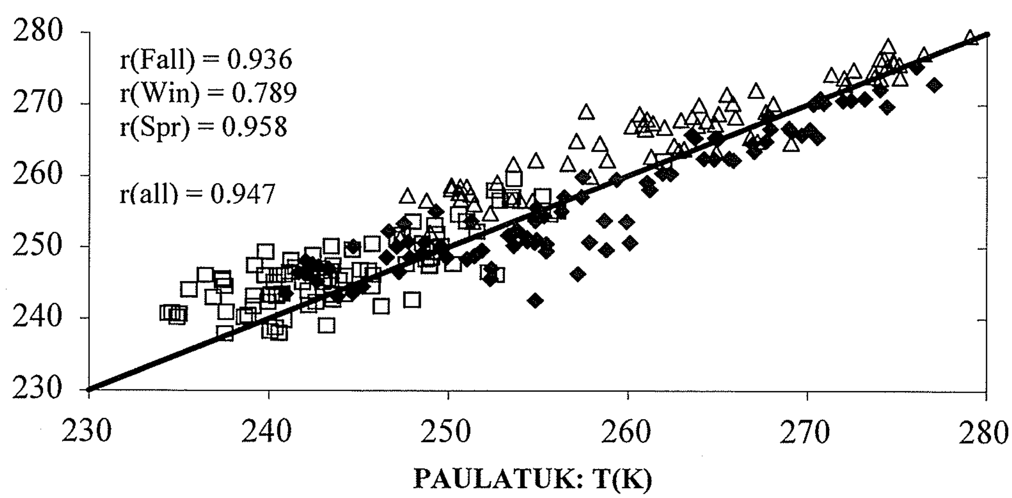
r(Fall) = 0.936
r(Win) = 0.789
r(Spr) = 0.958
r(all) = 0.947
280
270
260
250
240
230
230
240
250
260
270
280
PAULATUK: T(K)

(d)

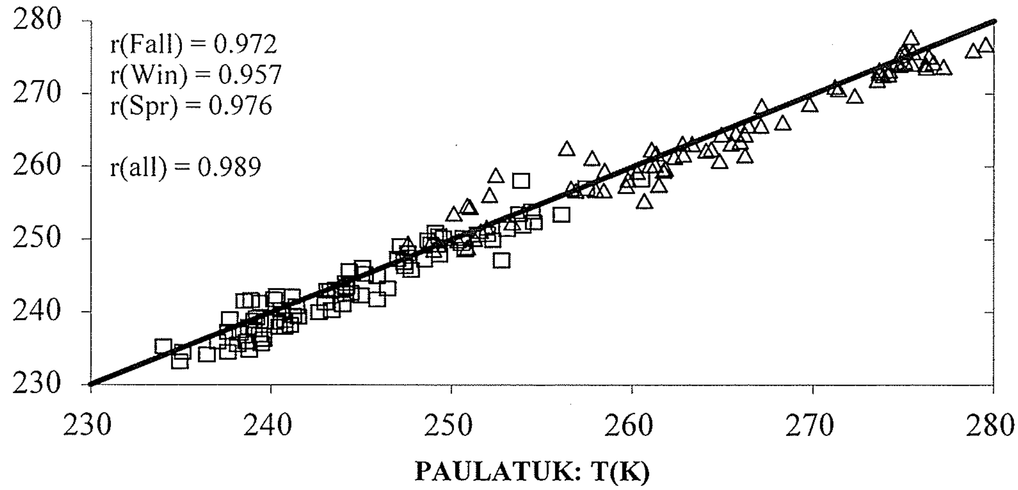


Figure 4.5: Same as Figure 4.3 for data from Paulatuk.

### 4.3.2 Pressure Representation

Pressure is well resolved amongst all model comparisons (*r* ranges from 0.964 to 0.999), however the ship's comparison with NARR stands out amidst the near perfect linearity of the other models. Recall that while calculating daily averages for comparison, the same methods were used as per the methods to obtain the daily averages per individual model. As previously described, NCEP I and NCEP II sets are comprised of 4-hourly daily averages, GEM of 2-hourly daily averages (00Z and 12Z), and NARR of 8-hourly intervals. In the case where time steps required for the calculation of the daily average were missing, the entry for that day was omitted. In the specific case of the ship, data are not continuous based on the number of observers on board at a given time; therefore, not all 8-hourly time steps are available to create a similar average with respect to NARR. In this case, NARR comparisons with the ship are done using a daily average calculated from all available ship data for that day. If no data exist for a particular day, the day is omitted from the set. As visually demonstrated, this allows for more entries than in any other case, but it also reveals large discrepancies, particularly in the winter months, that is not mirrored in the Paulatuk or the Cape Parry data set comparisons. When the whole-day daily average from the ship is used against the remaining three models, these discrepancies, mainly a handful of occasions during the winter months, are also apparent. These anomalies could be either a source of error from the observing station, a lag or delay, but it is also most likely result of largely incomplete daily data, allowing for a skewed average on particular days where pressure may have changed rapidly (not encompassing the entirety of the day's pressure changes by being incomplete). With that said, the remainder of the data set is near linear and NARR does well at fitting pressure observed at the ship, as do the remaining models for Cape Parry and Paulatuk. For the extremes, all models resolve the lowest recorded pressures well.

NCEP I and NCEP II both yield a best-fit line with slopes slightly less than one for all stations, where lower pressures are slightly overestimated, and higher pressures are slightly underestimated, best illustrated in the case of Paulatuk. GEM yielded the best results with RMSEs less than one for all stations and correlations very near unity. The models demonstrated the least variability with Cape Parry.

(a)

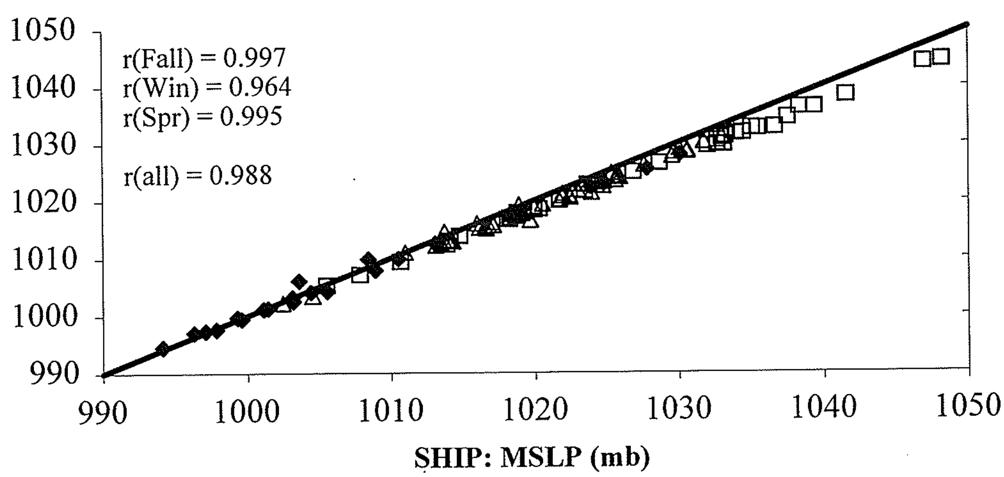

(b)

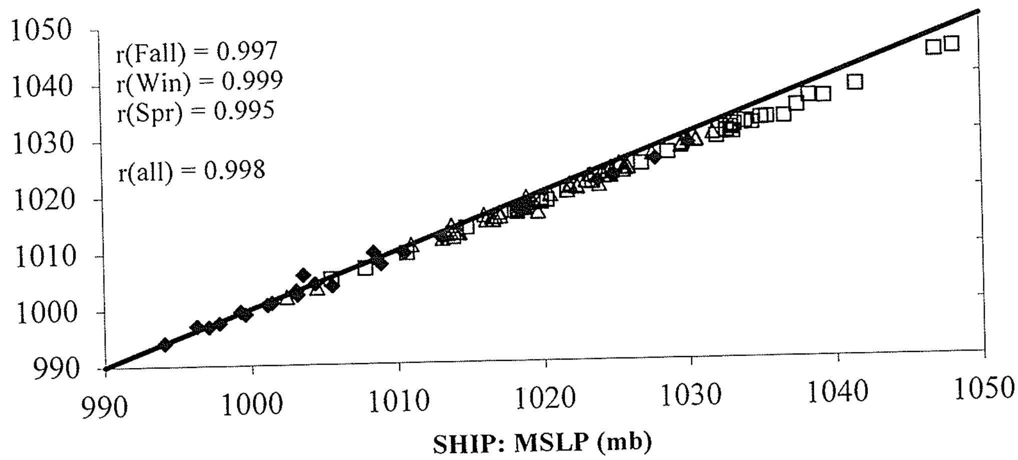


(c)

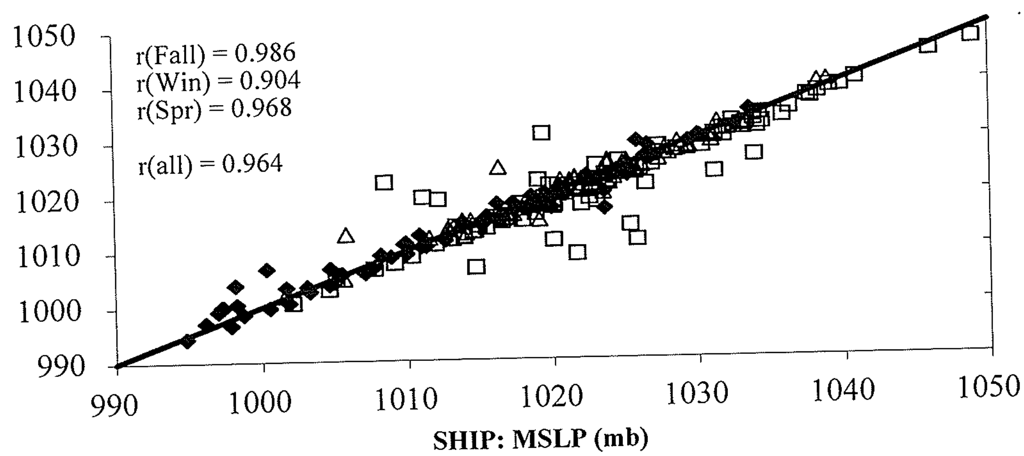


(d)

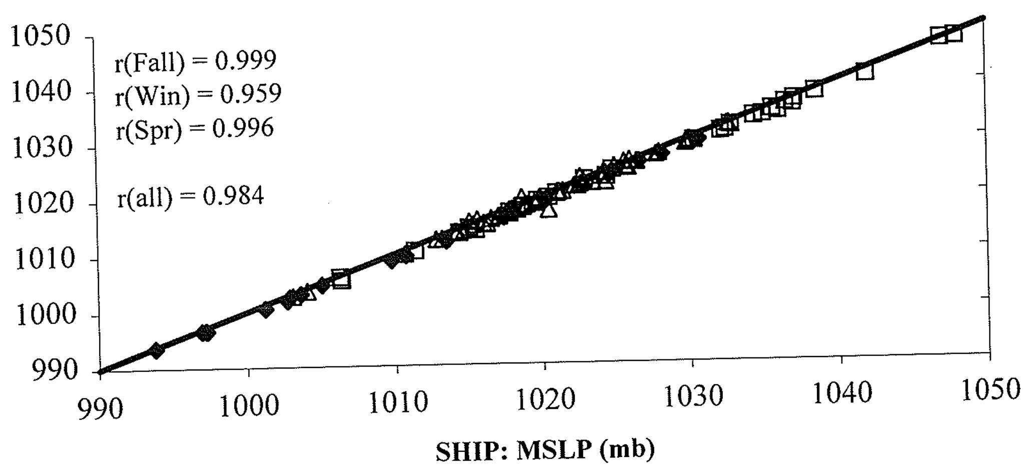


Figure 4.6: Mean Sea Level Pressure comparisons between ship data and data from (a) NCEP I, (b) NCEP II, (c) NARR, and (d) GEM. Solid diamonds represent Fall (OND) data, open squares the Winter (JFM), and open triangles the Spring (AMJ).

(a)

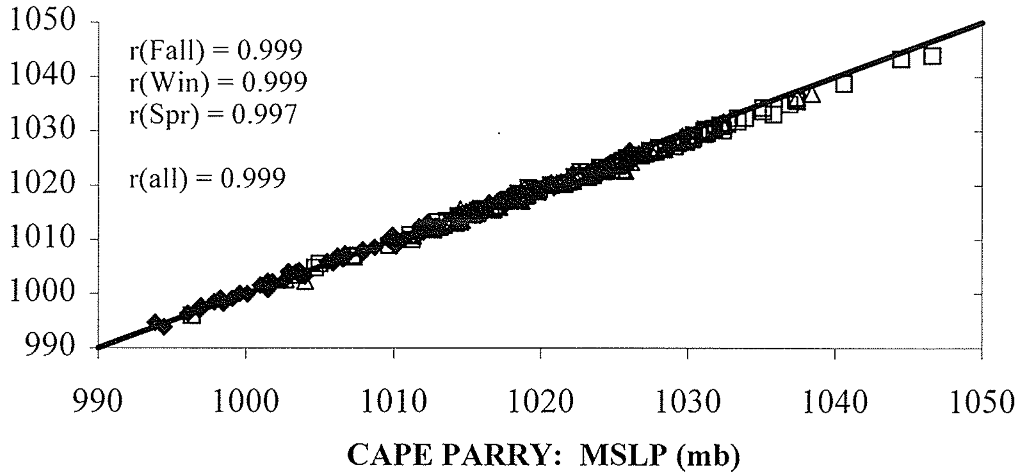
r(Fall) = 0.999
r(Win) = 0.999
r(Spr) = 0.997
r(all) = 0.999
1050
1040
1030
1020
1010
1000
990
990
1000
1010
1020
1030
1040
1050
CAPE PARRY: MSLP (mb)

(b)

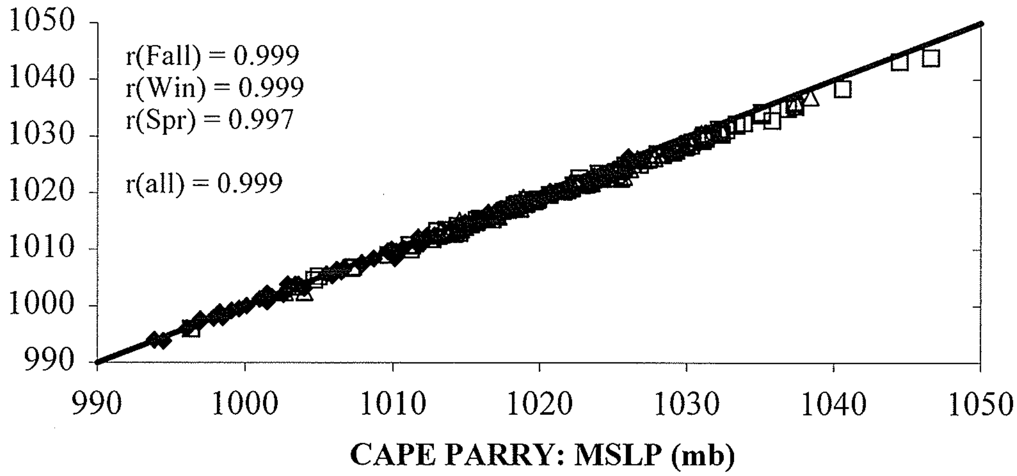
r(Fall) = 0.999
r(Win) = 0.999
r(Spr) = 0.997
r(all) = 0.999
1050
1040
1030
1020
1010
1000
990
990
1000
1010
1020
1030
1040
1050
CAPE PARRY: MSLP (mb)

(c)

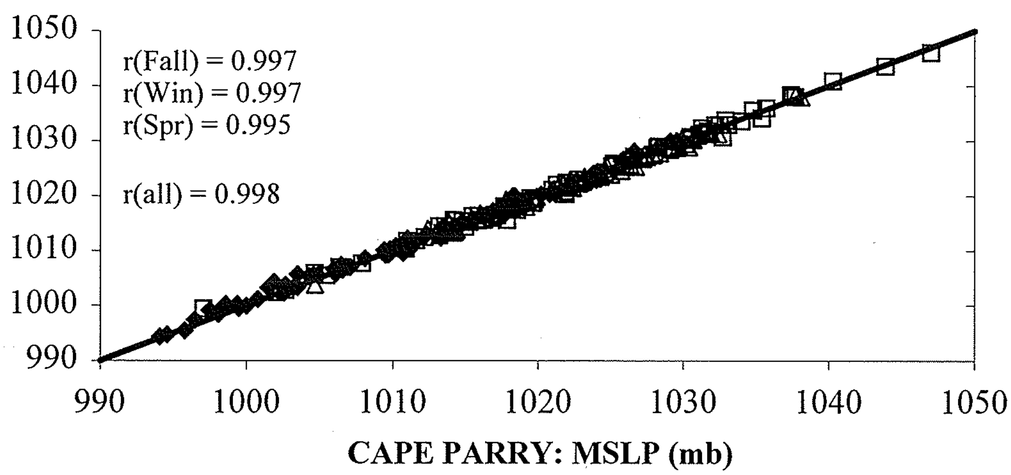
r(Fall) = 0.997
r(Win) = 0.997
r(Spr) = 0.995
r(all) = 0.998
1050
1040
1030
1020
1010
1000
990
990
1000
1010
1020
1030
1040
1050
CAPE PARRY: MSLP (mb)

(d)

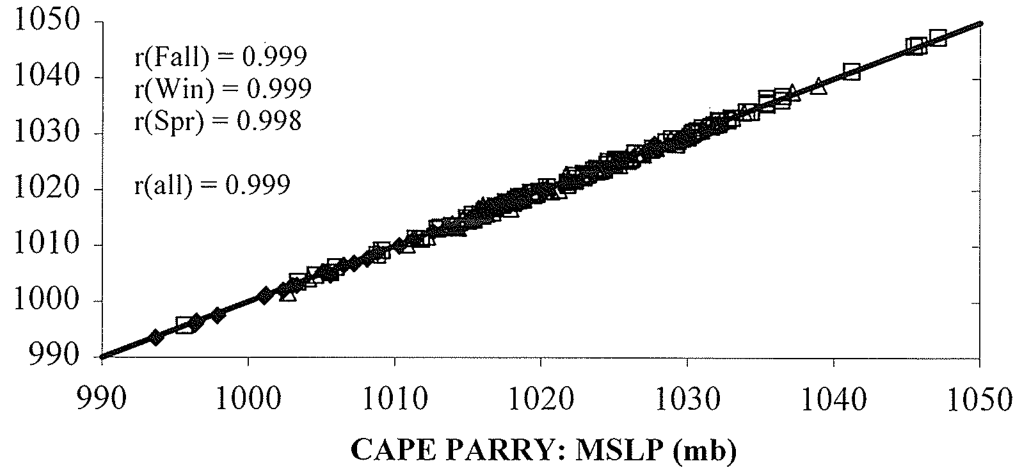


Figure 4.7: Same as 4.6 for data from Cape Parry.

(a)

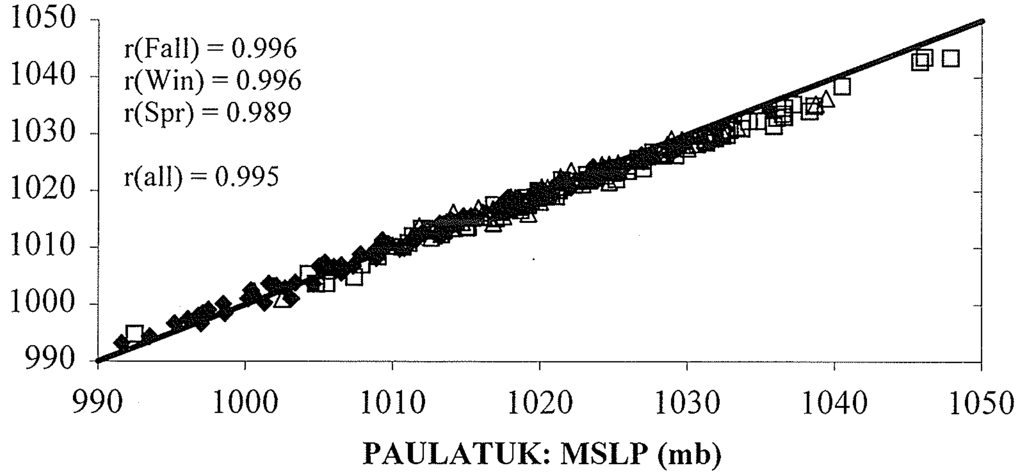
1050
1040
1030
1020
1010
1000
990
r(Fall) = 0.996
r(Win) = 0.996
r(Spr) = 0.989
r(all) = 0.995
990
1000
1010
1020
1030
1040
1050
PAULATUK: MSLP (mb)

(b)

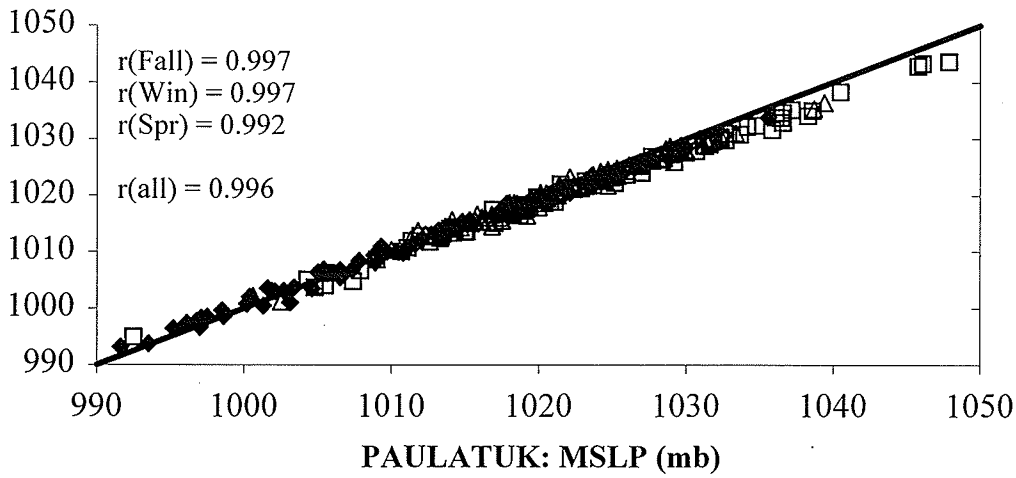
1050
1040
1030
1020
1010
1000
990
r(Fall) = 0.997
r(Win) = 0.997
r(Spr) = 0.992
r(all) = 0.996
990
1000
1010
1020
1030
1040
1050
PAULATUK: MSLP (mb)

(c)

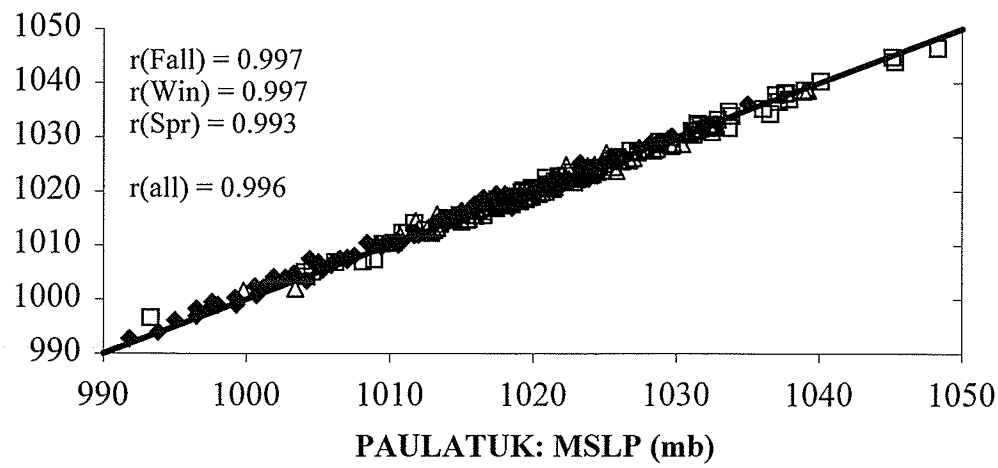
1050
1040
1030
1020
1010
1000
990
r(Fall) = 0.997
r(Win) = 0.997
r(Spr) = 0.993
r(all) = 0.996
990
1000
1010
1020
1030
1040
1050
PAULATUK: MSLP (mb)

(d)

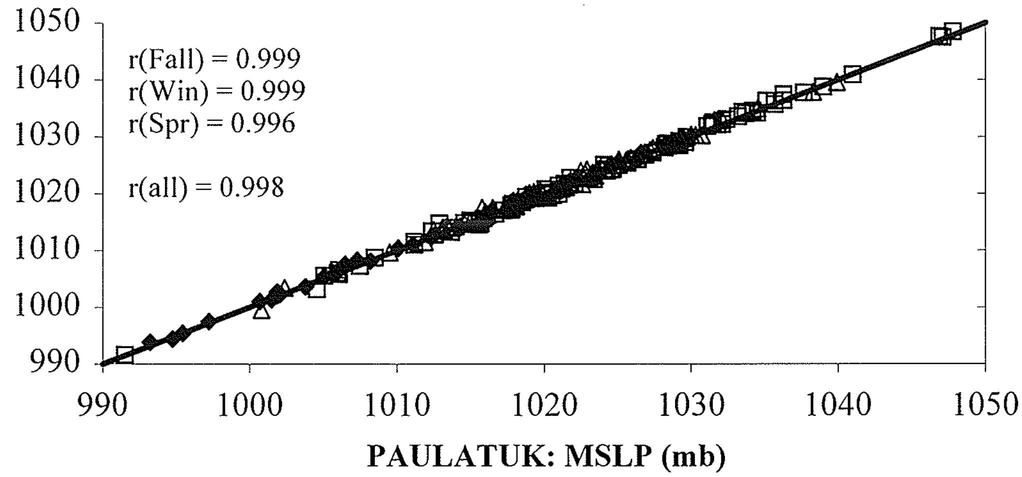


Figure 4.8: Same as 4.6 for data from Paulatuk.

### 4.3.3 Moisture Representation

Relative humidity (RH) and precipitable water vapour (PWV) are used to evaluate the representation of moisture among the stations and models. Unfortunately, not all stations and models provided a record of RH or PWV, which leads to a limitation in the overall study of moisture. Comparisons were done based on availability, as outlined below.

#### 4.3.3.1 Relative Humidity

Observations of RH were available from the CCGS *Amundsen* and from the Paulatuk station, and GEM and NCEP I provided a direct dataset of RH. Both models represented RH poorly for both station locations; however, GEM significantly outperformed NCEPI overall in both situations, as shown in Table 1. NCEP I underestimated the majority of the records from Paulatuk during the winter and spring seasons, by as much as 60% to 70%. Over the course of the study period, NCEP I fell short by -8.68%, with the greatest discrepancy found in February, with a bias of -31.69%.

The greatest negative bias for the ship fell in the month of May, with an average difference of -13.15%, and an overall bias of -7.01% for all months. Fall is generally overestimated by NCEP I, particularly in the case of the ship, though all seasons show a large range of variability. This inconsistency is reduced greatly in the case of GEM, and linear correlation is much improved, with an overall $r$ values of 0.65 and 0.89 for Paulatuk and the ship, respectively, compared to $r$ values of 0.49 and 0.56 for NCEP I. Seasonal variation is station-specific. Where all seasons are predominately underestimated in the ship's case, GEM overstates a portion of spring measurements from Paulatuk, mainly in the month of June, with a monthly average bias of +3.45%.

The largest negative bias between GEM and Paulatuk came at the end of winter (March; -10.77%), whereas the ship was most negatively represented at the beginning of spring (April; -6.06%), with both stations yielding overall negative biases for the study period of -3.06% and -5.96% for the ship and Paulatuk, respectively.

(a)

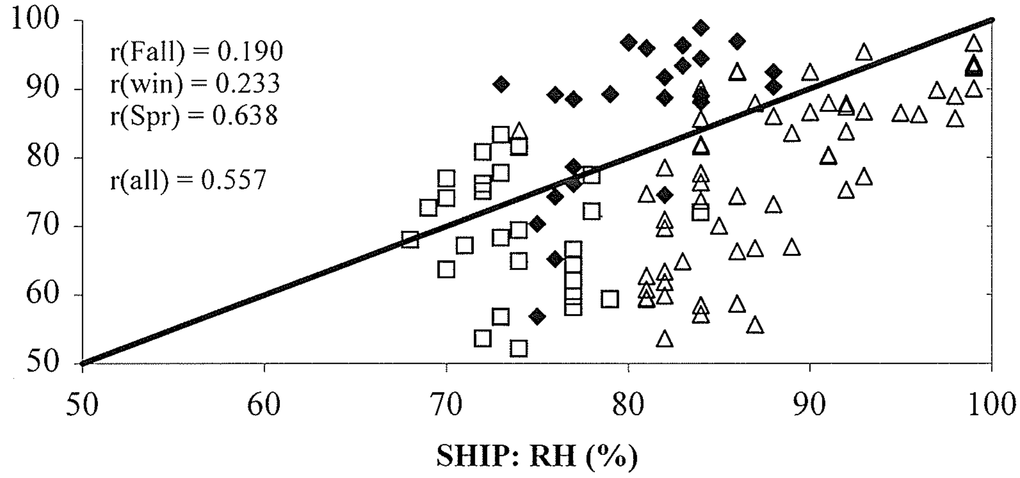


(b)

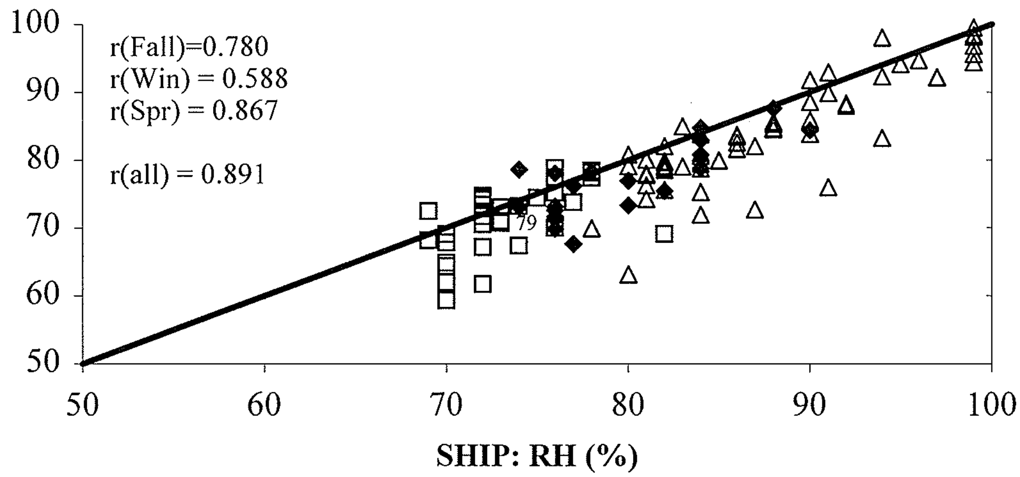


Figure 4.9: Relative humidity comparisons between ship data and data from (a) NCEP I, (b) GEM. Solid diamonds represent fall (OND) data, open squares the winter (JFM), and open triangles the spring (AMJ).

(a)

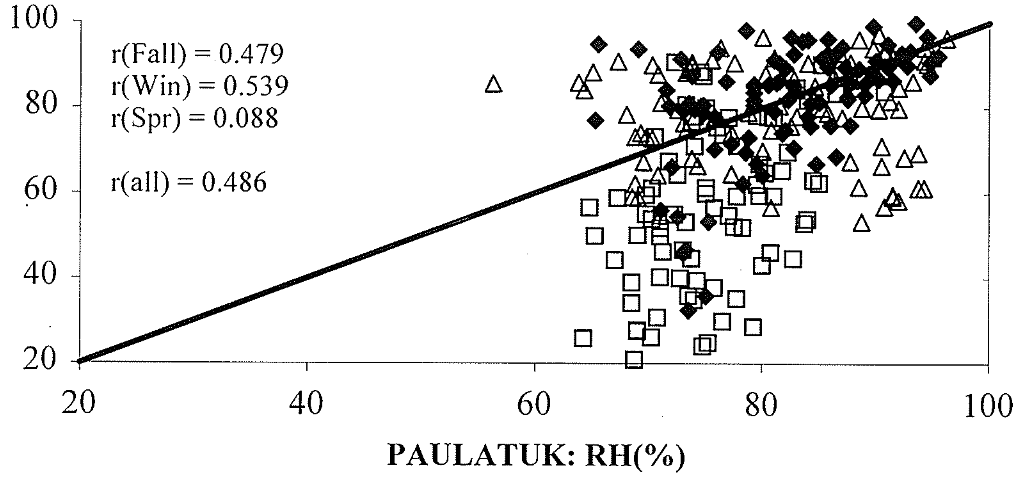


(b)

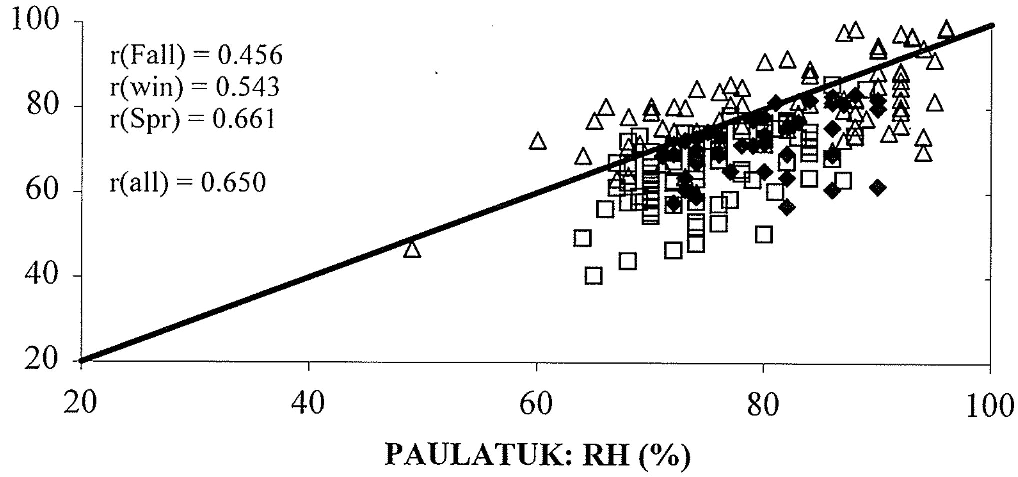


Figure 4.10: Same as 4.9 for data from Paulatuk.

#### 4.3.3.2 Precipitable Water Vapour

Measurements of PWV are limited to the CCGS Amudsen site by way of a microwave radiometer as part of the meteorological observing suite installed on the ship; this type of instrumentation is not standard at MSC reporting stations. NCEP I, NCEP II and NARR provided a PWV parameter in their dataset; PWV for GEM was calculated by integrating specific humidity over the 28 vertical levels, as explain in section 4.1.

There are many observations of PWV missing from the ship during the month of December and January due to a malfunction of the instrument, so a fair comparison during the winter months is not possible. To investigate the robustness of the data from microwave radiometer (MWR), PWV was calculated from soundings and matched with

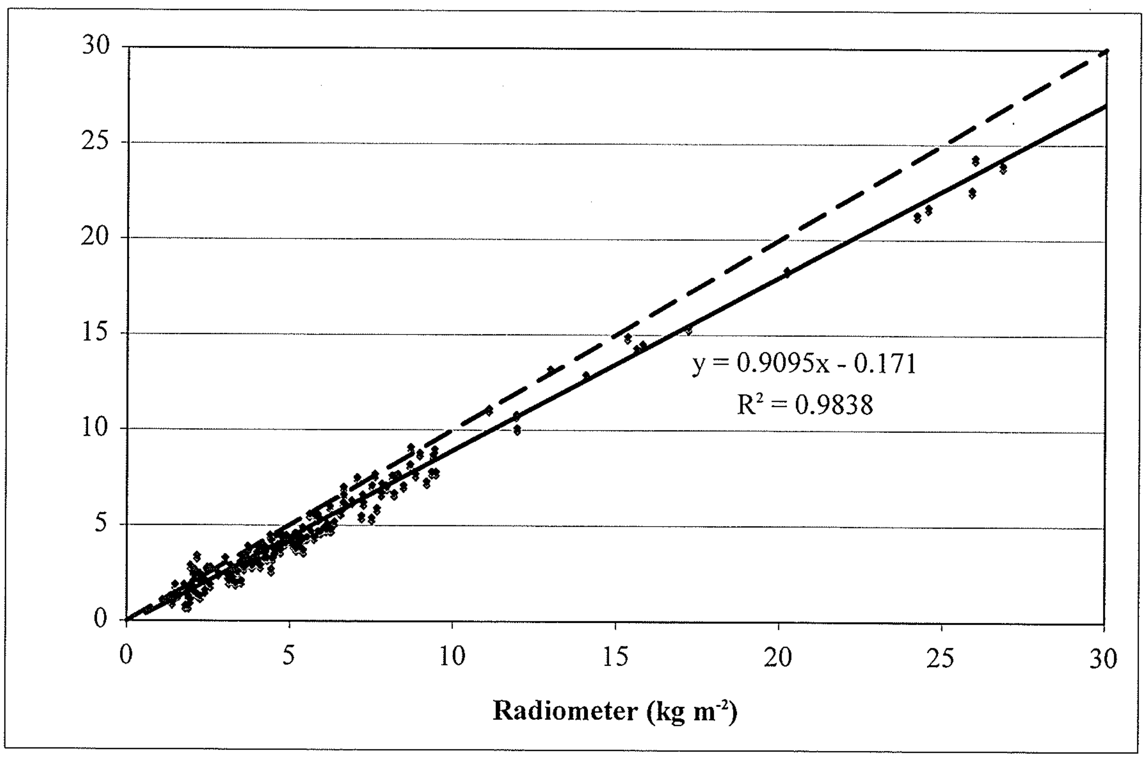


Figure 4.11: Comparison of precipitable water vapour (PWV) measurements recorded by the WVR-1100 and derived from radiosonde data. Solid line represents the linear regression (equation shown); dashed line is y=x.

data from the MWR (Figure 4.11) and illustrates the relationship between the PWV derived from the radiosondes and the data collected from the MWR. Linearity is well displayed ($r$ = 0.99) among the data, though the regression line shows that on the whole, the radiosonde estimate of precipitable water falls slightly short of the MWR measurements over the range of PWV values ($Data_{Radiosonde}$ /$Data_{MWR}$ = 0.91). The slight deviation is reinforced with an overall average bias of +0.73 $kg \cdot m^{-2}$, where bias is defined as the difference of $Data_{Radiosonde}$ from $Data_{MWR}$. This result is somewhat expected given the known dry bias that exists with the RS-80 radiosonde and the Humicap humidity sensor (Wang et al, 2002, Turner et. al., 2003, Westwater et. al., 2003). Having included the humidity correction in the calculation of PWV from the radiosonde data (Miloshevich et al. 2001), an RMSE of 1.06 $kg \cdot m^{-2}$ indicates a minimal presence of variability between the two datasets. In general, PWV measured from the MWR should hold well as a basis for comparison with model data.

Of the four models, GEM provided the best linear fit ($r$ = 0.93). Interestingly, all but NARR tended to consistently underestimate PWV throughout the study period. The largest variability came in the spring for all cases as measurements of water vapour in the atmosphere ranged into the higher values, particularly for NARR, which exhibited large positive and negative biases during the spring. While average monthly biases for April and May were slightly negative (-0.51 $kg \cdot m^{-2}$, -0.08 $kg \cdot m^{-2}$), the monthly average bias for June was slightly positive at +0.89 $kg \cdot m^{-2}$, indicating that the variability, though large (maximum deviations of +13.72 $kg \cdot m^{-2}$ day 170; -13.22 $kg \cdot m^{-2}$, day 148), is relatively proportionate. Mean Absolute Error (MAE) for the spring comparison with NARR yields an average deviation of 2.65 $kg \cdot m^{-2}$, where RMSE reveals and weighs the larger variability in this period (3.93 $kg \cdot m^{-2}$). By inspection of the data set, the large

(a)

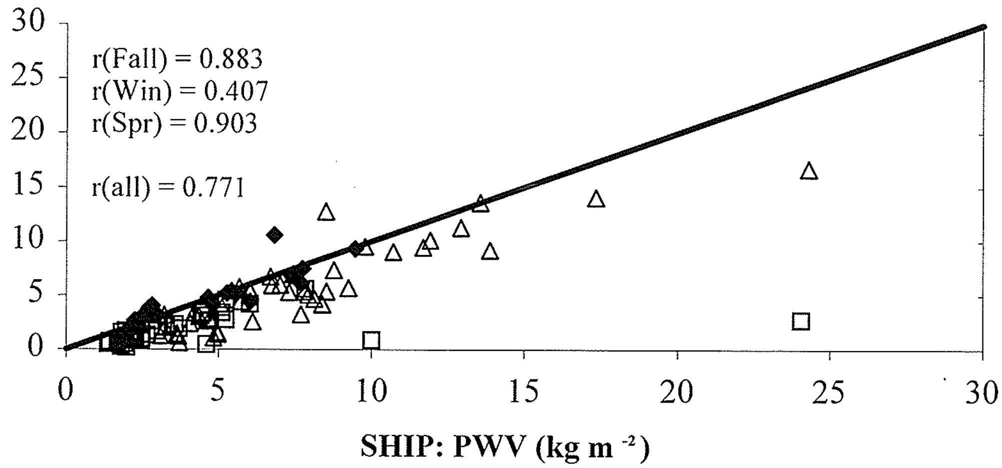
r(Fall) = 0.883
r(Win) = 0.407
r(Spr) = 0.903
r(all) = 0.771
0 5 10 15 20 25 30
0 5 10 15 20 25 30
SHIP: PWV (kg m -2 )

(b)

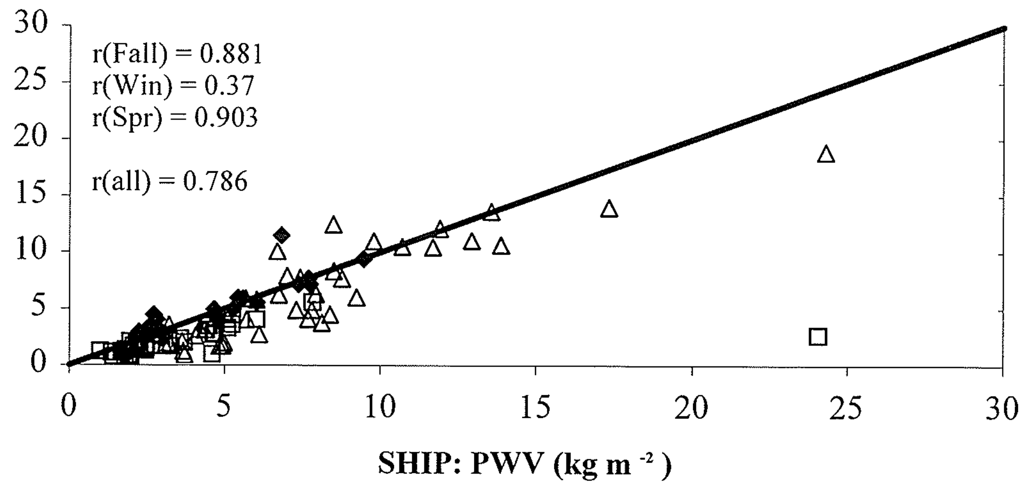
r(Fall) = 0.881
r(Win) = 0.37
r(Spr) = 0.903
r(all) = 0.786
0 5 10 15 20 25 30
0 5 10 15 20 25 30
SHIP: PWV (kg m -2 )

(c)

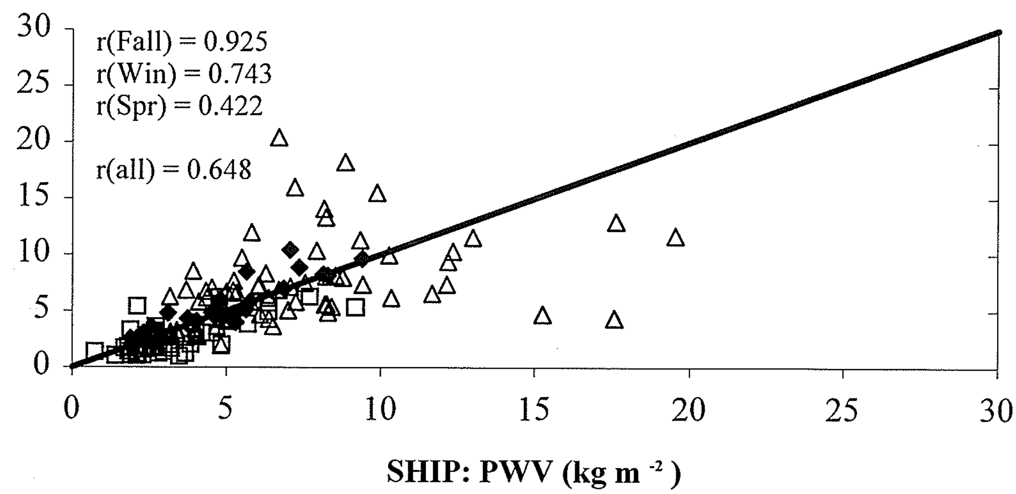
r(Fall) = 0.925
r(Win) = 0.743
r(Spr) = 0.422
r(all) = 0.648
0 5 10 15 20 25 30
0 5 10 15 20 25 30
SHIP: PWV (kg m -2 )

(d)

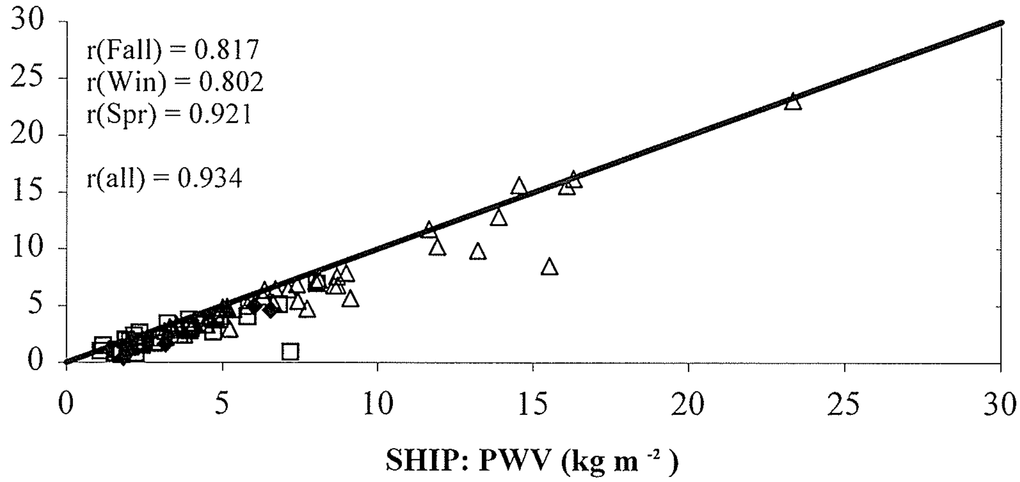


Figure 4.12: Precipitable water vapor (PWV) comparisons between ship data and data from (a) NCEP I, (b) NCEP II, (c) NARR, and (d) GEM. Solid diamonds represent fall (OND) data, open squares the winter (JFM), and open triangles the spring (AMJ).

variability coincides with the movement of the ship from its stationary position – the remaining 30 days of the study period. However, this isolated discrepancy may be a function of the difference in averaging done for each model comparison, where NARR, encompassing the most number of observations per daily average, may have caught values that otherwise would have been filtered out. Testing this by placing NARR values aside a 4-hourly average, the variability during the spring is significantly reduced (MAE of 1.17 $kg{\cdot}m^{-2}$, RMSE of 1.63 $kg{\cdot}m^{-2}$) and linearity is increased (r increases from 0.65 to 0.94), exceeding the performance of GEM overall.

### 4.3.4 Zonal Wind Representation

Of the three reporting stations, Cape Parry faired best amongst the four models in terms of zonal wind. With the exception of NARR, Cape Parry zonal winds yielded $r$ values greater than 0.9 in correlation with the models in question; GEM provided the best fit for Cape Parry and overall, linearly ($r$=0.95). While all comparisons seem to produce a general linear fit, this is not the case when investigating Paulatuk with respect to NCEP I and NCEP II. The comparison with Paulatuk and NCEP I produced an RMSE of 3.57 overall negative bias of -2.67 m $s^{-1}$, where December provided the greatest negative discrepancy on average (-4.09 m $s^{-1}$), and June the least (-1.13 m $s^{-1}$) of the study period, and where all months produced negative biases. The comparison of Paulatuk with NCEP II provided a similar yet augmented negative bias overall (-2.79 m $s^{-1}$), where both December and June again produced the maximum and minimum negative bias (-4.71 m $s^{1}$, -1.45 m $s^{-1}$). Variability is also augmented in the case of NCEP II with an RMSE of 4.22. It is interesting to note that most of the variability arises at lower yet still positive wind speeds, where the models returned large and negative corresponding values. Comparisons with GEM and NARR seem to account for these low, positive winds with much greater accuracy.

Variability was large across all comparisons of the ship data, having RMSE values between 6.73 m $s^{-1}$ (GEM) and 9.23 m $s^{-1}$ (NARR). NARR also faired the worst in linearity. As described earlier, due to the positioning of the ship during the over-wintering period, turbulent winds arriving at the ship's anemometer from a south-westerly direction provided a minimum from that direction in the ship's record. To investigate if this discrepancy was significant enough to have an effect on the comparison, winds from the Takatuk ice camp were averaged accordingly and compared. The wind record from Takatuk is limited from day 022 to day 145 of 2004. When these days are replaced in the dataset of the ship dataset, the overall correlation drops from 0.92 to 0.75 for GEM, but RMSE decreases from 6.73 to 4.66. The RMSE of the original dataset between day 022 and day 145 was 6.95 compared to 3.79. So while the old

(a)

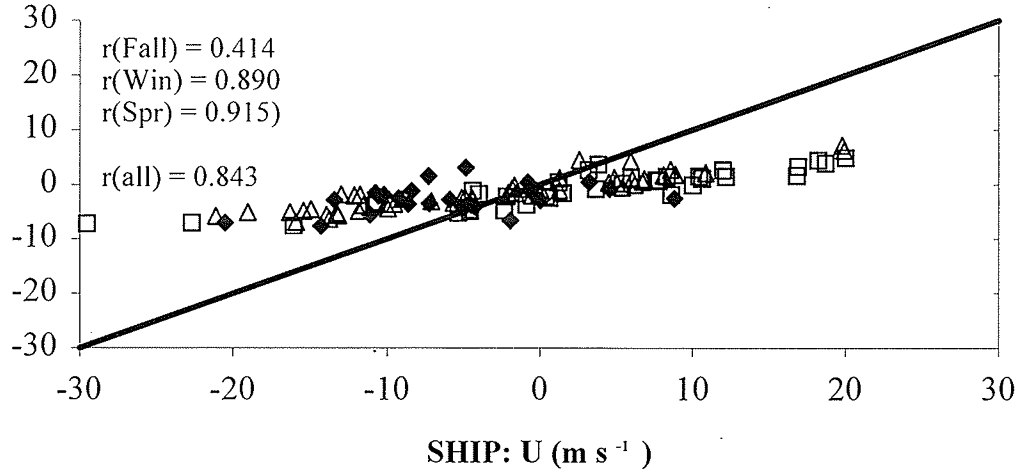

r(Fall) = 0.414
r(Win) = 0.890
r(Spr) = 0.915)
r(all) = 0.843
30
20
10
0
-10
-20
-30
-30
-20
-10
0
10
20
30
SHIP: U (m s -1 )


(b)

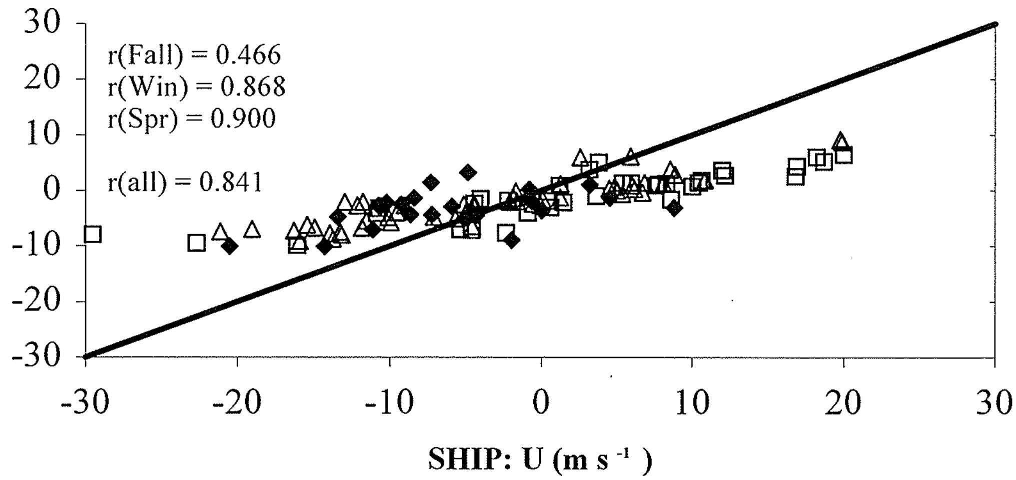

r(Fall) = 0.466
r(Win) = 0.868
r(Spr) = 0.900
r(all) = 0.841
30
20
10
0
-10
-20
-30
-30
-20
-10
0
10
20
30
SHIP: U (m s -1 )


(c)

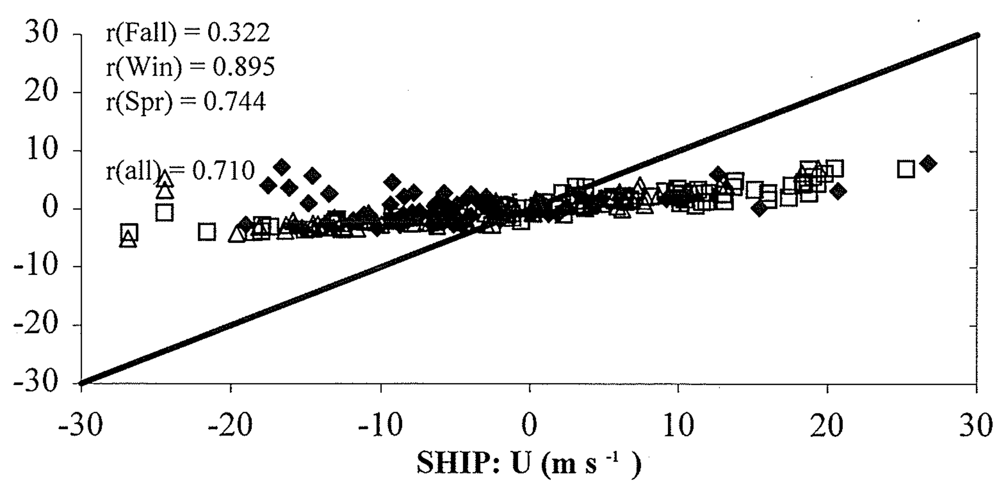

r(Fall) = 0.322
r(Win) = 0.895
r(Spr) = 0.744
r(all) = 0.710
30
20
10
0
-10
-20
-30
-30
-20
-10
0
10
20
30
SHIP: U (m s -1 )

(d)

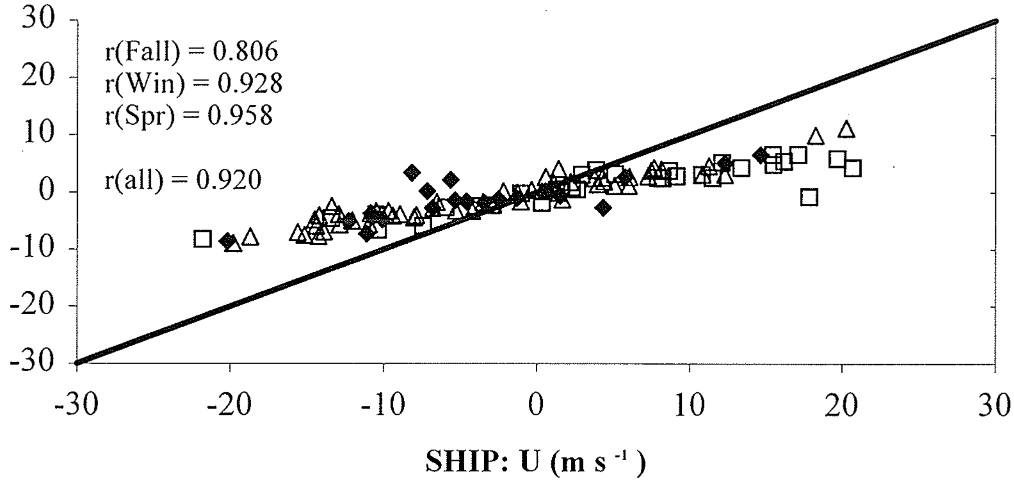


Figure 4.13: Zonal wind comparisons between ship data and data from (a) NCEP I, (b) NCEP II, (c) NARR, and (d) GEM. Solid diamonds represent fall (OND) data, open squares the winter (JFM), and open triangles the spring (AMJ).

dataset does provide a better fit linearly, the variability is much improved with Takatak's data. The range of values was reduced when the original ship data was replaced with that from Takatuk; the spread of zonal wind magnitudes went from -21.7 m $s^{-1}$ to +20.6 m $s^{-1}$ at the ship, where as Takatuk provided a range reduced by nearly a factor of 2, which can account for the reduction of variability in the new data set. In the remaining models, NARR and NCEP II performed much like GEM where variability was decreased but correlation was reduced. NCEP I was the opposite, with a reduction in correlation of 0.84 to 0.80 overall, and an increase in RMSE of 4.02 m $s^{-1}$ to 4.66 m $s^{-1}$ overall.

In all comparisons, the slopes of the linear relationships were less than one, indicating that on the whole the models tended to underestimate westerly winds and overestimate easterly winds.

(a)

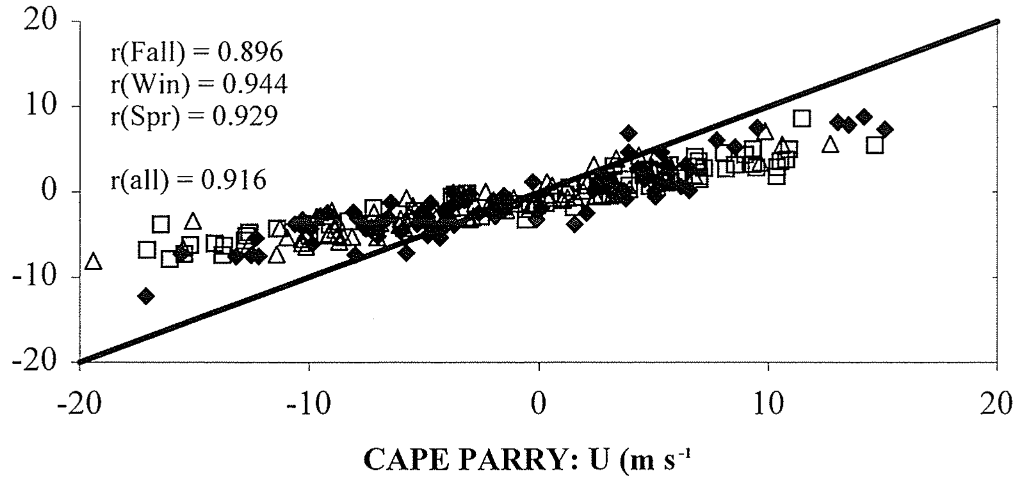
r(Fall) = 0.896
r(Win) = 0.944
r(Spr) = 0.929
r(all) = 0.916
20
10
0
-10
-20
-20
-10
0
10
20
CAPE PARRY: U (m s-1

(b)

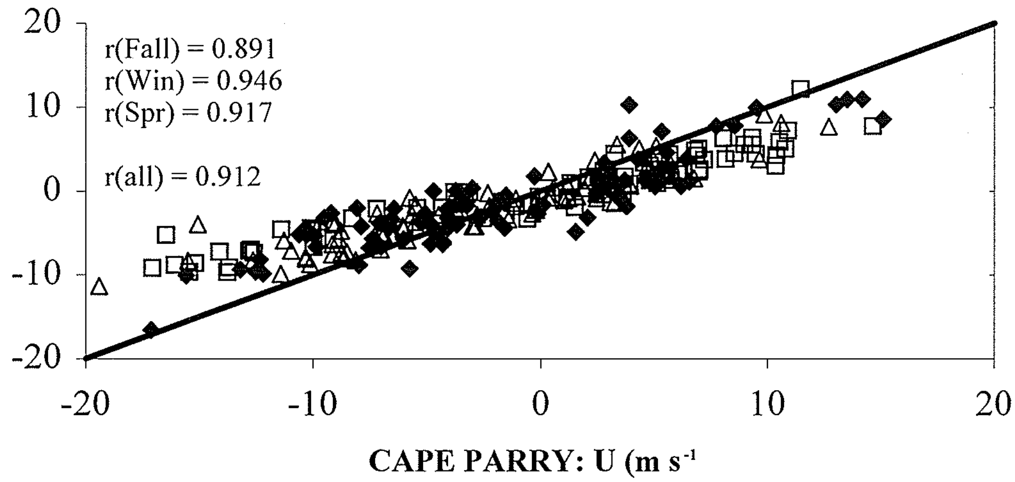
r(Fall) = 0.891
r(Win) = 0.946
r(Spr) = 0.917
r(all) = 0.912
20
10
0
-10
-20
-20
-10
0
10
20
CAPE PARRY: U (m s-1

(c)

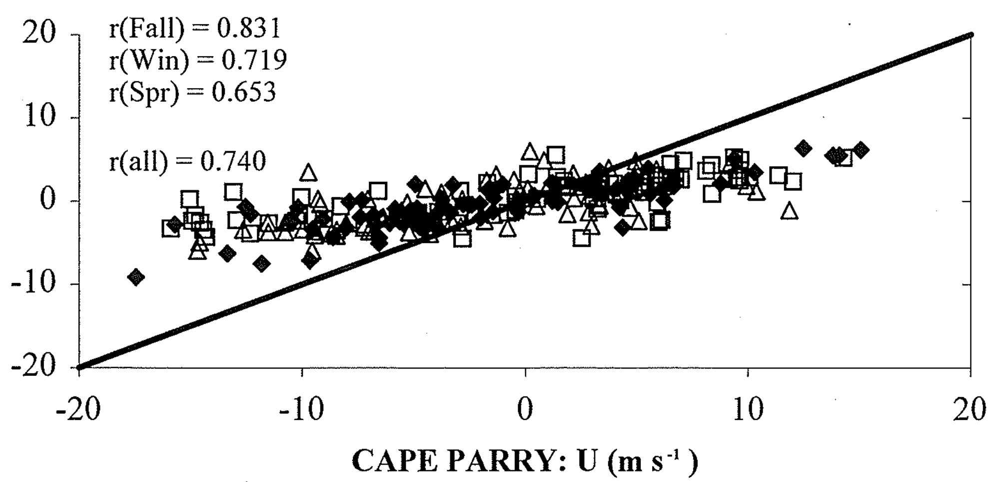
r(Fall) = 0.831
r(Win) = 0.719
r(Spr) = 0.653
r(all) = 0.740
20
10
0
-10
-20
-20
-10
0
10
20
CAPE PARRY: U (m s-1 )

(d)

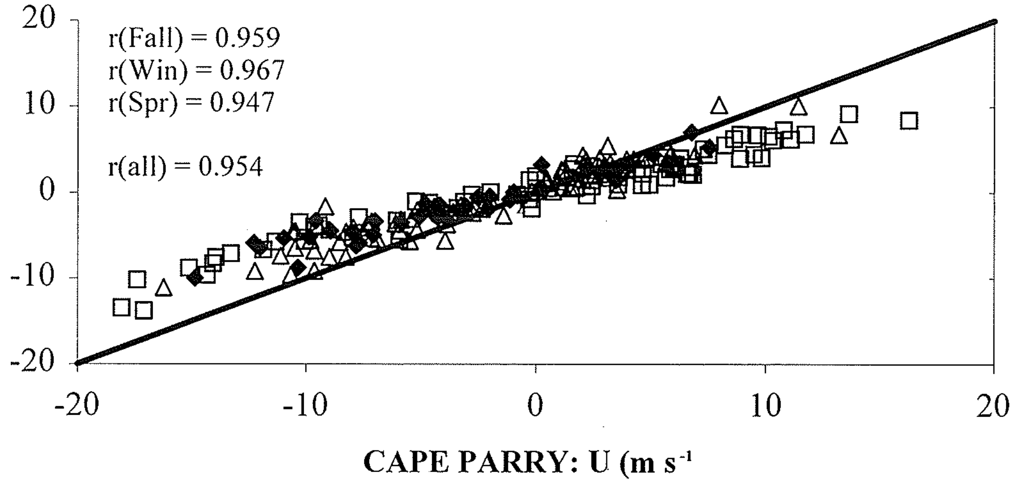


Figure 4.14: Same as 4.13 for data from Cape Parry.

(a)

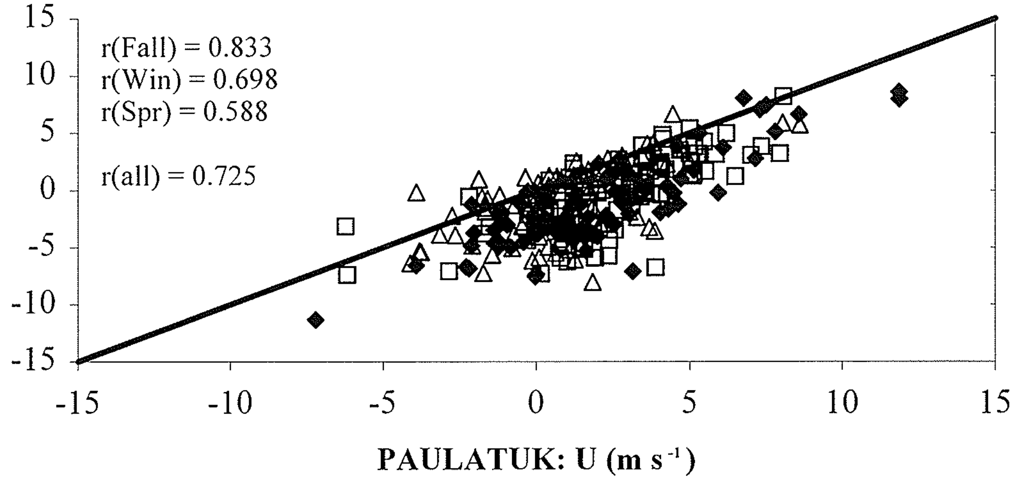

r(Fall) = 0.833
r(Win) = 0.698
r(Spr) = 0.588
r(all) = 0.725
15
10
5
0
-5
-10
-15
-15
-10
-5
0
5
10
15
PAULATUK: U (m s-1)


(b)

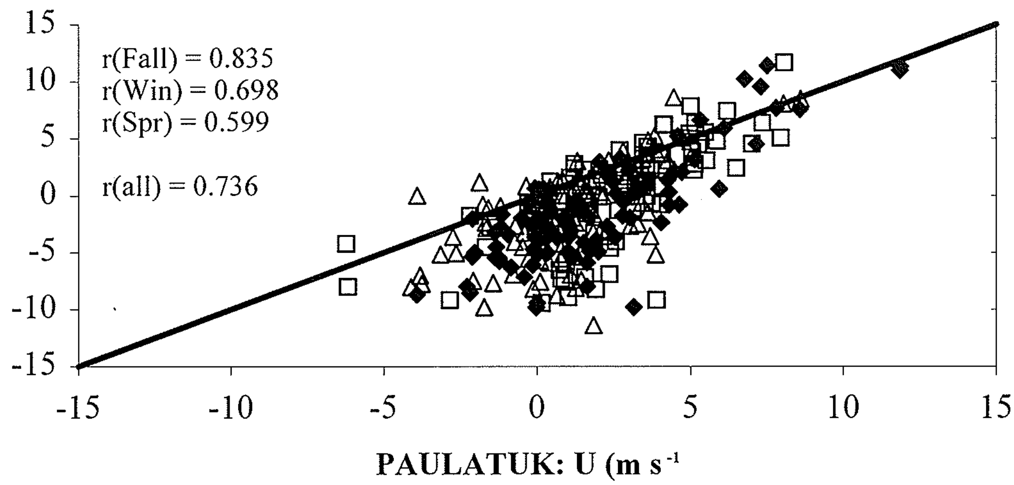

r(Fall) = 0.835
r(Win) = 0.698
r(Spr) = 0.599
r(all) = 0.736
15
10
5
0
-5
-10
-15
-15
-10
-5
0
5
10
15
PAULATUK: U (m s-1


(c)

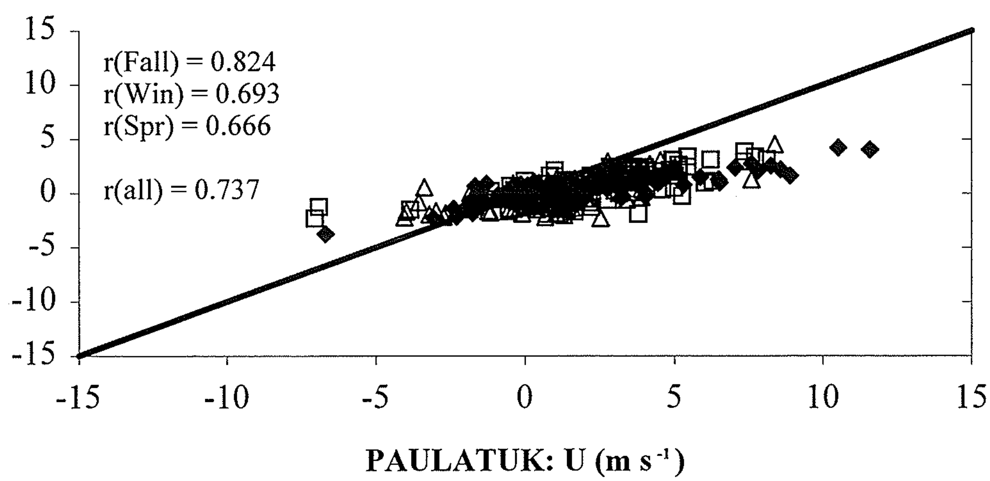

r(Fall) = 0.824
r(Win) = 0.693
r(Spr) = 0.666
r(all) = 0.737
15
10
5
0
-5
-10
-15
-15
-10
-5
0
5
10
15
PAULATUK: U (m s-1)

(d)

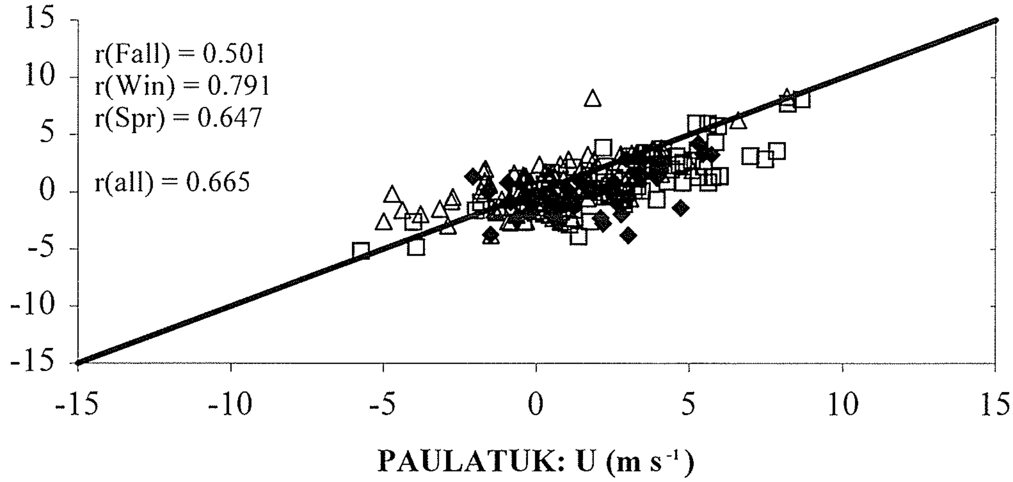


Figure 4.15: Same as 4.13 for data from Paulatuk.

### 4.3.5 Meridional Wind Representation

As with the zonal comparison, Cape Parry emerged as the station with the best correlation and least variability among the other station comparisons for meridional winds, with the exception of NARR, which produced a correlation of 0.53 with Cape Parry against correlations of 0.83 for the remaining models. RMSEs all remained below 2.0 m $s^{-1}$ for Cape Parry, including the case of NARR (1.96 m $s^{-1}$). GEM and NARR presented the best comparisons for Paulatuk, with correlations of 0.79 and 0.81, respectively, though the correlations with NCEP I and NCEP II were just slightly less at 0.75 and 0.74. Variability was consistent between the four models and Paulatuk, with NCEP II yielding the highest RMSE of 2.85 m $s^{-1}$. Comparisons with ship data faired the worst of the three stations, with high variability (RMSE of 3.80 to 4.85) and correlations between 0.66 and 0.71. All models produced fairly consistent results for the ship, with GEM providing the best correlation yet the worst range in error. Again, as with the zonal wind comparison, Takatuk winds were investigated as well to see whether or not the relationships would improve and reveal any inadequacies of the ship data itself. NARR was the only model to show a positive correlation change as well as a negative variability change (overall improvement). Correlation increased slightly from 0.65 to 0.67 with the replacement of ship data with Takatuk data between day 022 and day 145, and RMSE decreased from 4.15 m $s^{-1}$ to 3.21 m $s^{-1}$. In all other cases, correlation decreased, but RMSEs also decreased, giving light to a lower variability with the presence of Takatuk data. This suggests that wind measurements at the ship are most likely affected adversely by the architecture of the ship where turbulent flow may produce anomalous readings. Seasonal variability is minimal and overall, in parallel with the findings for zonal winds, large northerly winds were generally underestimated at the station sites; in other words, the slopes of the 'line of best fit' for all comparisons were less than one. Cape Parry came closest to unity with slopes around 0.83 for NCEP I, NCEP II and GEM.

(a)

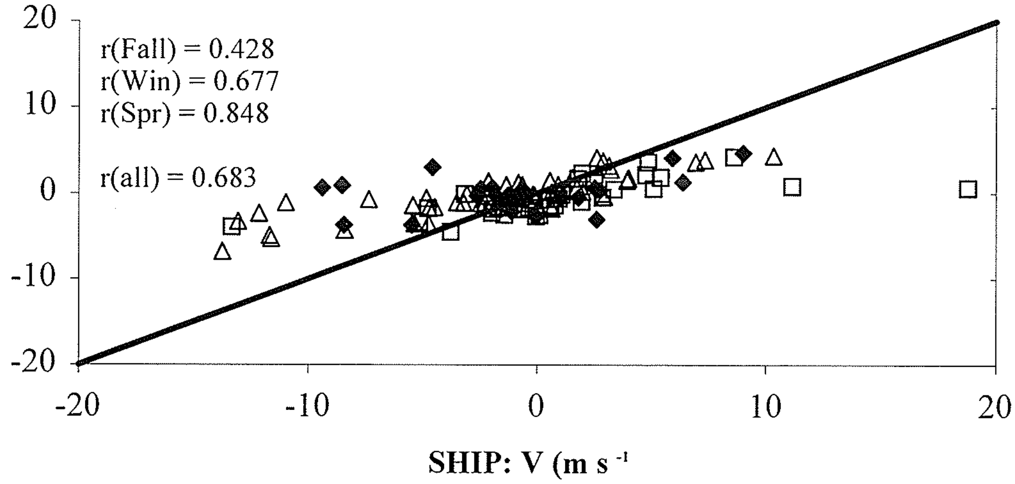

r(Fall) = 0.428
r(Win) = 0.677
r(Spr) = 0.848
r(all) = 0.683
20
10
0
-10
-20
-20
-10
0
10
20
SHIP: V (m s -1


(b)

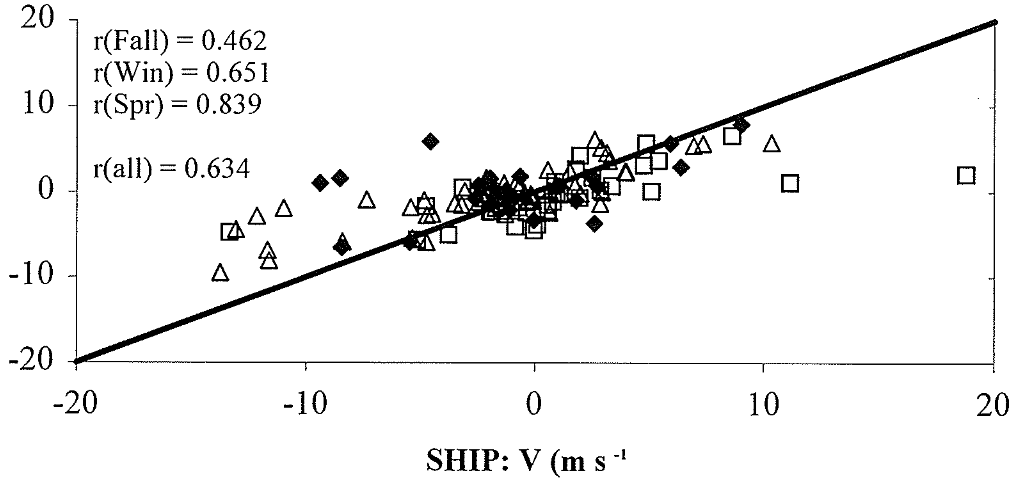

r(Fall) = 0.462
r(Win) = 0.651
r(Spr) = 0.839
r(all) = 0.634
20
10
0
-10
-20
-20
-10
0
10
20
SHIP: V (m s -1


(c)

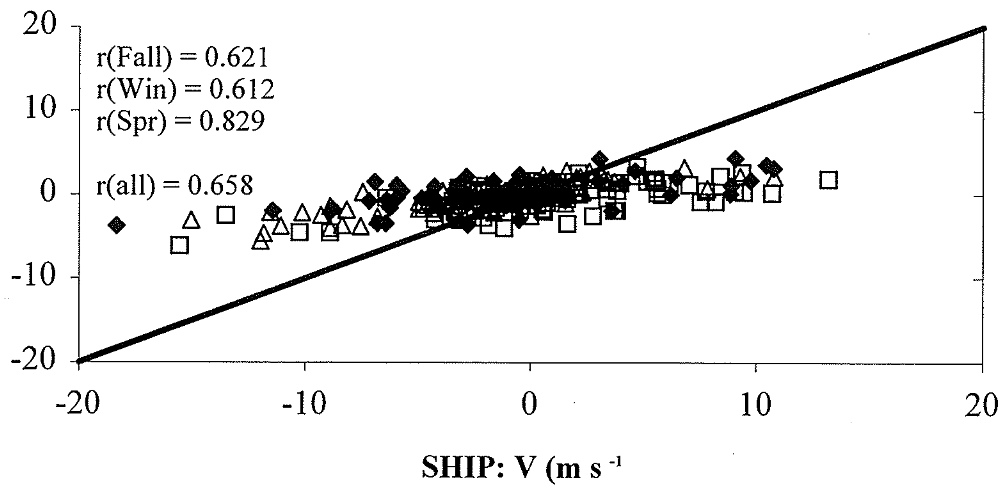

r(Fall) = 0.621
r(Win) = 0.612
r(Spr) = 0.829
r(all) = 0.658
20
10
0
-10
-20
-20
-10
0
10
20
SHIP: V (m s -1

(d)

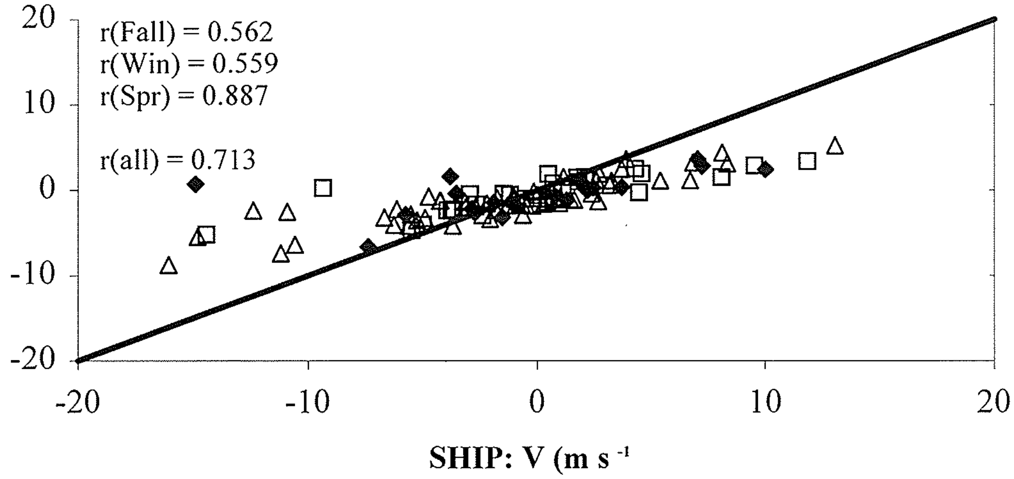


Figure 4.16: Meridional wind comparisons between ship data and data from (a) NCEP I, (b) NCEP II, (c) NARR, and (d) GEM. Solid diamonds represent fall (OND) data, open squares the winter (JFM), and open triangles the spring (AMJ).

(a)

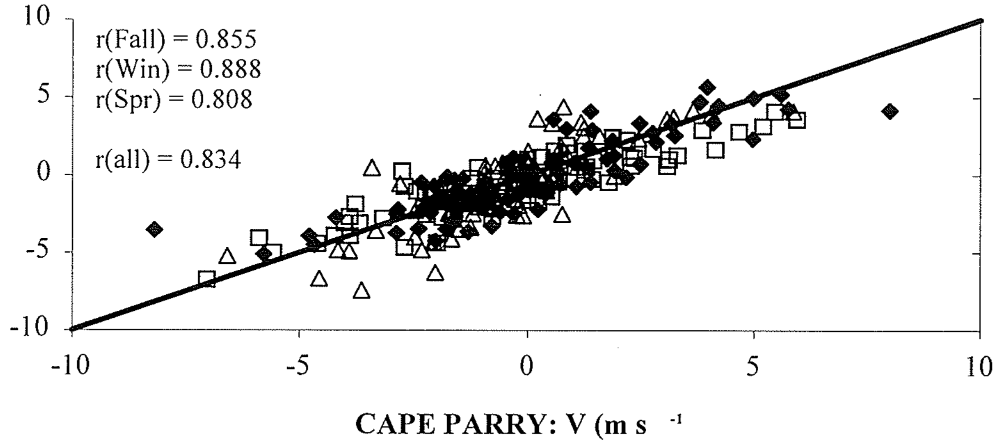
r(Fall) = 0.855
r(Win) = 0.888
r(Spr) = 0.808
r(all) = 0.834
10
5
0
-5
-10
-10
-5
0
5
10
CAPE PARRY: V (m s -1

(b)

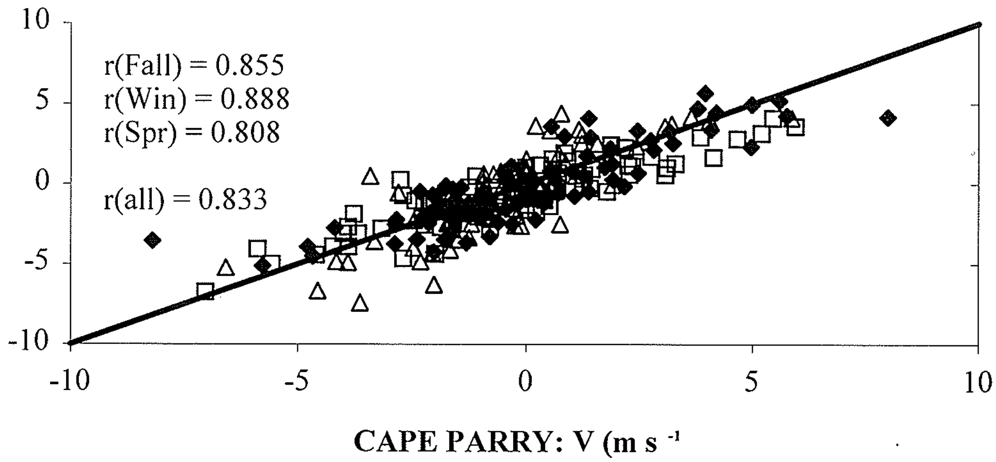
r(Fall) = 0.855
r(Win) = 0.888
r(Spr) = 0.808
r(all) = 0.833
10
5
0
-5
-10
-10
-5
0
5
10
CAPE PARRY: V (m s -1

(c)

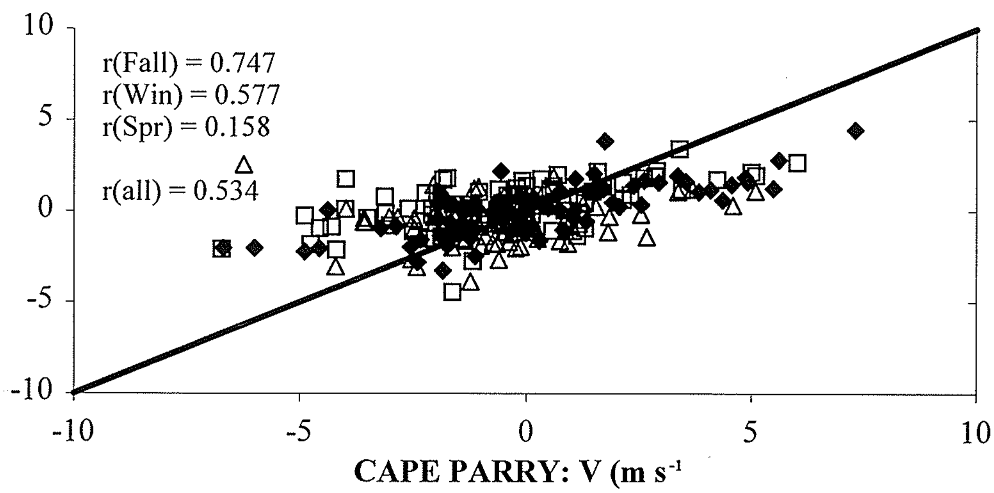
r(Fall) = 0.747
r(Win) = 0.577
r(Spr) = 0.158
r(all) = 0.534
10
5
0
-5
-10
-10
-5
0
5
10
CAPE PARRY: V (m s -1

(d)

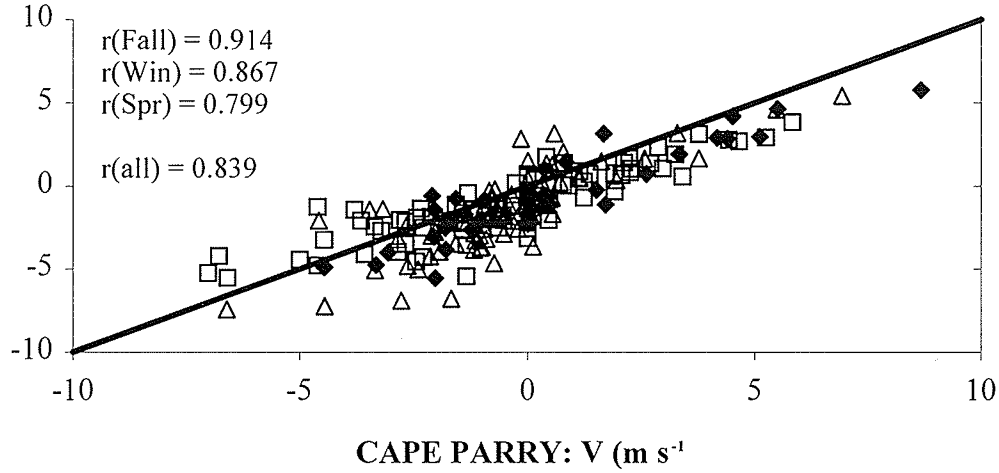


Figure 4.17: Same as 4.16 for data from Cape Parry.

(a)

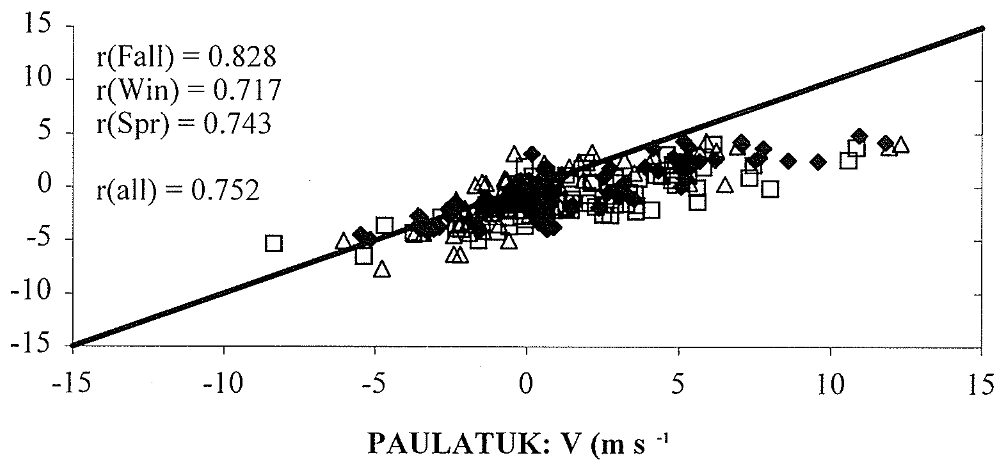

r(Fall) = 0.828
r(Win) = 0.717
r(Spr) = 0.743
r(all) = 0.752
15
10
5
0
-5
-10
-15
-15
-10
-5
0
5
10
15
PAULATUK: V (m s -1


(b)

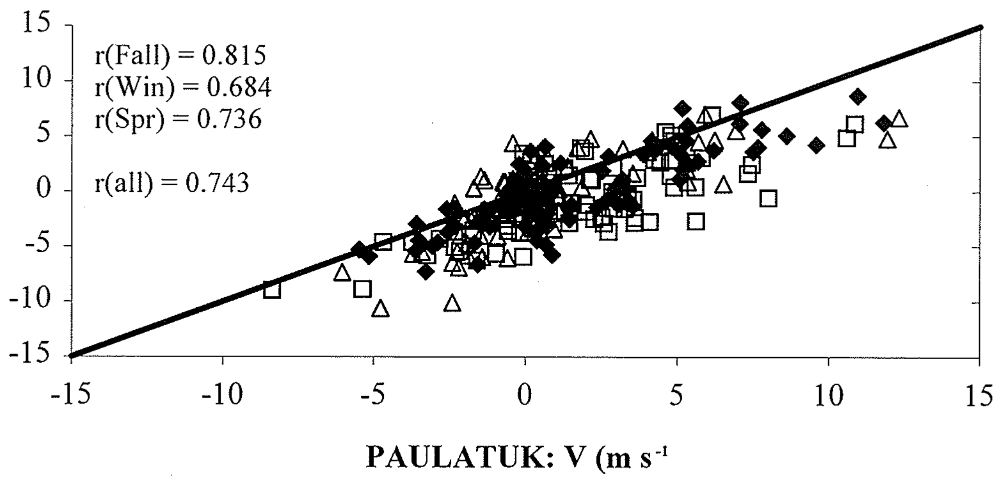

r(Fall) = 0.815
r(Win) = 0.684
r(Spr) = 0.736
r(all) = 0.743
15
10
5
0
-5
-10
-15
-15
-10
-5
0
5
10
15
PAULATUK: V (m s-1


(c)

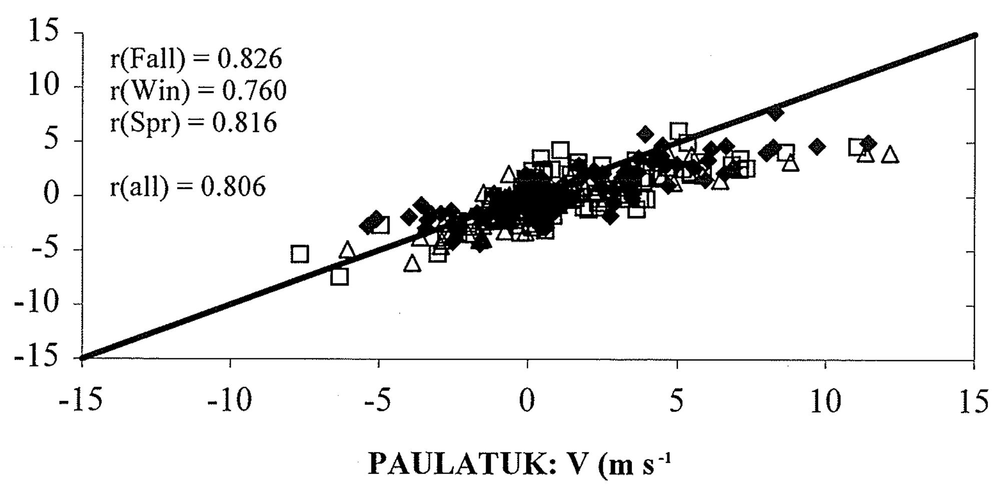

r(Fall) = 0.826
r(Win) = 0.760
r(Spr) = 0.816
r(all) = 0.806
15
10
5
0
-5
-10
-15
-15
-10
-5
0
5
10
15
PAULATUK: V (m s-1

(d)

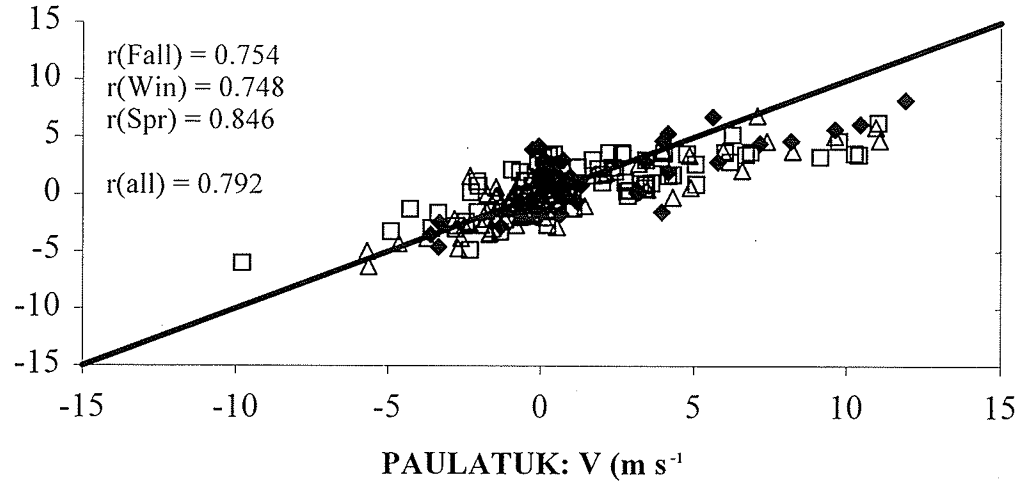


Figure 4.18: Same as 4.16 for data from Paulatuk.

# 5 Vertical Profile Data Comparison

As part of the full meteorological suite of instrumentation, vertical profiling was a key component. Along with measurements of total column PWV via the WVR-1100 microwave radiometer and cloud base height measurements from the ceilometer, over 300 radiosondes were released throughout the duration of the CASES project. The nature of operating an upper-air site in the arctic includes risks and hindrances in providing launches with the greatest accuracy. For the CASES project, launching from a ship platform, preparing sondes in sub-zero temperatures and launching during significant weather proved to be difficult. As much as 44% of the radiosondes launched had issues, including communications failure, early balloon failure, and lack of clearance of ship obstacles.

As previously shown in section 4.2.3, both the MWR and calculations from the radiosondes paint a similar picture in terms of measured PWV over the ship throughout the study period. Having investigated the accuracy of model data in comparison to surface variables, an investigation of the accuracy of model data in the vertical using the data retrieved from the radiosondes would be of great value.

## 5.1 Data and Methods

GEM was taken as the sole model to be used in the comparison, which has a total of 28 pressure levels at each 00z and 12z integration time, where temperature, dew point depression, and grid-referenced zonal and meridional winds were extracted at each level. Rotations of the winds were carried out as per the methods described in Section 4.1. GEM does not provide direct output for relative humidity (RH); RH was calculated based on the following relationship:

$$RH = 100 * \frac{es(T_d)}{es(T_{env})} \quad \textbf{(5.1);}$$

where $T_{env}$ is the environmental or ambient temperature, $T_d$ is the dew point temperature (calculated by subtracting the dew point depression from the environmental temperature), and $es$ is the saturation vapour pressure. Ship data was reduced to reflect a similar vertical structure as provided by GEM, by limiting the sounding data at the following 28 corresponding levels (in mb): 1015, 1000, 985, 970, 950, 925, 900, 875, 850, 800, 750, 700, 650, 600, 550, 500, 450, 400, 350, 300, 275, 250, 225, 200, 175, 150, 100, 50. More often than not, balloons terminated prior to reaching 50mb, so comparisons were limited to 100mb as the upper limit.

The investigation was split into three separate weather conditions in order to determine GEMs accuracy given specific atmospheric states, which are clear sky, overcast, and during blowing snow events. Given that these cases are relatively specific, and given the low rate of success with much of the radiosondes, the number of soundings that actually fit the categories remained quite small. A total number of eight clear sky and blowing snow cases were found to be suitable for inclusion. The overcast sky case encompassed 11 soundings. Rate of failure is not the sole reason for the lack of available soundings. Time of balloon release must also be taken into consideration, as data from GEM was taken at the 00z and 12z time periods. With this in mind, qualified soundings were limited to a ± 3-hour window around 00z and 12z.

The overall bias for each level was calculated as follows:

$$BIAS_{LEVEL} = \frac{1}{n}\sum_{k=1}^{n}(x_{GEM_k} - x_{SHIP_k}) \quad \textbf{(5.2);}$$

where the result at each level is the average of the difference of all available points at that level over ***n*** - the number of available data points at that level. Temperature, RH, U, and V (herein referenced according to case; ie: $T_{CLR}$, $T_{OVC}$, $T_{BS}$) are compared between GEM and the radiosondes released from the ship, and the results of each case are plotted in figures 5.1 to 5.12.

## 5.2 Results

Temperature in the lower layers of the atmosphere in all cases showed high variability, with RMSEs ranging considerably in the first 100 mb, particularly for clear sky and overcast cases (Figures 5.1 to 5.3). Variability appears to lessen above 900 mb in the case of $T_{OVC}$, and variability, while still present and somewhat large, remains mainly centered around the zero datum. Both $T_{BS}$ and $T_{CLR}$ prove to be consistently underestimated in the mid-levels. The GEM $T_{ovc}$ may be too cold in the boundary layer due to its typical lack of cloud cover generation. For $T_{BS}$, this is characterized by a smooth 'bulged' feature between 700 and 500 mb and a corresponding RMSE that appears to stabilize through the duration of the bulge at around 1.5 K; while there is a consistency in the mid-levels for a negative bias of $T_{BS}$, the low- and high-levels remain highly variable. As with $_{TBS}$, $T_{CLR}$ is highly variable at the low levels but variability does stabilize slightly with an increase in altitude.

The representation of RH varies widely between the three cases, and within each comparison (Figures 5.4 to 5.6). Surprisingly, RH was "best" represented in the blowing snow case, albeit with large variability. $RH_{CLR}$ exhibits no consistency with altitude as

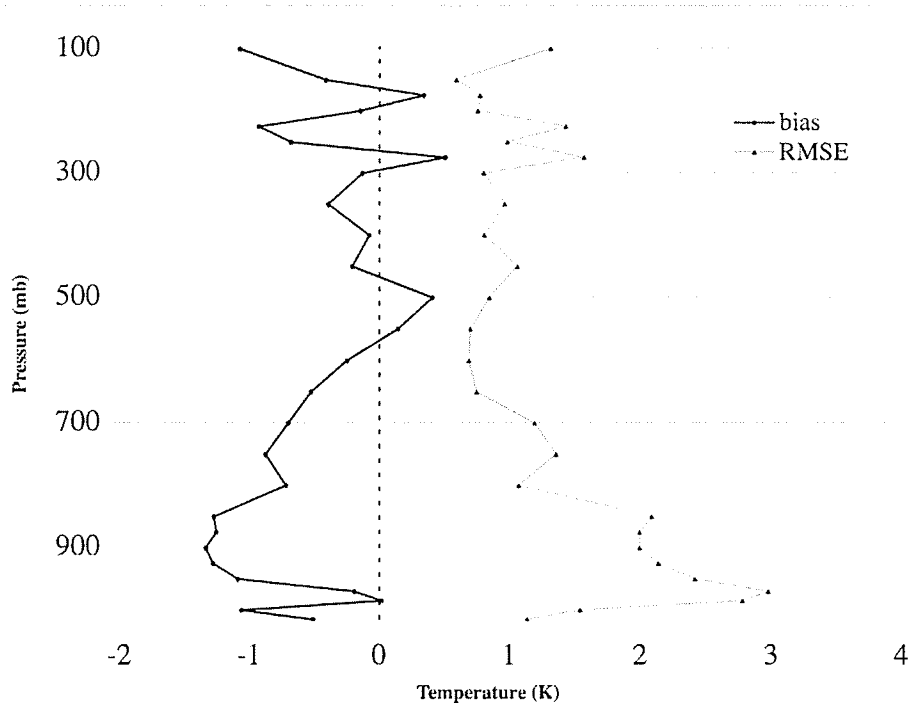


Figure 5.1: Average Clear-Sky temperature bias (dark black line) and RMSE (grey line) between GEM data and radiosonde data at 28 vertical pressure levels.

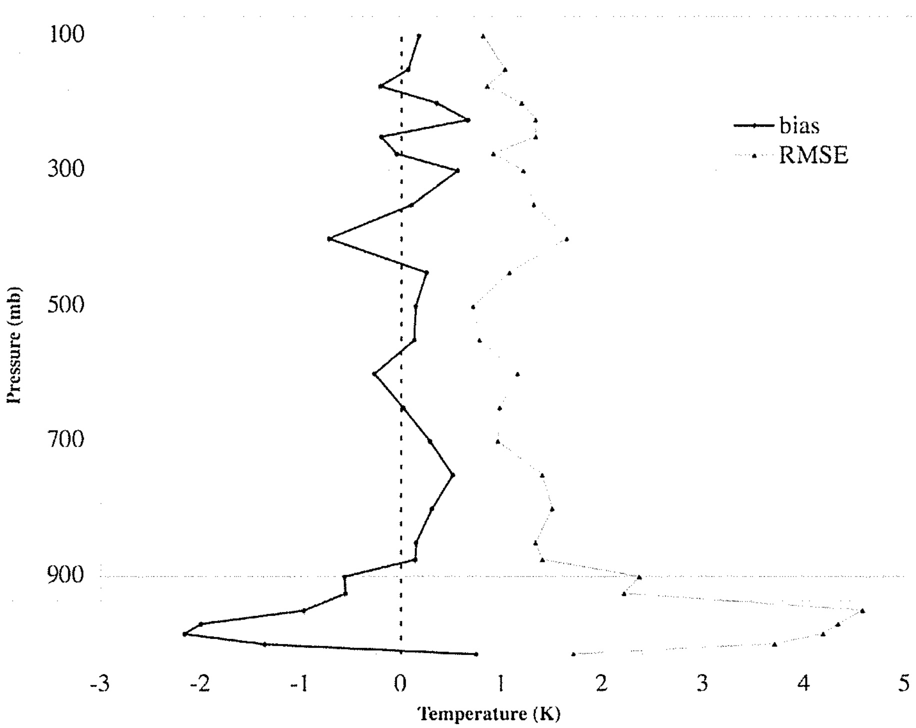


Figure 5.2: Same as Figure 5.1 for the Overcast (no precipitation) case.

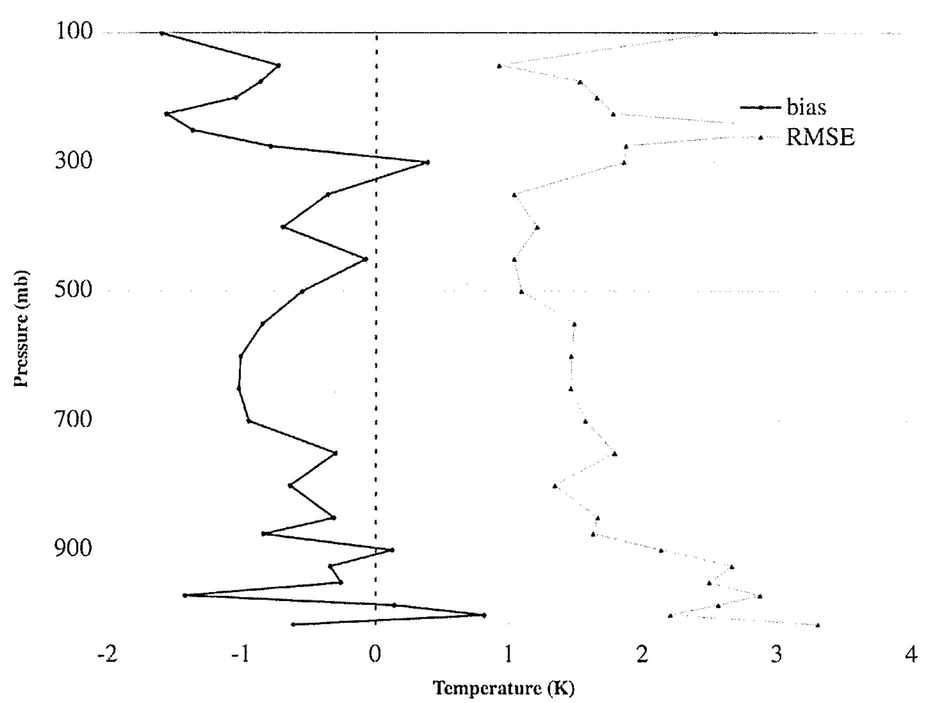


Figure 5.3: Same as Figure 5.1 for the Blowing Snow case.

bias jumps on either side of the zero line. Above 500 mb GEM highly overestimates $RH_{CLR}$ in the extreme upper and lower levels. Between 700 and 500 mb the bias changes from +10% to -5% before becoming positive again. Though the bias for $RH_{OVC}$ was largely positive at the surface, it remained mainly underestimated by GEM for all levels below 300 mb with large variability. Once again, the underestimation of RH in the boundary layer for clear and cloudy skies may be due to the lack of boundary layer cloud on many days. $RH_{BS}$,is no exception among the three cases where variability remains large for all altitudes.

Zonal winds in all three weather scenarios were mainly under-represented by GEM throughout the atmospheric column, with the best representations in all cases at the near surface (Figures 5.7 to 5.9). The best fit of $U_{CLR}$ came within the first and last 100 mb where bias was at most -2.0 m $s^{-1}$. From 900 mb to 300 mb the bias between GEM

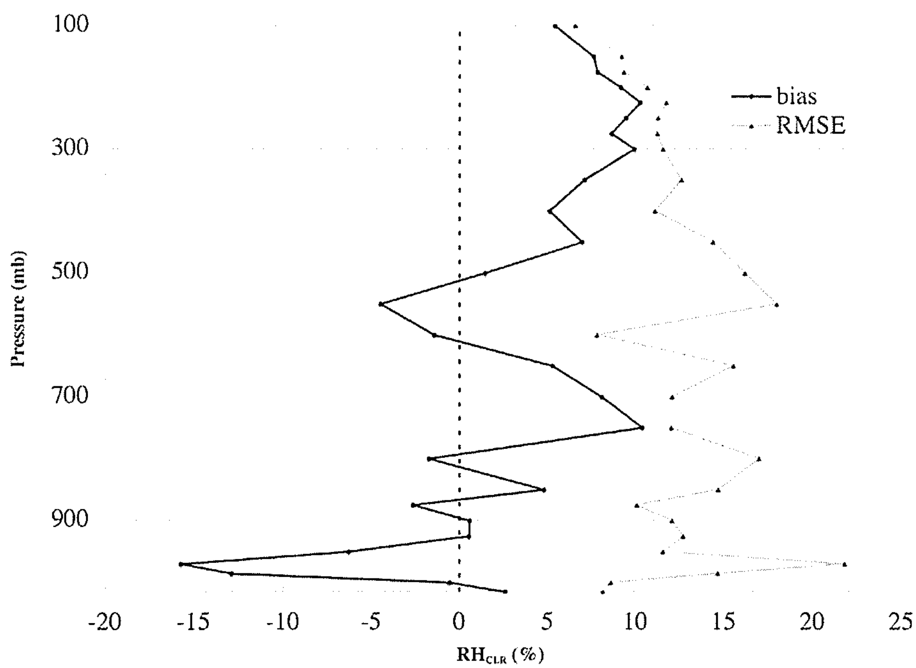


Figure 5.4: Average Clear-Sky relative humidity bias (dark black line) and RMSE (grey line) between GEM data and radiosonde data at 28 vertical pressure levels.

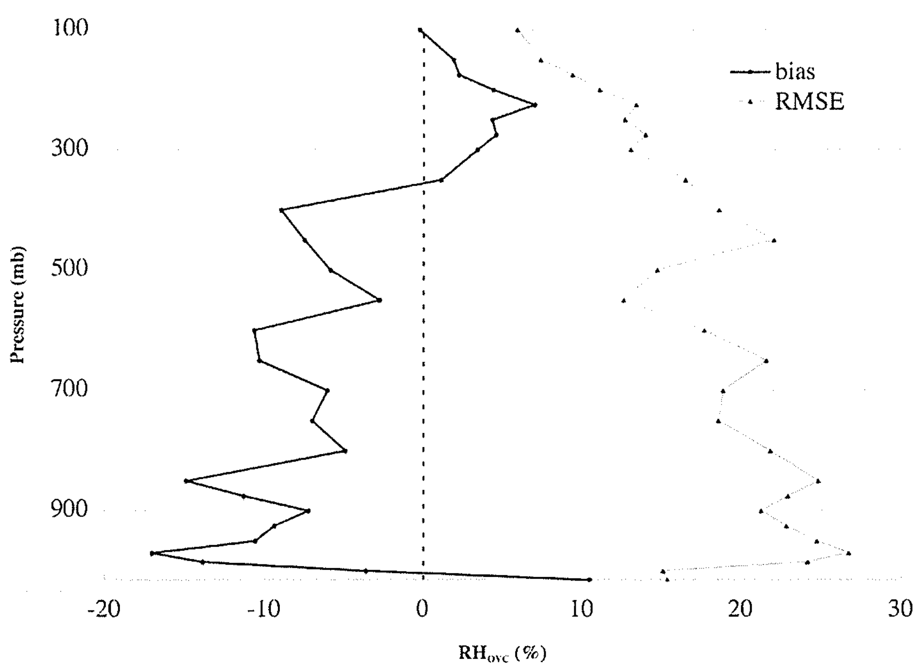


Figure 5.5: Same as Figure 5.4 for the Overcast (no precipitation) case.

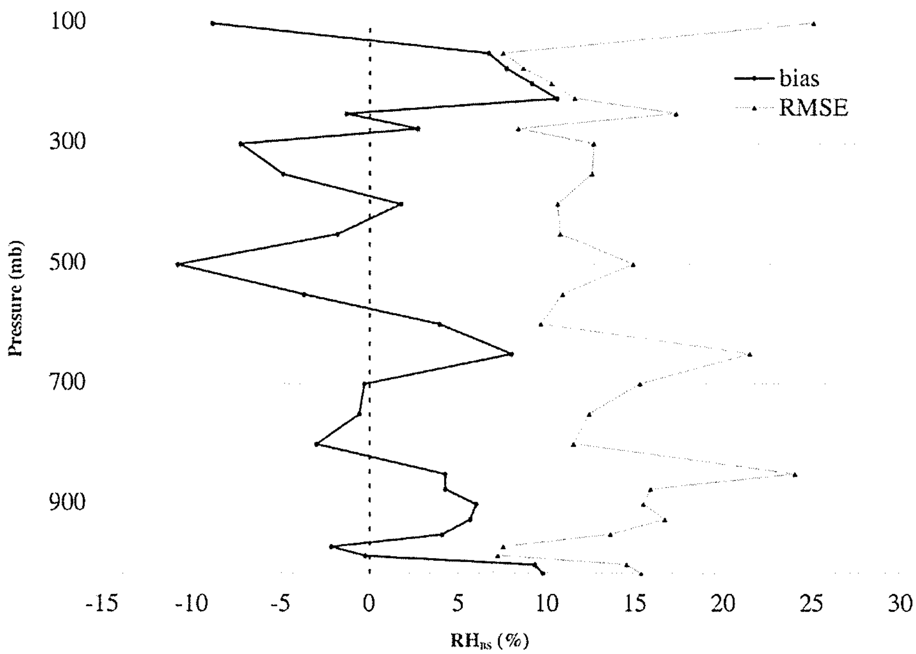


Figure 5.6: Same as Figure 5.4 for the Blowing Snow case.

and the radiosonde data became increasingly negative. The overcast case yielded a $U_{OVC}$ profile that remained relatively consistent throughout the troposphere, decreasing in bias from -2 m $s^{-1}$ to -5 m $s^{-1}$ to the top of the column, with the exception of the lower 100 mb. RMSE also decreased with height overall, though holding steady at 4 m $s^{-1}$ in the lower 100 mb, and peaking at 700 mb and 350 mb. RMSE for $U_{CLR}$ and $U_{BS}$ varied between 3 m $s^{-1}$ to 8 m $s^{-1}$, and as much as 12 m $s^{-1}$ for $U_{OVC}$. During blowing snow events the zonal winds bias, while associated with relatively high variability with height, exhibits a similar profile to that of the overcast sky case, remaining underestimated over all and varying between 2 m $s^{-1}$ and 4 m $s^{-1}$. All cases show a marked decrease in variability at 300 mb.

Meridional winds biases, particularly $V_{CLR}$ and $V_{BS}$, appeared to have much the same vertical structure as zonal wind biases (Figures 5.10 to 5.12). GEM underestimated

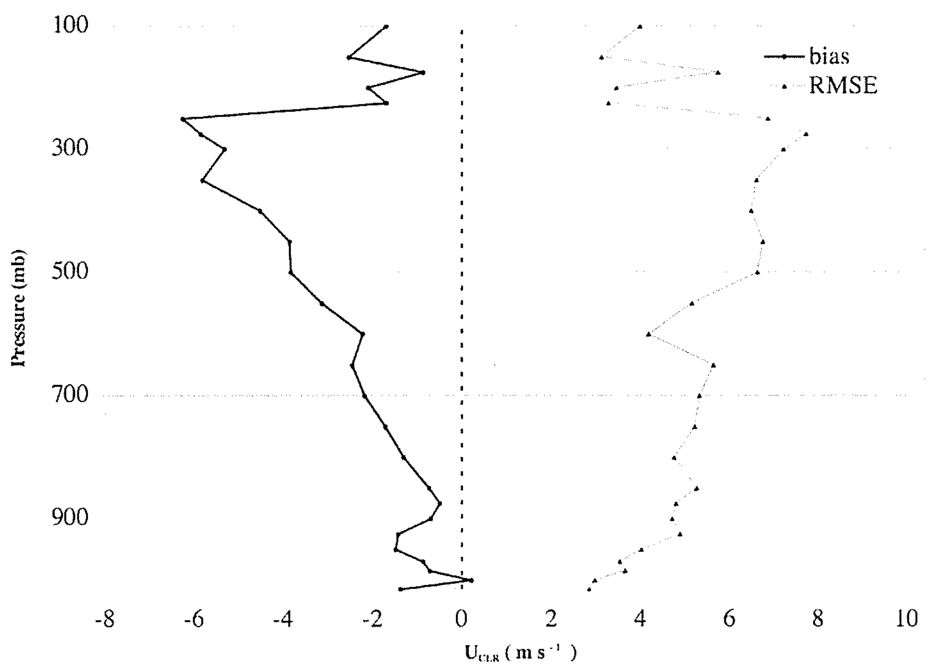


Figure 5.7: Average Clear-Sky zonal wind bias (dark black line) and RMSE (grey line) between GEM data and radiosonde data at 28 vertical pressure levels.

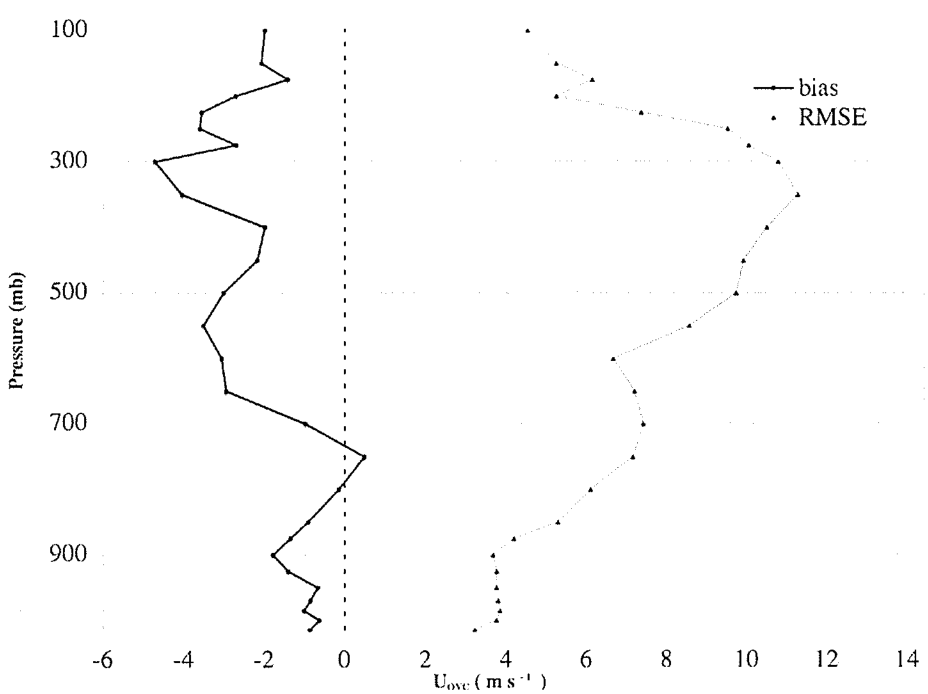


Figure 5.8: Same as Figure 5.7 for the Overcast (no precipitation) case.

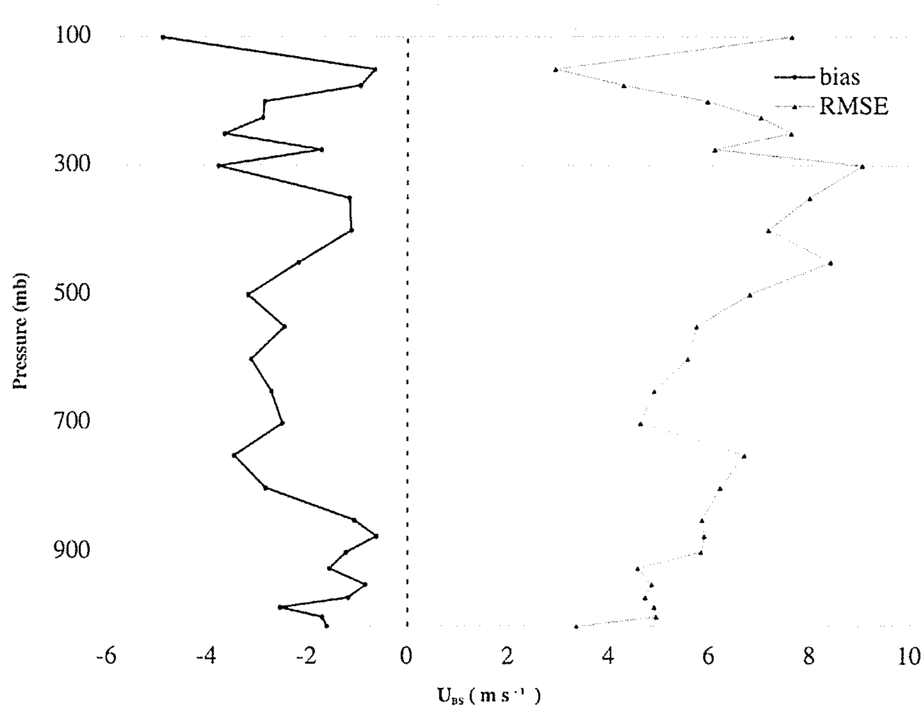


Figure 5.9: Same as Figure 5.7 for the Blowing Snow case.

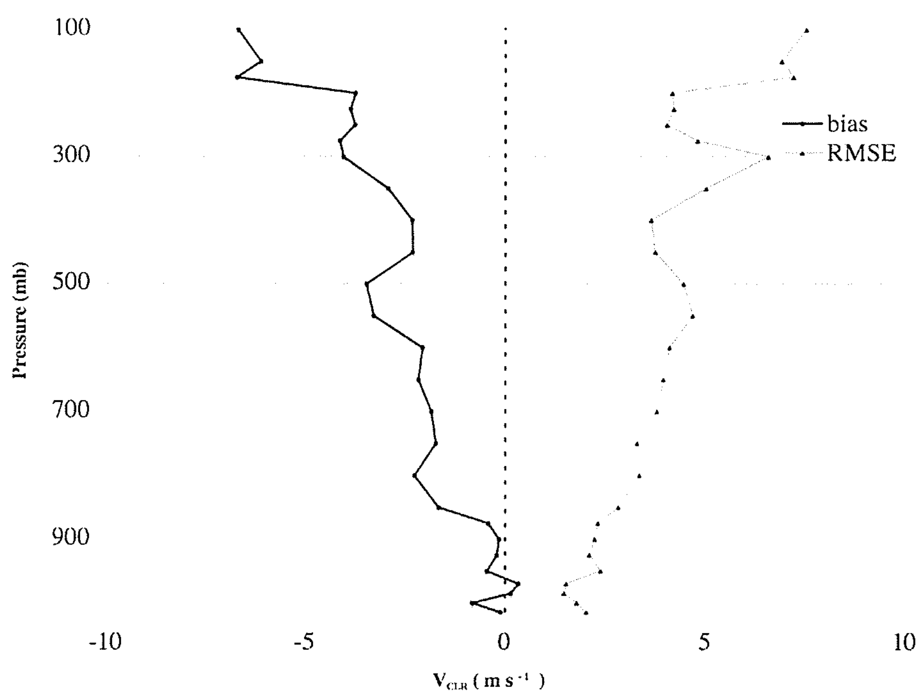


Figure 5.10: Average Clear-Sky meridional wind bias (dark black line) and RMSE (grey line) between GEM data and radiosonde data at 28 vertical pressure levels.

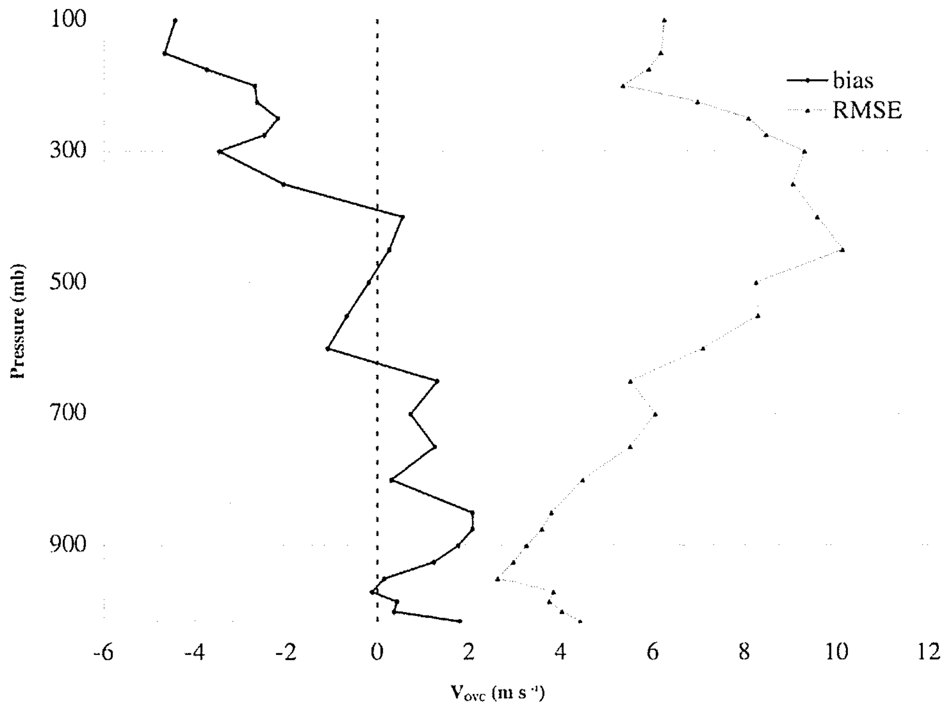


Figure 5.11: Same as Figure 5.10 for the Overcast (no precipitation) case.

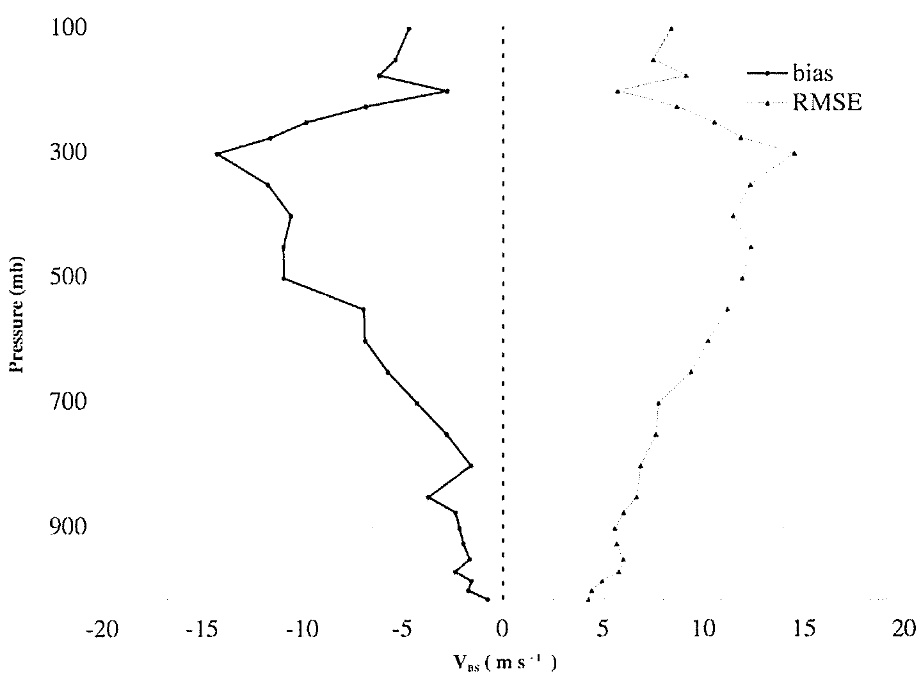


Figure 5.12: Same as Figure 5.10 for the Blowing Snow case.

both $V_{CLR}$ and $V_{BS}$ on the whole. In the case of $V_{OVC}$, however, GEM overstated northerly wind magnitudes for a substantial portion of the atmospheric column (up to 600 mb) within +2 m $s^{-1}$ before falling negative of the zero datum in the upper atmosphere. Variability, as in the previous zonal wind discussion, increased with altitude, making a sharp turn towards lower RMSEs at the 350 mb to 300 mb level, which coincides with the approximate location of the tropopause. $V_{BS}$ exhibited the most variability and illustrated the greatest bias (-14 m $s^{-1}$) at 300mb, where as VOVC and VCLR stay within -6 m $s^{-1}$.

Overall the comparison of GEM and radiosonde data in the vertical yielded high variability at each of the 28 pressure levels and on the whole, GEM mainly underestimated most variables throughout these levels.

# 6 Summary, Conclusions and Recommendations

## 6.1 Summary and Conclusions

Three distinct investigations have been presented to provide insight on the meteorological and climatological conditions observed during the CASES project to meet the requirements of the objectives set for the study. The first investigation was to provide an overall meteorological summary at three scales: the climate scale, the synoptic scale, and the local scale. The second investigation focused on the accuracy of model data in comparison to surface observations at the CCGS *Amundsen*, and MSC stations Cape Parry and Paulatuk. The third investigation, an extension of the second, was to test model data accuracy in the vertical against radiosonde observations collected from the CCGS *Amundsen*. A summary of the findings for each objective is outlined below.

1. ***To provide a climatological context for the CASES project.*** In order to address the first objective, NCEP I model data was used to compare meteorological variables from the CASES project to similar data representing the average of the last 30 years in order to reveal any significant anomalies. Temperatures were found to be above normal throughout the study period by as much as +7 °C over the Canadian Archipelago, where fall and early winter months over CASES were above normal by +1 °C to +5 °C. A weaker than normal Arctic High is likely to blame for these anomalies, which hindered the transfer of cold air from higher latitudes into the region. Large negative temperature anomalies were found in the mid to late winter months, corresponding to an increase of SLP and a return of

northerly cold flow into the region. Average monthly near-surface wind speed anomalies remained near normal, valuing between ±1 m $s^{-1}$ throughout the period. Average monthly PWV anomalies closely varied with temperature anomalies, being above normal during the fall/early winter and below normal for the late winter and early spring.

2. ***To provide additional knowledge into the trends of cyclonic activity in the Western Arctic.*** The findings in the synoptic investigation correlated with what was found in objective (1): that a weaker than normal arctic high in the late fall/early winter prevented the influx of cold air from the northern latitudes, and allowed for low pressure disturbances (LPDs) to migrate into the CASES region. It was found that a number of these LPDs began to dissipate prior to transiting the region, which left the CASES region mainly in the warm sector, contributing to above normal temperature and moisture content on average. The most synoptically active months were November (eight LPDs) and March (seven LPDs). Forty-one of these disturbances were recorded in total, with the majority of the systems originating north of the ship (56% of ARCTIC origin, 39% of PACIFIC origin, and 5% of IRREGULAR origin). A large percentage of disturbances, in comparison to previous studies, formed to the south and west of the ship location, which could suggest that during the CASES study period, the occurrence of Pacific-originating LPDs was above normal, or that mid-latitude storm tracks shifted slightly northward during the time-frame of the CASES project. Further study would be needed to conclude either scenario, which is discussed in section 6.2.

3. ***To provide a meteorological summary for the CASES project.*** A local summary of the weather recorded aboard the CCGS *Amudsen* was produced. Large temperature fluctuations were found in late fall, early and winter which corresponded to a peak in synoptic activity. The coldest day experienced at the ship was March 7, 2004 with a temperature of -38.3 °C, and the highest recorded temperature fell on June 12, 2004 at 5.5 °C. Blowing snow, light snow, and fog were the most reported weather types, and strataform-type clouds topped the most reported of cloud types throughout the study period, where November was the cloudiest month. Winds reported at the ship were predominantly easterly or westerly in direction.

4. ***To examine the differences between meteorological variables of surrounding stations.*** Time series of meteorological data were compared between the ship and two near-by reporting stations to determine discrepancies when attempting to use stations data in place of *in-situ* data. Cape Parry, the closer of the two reporting stations used in the study, stayed within ±1.5 °C of the monthly average temperatures at the ship. Pressure also varied similarly throughout the period, and with a calculated offset using current temperatures to account for elevation change, pressure could be used in this distance range. Winds at Cape Parry and the ship were both predominantly zonal; however, a monthly breakdown shows larger discrepancies between the stations. Late fall and early winter zonal wind anomalies were highly positive (winds at Cape Parry were much greater on average in comparison to the ship). Zonal wind anomalies were minimized

through the remainder of the winter and spring. Meridional wind anomalies remained within ±3.0 m $s^{-1}$. In the case of Paulatuk, pressure remained in good agreement, and average monthly temperature anomalies stayed within -1.7 °C to +3.6 °C. Ship recorded temperatures were warmer than Paulatuk on average from November to January. Zonal wind anomalies were mainly positive (stronger winds at Paulauk) throughout the period, but did compare well in late winter. Meridional wind anomalies were consistently positive with the most positive anomalies falling in November and June. In both cases, visibilities reported at the ship were larger then those resported at the respective stations, most likely caused by a systematic human error introduced by location where the measurements were being made (atop the wheelhouse) and with the aid of a videograph, also atop the ship. Replacing available visibility data from Takatuk yielded much lower visibilities in comparison with Paulatuk for the months available (Februrary to May). A better agreement was made for visibilities in both cases when an additional systematic error was minimized (the default maximum reported visibility at the ship was reduced to match those of the stations). Overall, pressure and temperature fields could be used with minimal error in place of on-ice data within the range of the stations presented here; however, the remaining fields did not exhibit the consistency necessary in their comparisons to conclude the same.

5. ***To investigate the accuracy of model data within the CASES region.*** Two studies, broken into sections referring to surface and vertical data, were carried out.

    a. Firstly, four models, NCEP I, NCEP II, NARR and GEM, were used to investigate their accuracy against data from the CCGS Amudsen, Cape Parry and Paulatuk. Time series data were created to represent of each of the stations' surface position in order to carry out the comparison. GEM provided the best fit amongst all four models in regards to temperature, particularly with Paulatuk. NARR presented a larger discrepancy with pressure compared to the remaining models, most likely caused by the averaging technique and missing data. Relative humidity (RH) was generally resolved poorly, though GEM outperformed NCEP I overall. In terms of PWV, the largest variability appeared in the spring, and all but NARR consistently underestimated PWV measured at the ship. GEM, again, provided the best fit among the four models in regards to zonal winds, in the case of Cape Parry. The NCEP products had difficulty with Paulatuk's location, particularly with low, positive wind speeds. Takatuk wind data was included in the ship dataset to minimize some of the noted wind errors from aboard the ship. It was found that overall the unaltered ship dataset provided the best linearity correlation with model data, though variability was reduced with the addition of the data from Takatuk. This was true for NARR, GEM and NCEP II, however NCEP I showed a decrease in performance when Takatuk data was in place. For meridional winds, comparisons for Cape Parry faired the best with the exception of NARR. When winds from Takatuk were integrated into the dataset for the ship, NARR was the only model to show an improvement in linear correlation and variability. All models underestimated wind magnitudes for the ship, Paulatuk, and Cape Parry; i.e., the models mainly underrepresented larger magnitudes of reported zonal or meridional winds. While GEM provided the best fit overall, it has been noted in recent studies that a larger-than- necessary surface roughness term used in the boundary layer scheme could be contributing to the under-representation of winds at the surface (John Hanesiak, personal communication). As GEM has been shown to provide the best representation of all stations in all fields (with the exception of winds) among the four models considered, it can be recommended for use in the Western Arctic for verification and investigative studies.

b. Secondly, vertical data collected from radiosondes released from the ship were compared to vertical data matched from GEM Regional model output. Vertical profiles were broken into three distinct meteorological conditions (Clear Sky, Overcast Sky (no precipitation), and Blowing Snow) to compare temperature, pressure, relative humidity, zonal wind and meridional winds. Most of the comparisons yielded large variability at all levels, particularly in the lower levels for temperature and upper levels for both zonal and meridional winds. Each variable presented a unique bias and RMSE profile for each case and consistency cannot be concluded; however, the temperature comparison in the Overcast Sky case provided the best overall comparison in the study, with RMSE ranging between +1 °C and +2 °C and bias between ±1°C above 900mb. Large RMSE values were the norm in most cases. Among the poorest representations were the wind comparisons, with RMSEs ranging between 4 m $s^{-1}$ and 15 m $s^{-1}$, and were consistently underestimated throughout the tropospheric column. Error sources may stem from sonde error, or interpolation error of the model data.

## 6.2 Recommendations

The nature of the thesis presented gives way to a number of recommendations for future work and further analysis. Each of the three studies (climatological/meteorological summary, data comparison, model verification) was limited to a 'first look' where more details would be necessary before coming to full conclusions.

In the first study, the observed synoptic activity may have subjected the CASES region to an above-average number of storms originating from the PACIFIC region. The bases for this conclusion were studies focusing on year-round arctic synoptic activity, whereas our study is limited only to the late fall/winter/spring months of one particular region of the Arctic. While Hudak et. al. 2002 provided a long-term summary of summer storms in the Beaufort Sea, it would be useful to create a climatology of year round and seasonal synoptic activity in this region to come to conclusions about trends in origin, frequency and intensity. Also, while we know large-scale atmospheric mass shifts give way to storm track deviations, investigating the linkages between synoptic activity and variables such as sea ice concentrations and/or regional SST could be worthwhile.

In the model verification study, interpolations were done using an inverse distance weighted scheme. A more advanced interpolation scheme, or a scheme that included terrain effects may have provided a better fit to actual recorded data, particularly in terms of winds and moisture. Along the same lines, interpolation in the vertical profile study was done using the same distance-weighting technique. Radiosondes unfortunately do not remain directly above the launch site, and so using the same four grid point references may not always been the best-case scenario at particular levels. Creating a vertical profile of GEM data with this in mind was beyond the time frame of this thesis; however, considering the poor results in the vertical profile study, it may be worthwhile to investigate this avenue. In addition, the number of available sondes in each case was quite low, and it is difficult to come to conclusions regarding a particular case limited to small numbers of available sondes per meteorological case. Inherent errors in launching aboard a ship in the Arctic Ocean did unfortunately arise. The recommendation here is to continue to provide the resources for similar campaigns in the future (not limited to the Beaufort Sea region) to continue the vertical data verification of GEM.

# List of References


ACIA, 2004: *Impacts of a Warming Climate*. Arctic Climate Impact Assessment, Hassol, S.J., et al., eds. Cambridge University Press, Cambridge, UK.

Anderson, S., R. Tonboe, L. Kaleschke, G. Heygster, and L.T. Pedersen, 2007: Intercomparison of passive microwave sea ice concentration retrievals over the high-concentration Arctic sea ice. *Journal of Geophysical Research*, **112**, C08004, doi: 10.1029/2006

Barber, D.G. and J.M. Hanesiak, 2004: Meteorological forcing of sea ice concentration in the southern Beaufort Sea over the period 1979 to 2000. *Journal of Geophysical Research*, **109**, C06014, doi: 10.1029/2003JC002027.

Briegler, B.P. and D.H. Bromwich, 1998: Polar climate simulation of the NCAR CCM3. *Journal of Climate*, **11**(6), 1270-1286.

Bromwich, D.H., J.J. Cassano, T. Klien, G. Heinemann, K.M. Hines, K. Steffen, and J.E. Box, 2001: Mesoscale modeling of katabatic winds over Greenland with Polar MM5. *Monthly Weather Review*, **129**(9), 2290-2309.

Buehler, S.A., M. Kuvatov, V.O. John, U. Leiterer, and H. Dier, 2004: Comparison of microwave satellite humidity data and radiosonde profiles: A case study. *Journal of Geophysical Research*, **109**, D13103, doi: 10.1029/2004JD004605.

Comiso, J.C., 2006: Abrupt decline in the Arctic winter sea ice cover. *Geophysical Research Letters*, **33**, L18504, doi: 10.1029/2006GL027341.

Côté, J., S. Gravel, A. Méthot, A. Patoine, M. Roch, and A. Staniforth, 1998: The operational CMC-MRB global environmental multiscale (GEM) model. Part 1: Design considerations and formulation. *Monthly Weather Review*, **126**(6), 1373-

1395.

Côté, J., J.G. Desmarais, S. Gravel, A. Méthot, A. Patoine, M. Roch, and A. Staniforth, 1998: The operational CMC-MRB global environmental multiscale (GEM) model. Part II: Results. *Monthly Weather Review*, **126**(6), 1397-1418.

Crane, R.G. and R.G. Barry, 1984: Review Paper: The influence of clouds on climate with a focus on high latitude interactions. *Journal of Climatology*, **4**(1), 71-93.

Cullather, R.I., D.H. Bromwich, and M.C. Serreze, 2000: The atmospheric hydrologic cycle over the arctic basin from Reanalyses. Part I: Comparison with observations and previous studies. *Journal of Climate*, **13**(5), 923-937.

Dickson, R.R., T.J. Osborn, J.W. Hurrell, J. Meincke, J. Blindheim, B. Adlandsvik, T. Vinje, G. Alekseev, and W. Maslowski, 2000: The Arctic Ocean response to the North Atlantic Oscillation. *Journal of Climate*, **13**(15), 2671-2696.

Dumas, J.A., G.M. Flato, R.D. and Brown, 2006: Future Projections of landfast ice thickness and duration in the Canadian Arctic. *Journal of Climate*, **19**(20), 5175-5189.

Gregory, J.M., P.A. Scott, D.J. Cresswell, N.A. Rayner, C. Gordon, and D.M.H. Sexton, 2002: Recent and future changes in arctic sea ice simulated by the HadCM3 AOGCM. *Geophysical Research Letters*, **29**(24), doi: 10.1029/2001GL014575.

Holland, M.M. and J. A. Curry, 1999: The role of physical processes in determining the interdecadal variability of central Arctic sea ice. *Journal of Climate*, **12**(11), 3319-3330.

Hudak, D. and J.M.C. Young, 2002: Storm climatology of the Southern Beaufort Sea. *Atmosphere-Ocean*, **40**(2), 145-158.

IPCC, 2001: *Climate Change 2001: The Scientific Basis.* Intergovernmental Panel on

Climate Change (IPCC) Working Group I, J.T. Houghton, Y. Ding, D.J. Griggs, M. Noguer, P.J. van der Linden and D. Xiaosu (Eds.) Cambridge University Press, Cambridge, UK, pp 944

IPCC AR4, 2007: *Climate Change 2007: The Physical Science Basis.* Intergovernmental Panel on Climate Change (IPCC) Working Group I, Solomon, S. et al., eds. Cambridge University Press, Cambridge, UK.

Kalnay, E., M. Kanamitsu, R. Kistler, W. Collins, D. Deaven, L. Gandin, M. Iredell, S. Saha, G. White, J. Woollen, Y. Zhu, M. Chelliah, W. Ebisuzaki, W. Higgins, J. Janowiak, K.C. Mo, C. Ropelewski, J. Wang, A. Leetmaa, R. Reynolds, R. Jenne, and D. Joseph, 1996: The NCEP/NCAR 40-year reanalysis project. *Bulletin of the American Meteorological Society*, **77**(3), 437-471.

Kanamitsu, M., W. Ebisuzaki, J. Woollen, S-K. Yang, J.J. Hnilo, M. Fiorino, and G.L. Potter, 2002: NCEP-DOE AMIP-II Reanalysis (R-2). *Bulletin of the American Meteorological Society*, **83**(11), 1631-1643.

Konosuke, S., D. Yang, T. Ohata, 2003: Systematic error aspects of gauge-measured solid precipitation in the Arctic, Barrow, Alaska. *Geophysical Research Letters*, **30**(4), 1192, doi: 10.1029/2002GL15547.

Lambert, S.J., 1995: The effect of enhanced greenhouse warming on winter cyclone frequencies and strengths. Notes and Correspondence, *Journal of Climate*, **8**(5), 1447-1452.

Lindsay, R.W. and J. Zhang, 2005: The Thinning of Arctic Sea Ice, 1988-2003: Have We Passed A Tipping Point? *Journal of Climate*, **18**(22), 4879-4894.

Manabe, S. and R.J. Stouffer, 1994: Multiple-century response of a coupled ocean-atmosphere model to an increase of atmospheric carbon dioxide. *Journal of*

*Climate*, 7(1), 5-23.

Maslowski, W., B. Newton, P. Schlosser, A. Semtner, D. Martinson, 2000: Modeling recent climate variability in the Arctic Ocean. *Geophysical Research Letters*, **27**(22), 3743-3746.

McCabe, G.J., M.P. Clarke, and M.C. Serreze, 2001: Trends in Northern Hemisphere surface cylcone frequency and intensity. *Journal of Climate*, **14**(12), 2763-2768.

McMillin, L. M., J. Zhao, M. K. Rama Varma Raja, S. I. Gutman, and J. G. Yoe, 2007: Radiosonde humidity corrections and potential Atmospheric Infrared Sounder moisture accuracy. *Journal of Geophysical Research*, **112**, D13S90, doi:10.1029/2005JD006109.

Mesinger, F., G. DiMego, E. Kalnay, K. Mitchell, P.C. Shafran, W.Ebisuzaki, D. Jovic, J. Woollen, E. Rogers, E.H. Berbery, M.B. Ek, Y. Fan, R. Grumbine, W. Higgins, H. Li, Y. Lin, G. Mankin, D. Parrish, and W. Shi, 2006: North American Regional Reanalysis. *Bulletin of the American Meteorological Society*, **87**(3), 343-360

Miloshevich, L. M., H. Vömel, A. Paukkunen, A. J. Heymsfield, and S. J. Oltmans, 2001: Characterization and correction of relative humidity measurements from Vaisala RS80A radiosondes at cold temperatures. *Journal of Atmospheric and Oceanic Technology*, **18**, 135 – 155.

Miloshevich, L. M., H. Vömel, D. N. Whiteman, B. M. Lesht, F. J. Schmidlin, and F. Russo, 2006: Absolute accuracy of water vapor measurements from six operational radiosonde types launched during AWEX-G and implications for AIRS validation. *Journal of Geophysical Research,* **111**, D09S10, doi:10.1029/2005JD006083.

Rothrock, D.A., Y. Yu, and G.A. Maykut, 1999: Thinning of the arctic sea-ice cover. *Geophysical Research Letters*, **26**(23), 3469-3472.

Schweiger, A.J. and J.R. Key, 1992: Arctic cloudiness: Comparison of ISCCP-C2 and *Nimbus-7* satellite-derived cloud products with a surface-based cloud climatology. *Journal of Climate*, **5**(12), 1514-1527.

Serreze, M.C., R.G. Barry, 1988: Synoptic activity in the Arctic Basin, 1979-85. *Journal of Climate*, **1**(12), 1276-1295.

Serreze, M.C., J.E. Box, R.G. Barry, and J.E. Walsh, 1993: Characteristics of arctic synoptic activity, 1952-1989. *Meteorology and Atmospheric Physics*, **51**(3-4), 147-164

Serreze, M.C., T.L. Demaria, R.G. Barry, and D.A. Robinson, 1991: Atmospheric forcings on large scale patterns of parameterized albedo over arctic sea ice: case studies for June 1975 and 1988. *Preprint Volume of the Fifth Conference on Climate Variations, Denver, CO*, American Meteorological Society, 396-399.

Soden, B.J., D.D. Turner, B.M. Lesht, and L. M. Miloshevich, 2004: An analysis of satellite, radiosonde, and lidar observations of upper tropospheric water vapour from the Atmospheric Radiation Measurement Program. *Journal of Geophysical Research*, **109**, D04105, doi: 10.1029/2003JD003828.

Stroeve, J., M.M. Holland, W. Meier, T. Scambos, and M. Serreze, 2007: Arctic sea ice deline: Faster than forecast. *Geophysical Research Letters*, **34**, L09501, doi: 10.1029/2007GL29703.

Sugiura, K., D. Yang, and T. Ohata, 2003: Systematic error aspects of gauge-measured solid precipitation in the Arctic, Barrow, Alaska. *Geophysical Research Letters*,

**30**(4), doi: 10.1029/2002GL015547

Thompson, D.W.J. and J.M. Wallace, 1998: The Arctic Oscillation signature in the wintertime geopotential height and temperature fields. *Geophysical Research Letters*, **25**(9), 1297-1300.

Turner, D.D., B.M. Lesht, S.A. Clough, J.C. Liljegren, H.E. Revercomb, and D.C. Tobin, 2003: Dry bias and variability in Vaisala RS80-H radiosondes: The ARM Experience. *Journal of Atmospheric and Oceanic Technology*, **20**, 117-132.

Walsh, J.E., W.L. Chapman, and T.L. Shy, 1996: Recent decrease of seal level pressure in the central Arctic. Notes and Correspondence, *Journal of Climate*, **9**(2), 480-486.

Walsh, J.E., V.M. Kattsov, W.L. Chapman, V. Gorvorkova, and T. Pavlova, 2002: Comparison of Arctic slimate simulations by uncoupled and coupled global models. *Journal of Climate*, **15**(12), 1429-1446.

Wei, H., W.J. Gutowski, Jr., C.J. Vorosmarty, and B.M. Fekete, 2002: Calibration and validation of a regional climate model for pan-Arctic hydrologic simulation. *Journal of Climate*, **15**(22), 3222-3236.

Westwater, E.R., B.B. Stankov, D. Cimini, Y. Han, J.A. Shaw, B.M. Lesht, and C.N. Long, 2003: Radiosonde humidity soundings and microwave radiometers during Nauru99. *Journal of Atmospheric and Oceanic Technology*, **20**, 953-970.

Zhang, J., D. Rothrock, and M. Steele, 2000: Recent changes in arctic sea ice: The interplay between ice dynamics and thermodynamics. *Journal of Climate*, **13**(17), 3099-3114.

Zhang, X., J.E. Walsh, J. Zhang, U.S. Bhatt, and M. Ikeda, 2004: Climatology and interannual variability of arctic cyclone activity: 1948-2002. *Journal of Climate*,

**17**(12), 2300-2317.